Coupling the thermodynamic state with the dynamics of lipid interface layers

- and its possible role for biology -

Dissertation zur Erlangung des Doktorgrades
der mathematisch-naturwissenschaftlichen Fakultät
der Universität Augsburg
vorgelegt von

Stefan Bössinger

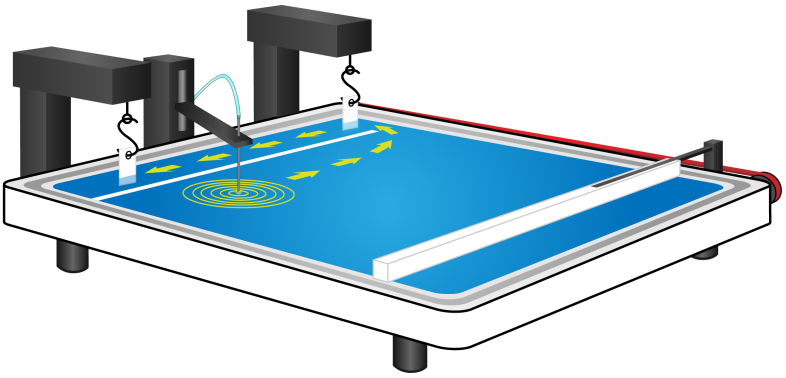

Lehrstuhl für Experimentalphysik I
Institut für Physik
Universität Augsburg
9. Juni 2012

Erster Gutachter:	Prof. Matthias Schneider
Zweiter Gutachter:	Prof. Armin Reller
Tag der Einreichung:	9. Juli 2012
Tag der mündlichen Prüfung:	18.September 2012

"A new scientific truth does not triumph by convincing its opponents and making them see the light, but rather because its opponents eventually die, and a new generation grows up that is familiar with it."

"Eine neue wissenschaftliche Wahrheit pflegt sich nicht in der Weise durchzusetzen, daß ihre Gegner überzeugt werden und sich als belehrt erklären, sondern vielmehr dadurch, daß ihre Gegner allmählich aussterben und daß die heranwachsende Generation von vornherein mit der Wahrheit vertraut gemacht ist."

Max Planck

Contents

Abstract

Hydrated interfaces and lipid membranes are ubiquitous throughout the biological world. Although these systems have been thoroughly studied under static conditions over the past decades, their dynamic properties are only poorly understood. In particular, longitudinal waves in lipid monolayers have not received much attention in biology. However, it has been proposed recently that such waves might be the underlying principle for the propagation of action potentials in nerves. The central topic of this thesis is therefore to investigate the properties of sound wave propagating in lipid-based interfaces. Experimentally this is accomplished by the excitation of pressure pulses resulting from the fusion of a solvent drop with the air-water interface of a lipid monolayer.

The initial development of a comprehensive understanding for the excitation process of longitudinal lipid monolayer waves delivers a sound foundation for further experiments conducted within the scope of this thesis. For this purpose, pressure pulses were excited by fusion of solvent droplets with the aqueous interface of a lipid monolayer. Despite the highly non-linear compressibility profile of the lipid membrane, a linear stress-strain relation was found for the amplitude of the wave. In combination with the elucidated influence of the type of solvent molecules, a comprehensive picture for the excitation process was found, which allows to precisely determine the excitability of the monolayer. In the next step a detailed study about wave excitation by the vapor phase exerted from solvent drops was conducted. With this contactless excitation method it was possible to induce long-term auto-oscillations of membrane tension. Investigation of the relaxation characteristics of the showed coinciding maxima of relaxation time and monolayer compressibility. In order to study the propagation of waves in an even more realistic model of the cell membrane, monolayers formed from lipids with a poly(ethylene glycol)-conjugated headgroup were used. The latter represents a highly hydrophilic moiety which closely mimics carbohydrate residues that constitute the glycocalyx of cells. The increased interaction with the supporting aqueous sub phase led to augmented damping of the waves and linearized their velocity profile. In subsequent experiments, a drastic reduction of membrane excitability was found upon the introduction of Gadolinium ions to the sub phase. Even submillimolar concentrations were sufficient to abolish excitability of the interface. A similar effect was found for other lanthanides e.g. Lanthanum

and Neodymium. It seems very likely that the blockage of monolayer waves by these highly charged ions is due to a complexation of phospholipid molecules. Moreover, the resulting solidification of the membrane could represent a potential explanation as to why lanthanides are also potent blockers of mechanogated ion channels in nerves and muscles. Finally, the effects upon collision of longitudinal monolayer waves was investigated. In a nerve cell, two colliding action potentials annihilate each other. In contrast, two colliding monolayer waves create interference patterns in surface tension. By considering the path length for each pulse, these patterns can be calculated, proofing the classical wave behavior of the phenomenon observed.

The experimental results on the properties of acoustic monolayer waves presented in this thesis will contribute to a better understanding of pulse propagation in biological systems and in particular of action potential propagation in nerves.

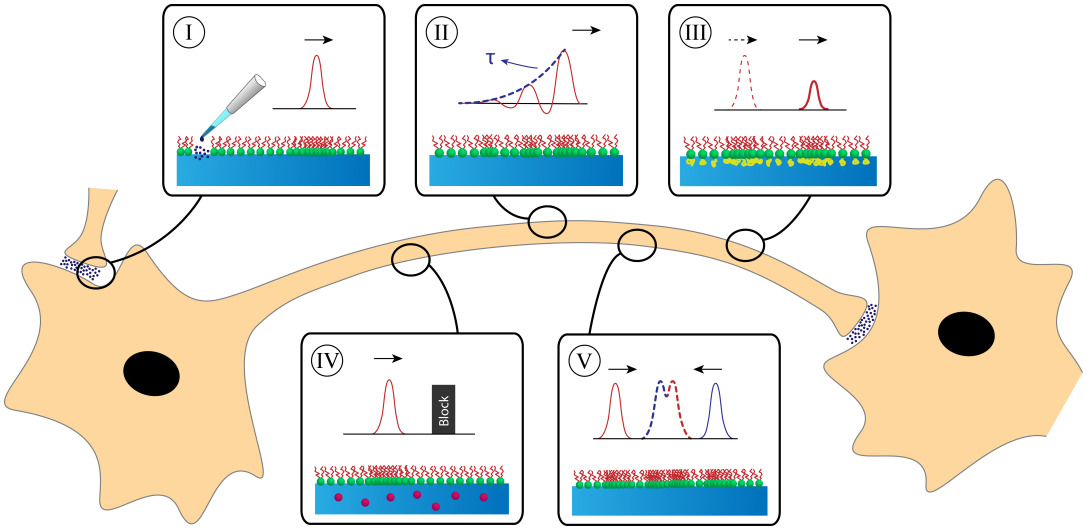

Figure 0.1.: Schematic drawing of signal transmission in nerve cells and the potential relevance of the experiments conducted within this thesis for the processes involved:
I: Excitation of longitudinal pulses by chemical transmitters at the synapse, imitated here by the application of ambipolar solvents to a lipid monolayer-water interface. **II:** Relaxation behavior of excited pressure pulses. **III:** Influence of the glycocalyx on propagating pulses, simulated by the incorporation of glycolipids into the monolayer. **IV:** Block of pulse propagation by lanthanide ions. **V:** Superposition of longitudinal monolayer waves upon collision.

Chapter 1: Introduction

The publication of Luigi Galvani's work about the *"elettricita animale"* in 1791 can be considered as the dawn of electrophysiology [1]. In his writings he described his discovery of inducing twitches in a frog's nerve-muscle-preparation, when brought into contact with a bimetallic arc (see fig. 1.1 left). Galvani explained his findings in analogy to the Leiden Jar (see fig. 1.1 middle), a precursor of the capacitor that can accumulate charges of opposite sign on electrodes in- and outside of a glass jar. He concluded that the contact of the bimetallic arc allows the discharge of the, what he called, *animal electricity* stored inside the muscle, causing the latter to twitch. This result fascinated and inspired people throughout Europe, but also started a debate about the nature of electricity and the nerve excitation. The discussion continued for almost ten years, until Alessandro Volta finally showed by the invention of the Volta pile (fig. 1.1 right) that the bimetallic arc by itself is a continuous source of electricity, able to induce nervous activity. In the following, regular electricity was established as the main tool to investigate the so-called action potentials propagating in nerve cells. Thus, it is not surprising that the current

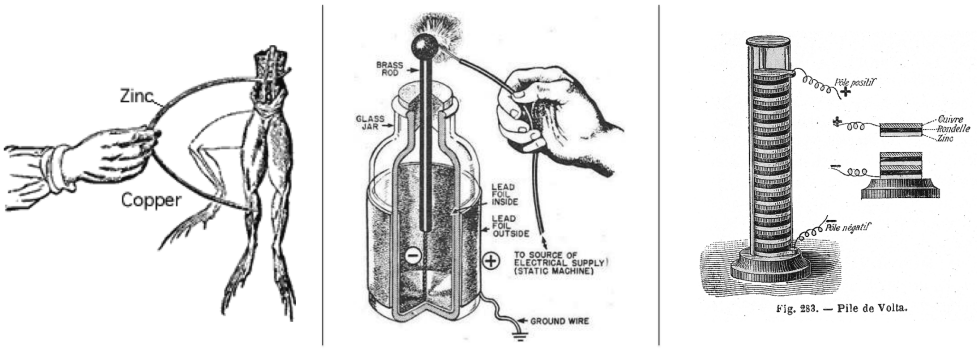

Figure 1.1.: Left: Twitch in a muscle-leg-preparation of a frog induced through the contact of a bimetallic arc (figure from [2]). **Middle:** Systematic drawing of a Leiden Jar (figure from [3]). **Left: The Volta pile** Stacked alternating discs of silver and zinc producing an electromotive force (figure from [4]).

concept in neurophysiology is based on the purely electrical theory formulated by Hodgkin and Huxley [5]. Through a refining of the experimental approach of Galvani and Volta by using single nerve fibers of squids, Hodgkin and Huxley were able

to record individual action potentials propagating on the cell wall of an axon. A standard example can be seen in figure 1.2. The conductivity change during such

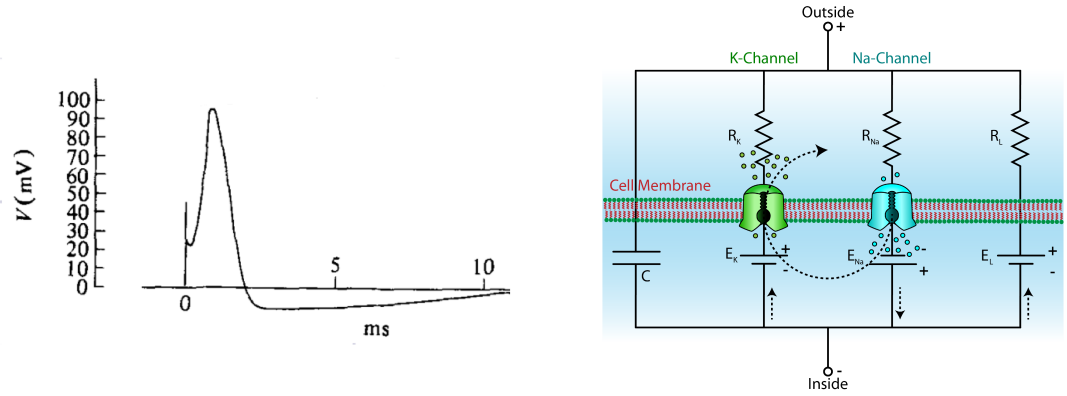

Figure 1.2.: Left: Action potential recorded on a squid giant axon, taken from [5] **Right:** Equivalent circuit representing membrane. R_L and C are the membrane's resistance and capacity. R_{Na} and R_K are the ion-selective resistances varying with time and membrane potential. $E_{Na,K,L}$ are the corresponding ion-selective membrane potentials. Figure adapted from [5, 6]

a pulse is explained by employing an equivalent circuit (compare fig: 1.2), which is motivated from basic cable theory, since in terms of electricity the neuron's axon resembles a classic telephone cable. Here, the nerve cell's membrane is treated as an insulating capacitor in which ion channels are embedded, enabling the selective influx of Na^+ ions and subsequently the efflux of K^+ ions. The channels are triggered by changes in the cellular potential, forcing the resulting local currents to propagate along the membrane. The resulting differential equation, describing the temporal course of voltage is the famous Hodgkin and Huxely equation:

$$\frac{a}{2Rc^2}\frac{\partial^2 V}{\mathrm{d}t^2} = K\left\{\frac{\partial V}{\mathrm{d}t} + \frac{1}{C_m}\left[\bar{g}_K n^4 (V - V_K) + \bar{g}_{Na} m^3 h (V - V_{Na}) + \bar{g}_l (V - V_l)\right]\right\} \qquad (1.1)$$

When numerically calculated, equation 1.1 mimics the action potential recorded (compare figure 1.2), but also consists of at least four independent fit parameters. Quoting John von Neumann, who declared [7]:

Give me four parameters, and I will draw an elephant for you; with five I will have him raise and lower his trunk and his tail!

might resolve the reason, why Hodgkin and Huxley stated by themselves [5]:

For the sake of illustration we shall try to provide a physical basis for the equations, but must emphasize that the interpretation given is unlikely to provide a correct picture of the membrane.

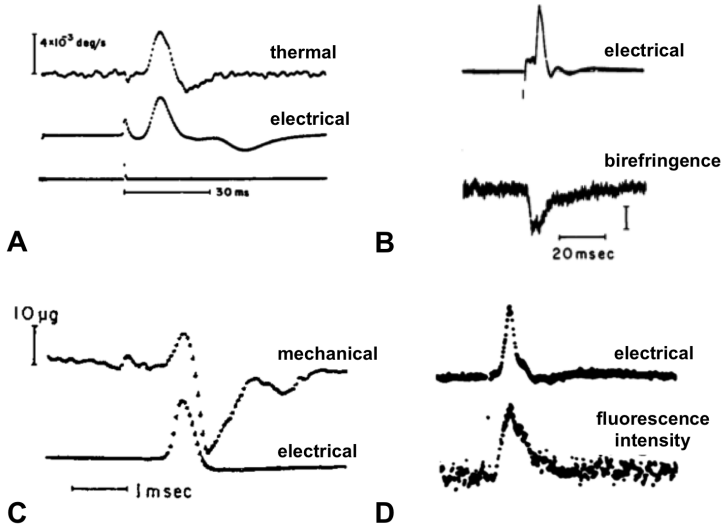

Figure 1.3.: Action potentials are invariably accompanied by nonelectrical concomitants. This includes temporally and spatially coinciding changes in the nerve membrane's temperature (A), birefringence (B), thickness (C) and fluorescence intensity (D). Adapted from [8–10]

With the improvement of measurement techniques however, it was later shown that an action potential is accompanied by thermal [9, 11–13], optical [10] and mechanical [8, 9] changes in the cell membrane that coincide spatially and temporally with the electric signal (compare 1.3). Despite all efforts of explaining those phenomena within the theory of Hodgkin and Huxley [14], all reservations couldn't be overcome. Especially the *consumption of heat* in the second half of a passing pulse couldn't be explained sufficiently by the ion channel theory [9, 12, 13], since the employed conducting proteins can only work as *heat producing* resistors. Moreover, the net change within all variables during an action potential was measured to be almost zero, which implies a reversible nature of the phenomenon [8–10, 12, 13]. Those mentioned reservations inspired the development of an alternative theory in which the nerve impulse could be understood as a longitudinal, sound-like wave, conducted within the cell membrane [15–18]. The integrative nature of the underlying thermodynamic approach could not only explain the phenomenon of heat release and consumption, but also account for the optical, mechanical and electrical changes occurring during an action potential. To address key aspects of this fundamental debate in physiology is the central aim of this thesis. The pure existence of the longitudinal wave mode in lipid layers has already been shown [19–22], but are those waves able to exhibit major features measured on nerve cell membranes? In order to challenge this picture of a propagating sound wave in nerve cells experimentally, a lipid monolayer, the simplest model of a cell membrane, was applied to study excitation, blockage and collision of the described interfacial waves.

A simple hydrodynamic theory of longitudinal waves in lipid monolayers was readily verified by the prediction that the velocity of the 2-dimensional sound wave is correlated to the monolayer's compressibility κ_T [23]. Additionally, along with the lipid density pulse, a dynamic change in the surface potential was identified, whose shape resembled the alteration measured in surface tension [24]. These results not only imply the coupling of different thermodynamic susceptibilities (here κ_T and C_π), but allows to conclude for coinciding mechanical, optical and electrical pulses upon passing of a pressure pulse.

As a first part of this thesis, the wave excitation by alcohols and organic acids such as acetic acid, which is produced upon hydrolyzation of the neurotransmitter acetylcholine in the synaptic cleft, was studied thoroughly. It was found that although acetic acid carries a permanent charge, as compared to ethanol, the length of the aliphatic carbon chain is the main factor that determines the amplitude of the resulting pressure pulse. Also the number of molecules applied to the surface correlates linearly with the pulse amplitude, even within the high non-linear phase transition regime. Moreover, without any mechanical contact, the vapor phase of a solvent is capable of exciting a wave. In particular, volatile members of the carboxylate ester group revealed a strong impact when brought into the vicinity of the membrane. The chemical excitation of waves in lipid monolayers can therefore be understood as a local displacement of lipids, which results in a pressure pulse that is conducted along the interface.

Moreover, the thermodynamic state of the membrane was found to determine the relaxation time τ of the excited wave, as predicted by an Onsager-type ansatz. As a consequence, the maximum in compressibility κ_T coincides with the maximum in relaxation time, when plotted against the membrane pressure. The established correlation between τ and κ_T is conserved under thermodynamic (Π, T), excitation (Ethanol, Chloroform) and molecular (lipids) variations.

To more closely mimic the membrane of a nerve cell, which is covered by a layer of carbohydrates (glycocalyx), the influence of highly hydrated polyethylene glycol (PEG) molecules, covalently bonded to the lipid headgroup, was probed. Compared to experiments done on regular lipids, the polymer caused a slowing down of pulses. Also, the pulse's amplitude was highly damped. From a molecular point of view, the influence can be correlated to the number of ethylene glycol monomers, which determines the capacity to form hydrogen bonds to the surrounding water. The longer the polymer, the more water has to be dragged along with a pulse in the lipid membrane.

In order to investigate the monolayer wave with substances that are probably capable of blocking an action potential, Gadolinium (Gd^{+3}) is of particular interest due to its property to nonspecifically block ion channels. This threefold charged ion

revealed a high affinity towards even slightly charged membranes, changing severely the membrane structure and thereby its dynamic properties. In the range of physiological membrane pressures, the conduction of lateral density pulses was found to be strongly impeded, what might suggest an entirely new mechanism for the blocking effect of Gd^{+3} on nerve signals.

A central point of interest regarding a thermodynamic theory of nerve pulses is the behavior of two signals upon collision. While in nerve cells it was observed that two action potentials cancel each other upon collision, waves in lipid monolayers form inference patterns. Employing the linear superposition principle, the interference pattern can be calculated from the time delay in between two single pulses. This principle was found to hold within all phase states of the membrane.

In conclusion, this thesis presents a variety of results on the properties of acoustic monolayer waves, which provide a solid basis for a scientific debate on the contribution of the lipid layer to the nervous impulse.

Chapter 2: Physics and chemistry of lipid membranes

Lipids are integral parts of living organisms. Their ability of forming self-organized, impermeable membranes compartmentalizes space and thus provides protected areas, where life can develop. Also the beforehand mentioned cell membrane of neurons, responsible for the transport of action potentials, consists mainly of proteins and lipids. Since the latter are the central material under investigation in this thesis, this chapter shall provide a short overview over the molecular structure of lipids and describe the methodology used to investigate them. A more thorough description of lipids can be found in [25, 26], whereas the thermodynamic perspective to this topic is mostly provided in [27].

2.1. Chemical structure of lipids

Among the chemical family of lipids, phospholipids are the most prominent representatives. Especially neurons exhibit a high percentage of roughly 80% of phospholipids in their membranes [27]. These lipids are composed of a glycerol backbone, where two fatty acids and one phosphoric acid are attached via ester bondings (compare figure 2.1). The amphiphilic structure of the resulting molecule with a hydrophobic tail (repelled from water) and a hydrophilic head (attracted to water), forces the lipid to orientate along water-air or water-oil interfaces. The driving force for this lipid orientation is the entropically driven hydrophobic effect of water (expulsion of lipids from water), because the hydrophyobic tail cannot engage hydrogen bonds with its surrounding water molecules. Thus, the lipid molecules accumulate on the surface, reducing the surface tension of water according to the Gibbs adsorption isotherm [28]:

$$\frac{-\mathrm{d}\gamma}{RT} = \sum_i \left(\Gamma_i \ln\left(a_i\right)\right) \tag{2.1}$$

Here, γ represents the surface tension, Γ the surface excess of component i and a_i the activity of this component. R and T are the ideal gas constant and the temperature respectively. The hydrophilic headgroup on the contrary can engage

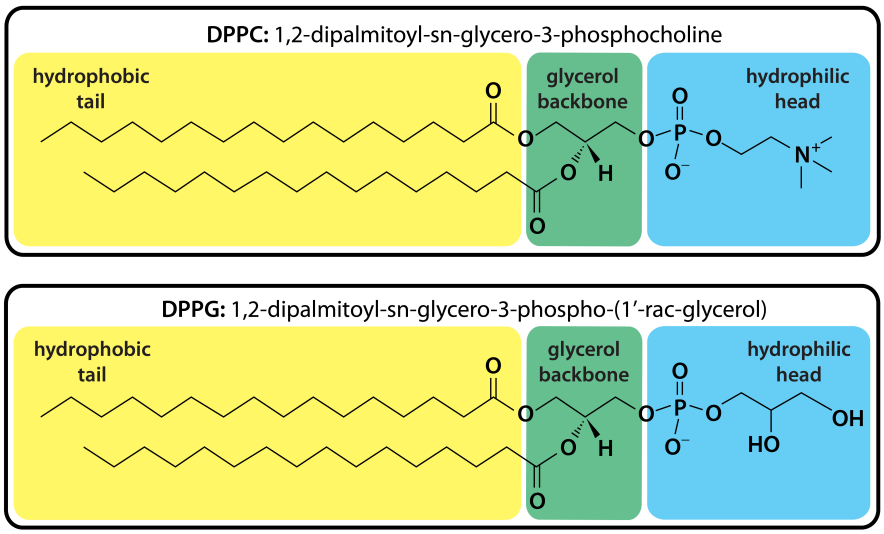

Figure 2.1.: Structure of lipids mainly used in this work. At neutral pH, DPPC remains neutrally charged with a resulting dipole moment, while DPPG is negatively charged. Since neuronal membranes bare 10-20% negatively charged lipids [27], the mainly used lipid composition was DPPC:DPPG (9:1)

hydrogen bonds i.e. via the phosphoric acid and moreover the ampholytic character of this acid allows the lipid to change its net charge accoringly to the bulk pH. The pK value of the whole lipid can also be altered by additional molecules attached to the headgroup as choline in the case of *1,2-dipalmitoyl-sn-glycero-3-phosphocholine* (abbreviated DPPC, compare upper figure in 2.1) or the ionic background [29].

2.2. Self-aggregation and structure of lipid membranes

The amphiphilic character of lipids and the accordingly low solubility in water favors agglomerations in order to avoid contact of the hydrophobic tails with bulk water. Depending on the geometry and concentration of the lipids, micells or vesicles are formed to shield the hydrocarbon chains from water [30]. Also more complex structures as sponge or cubic phases can be formed at higher concentrations and are thoroughly described in [27].

Vesicles are sphere like conglomerates, composed of lipid bilayers, in which the hydrocarbon chains are pointing towards each other. In the simplest case, only one bilayer comprises the membrane, resembling the situation of a cell wall, where different types of lipids in one lamellar sheat are acting as a plattform for embedded proteins. This model of a cell membrane is called the *fluid mosaic model* [31], which

was later improved according to the idea of hydrophobic matching. This refinement is referred to as the *mattress model*, where lipids and proteins with similar length of hydrophobic sites optimize their free energy through the formation of clusters within the membrane [32]. Furthermore, vesicles are composed of two lightly coupled monolayers, which form when the vesicles are approaching a water-air interface or the lipids are directly spread onto the water surface.

The arrangements of lipid structures and thus their macroscopic properties depend among others on the geometry of the lipids themselves [30]. While at lower temperatures the lipids display predominantly all-*trans* configuration and the hydrocarbon chain is mostly oriented in a straight line, at higher temperatures also the *gauche*$^+$ and *gauche*$^-$ states are equally populated causing the lipids to access a larger average area per molecule [27]. During the *main transition* of the lipid

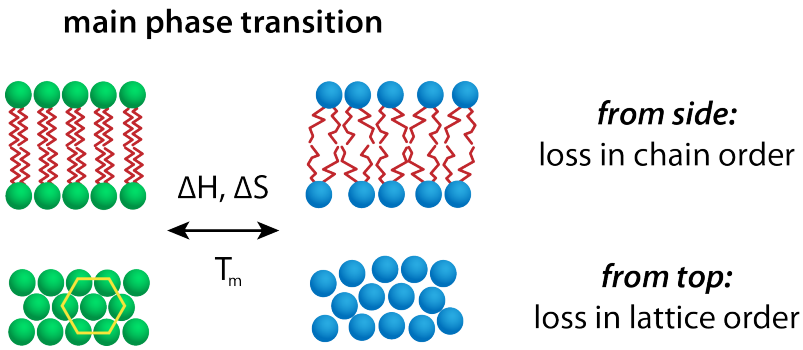

Figure 2.2.: Schematic drawing of the main phase transition (first order) from the solid-ordered to the liquid-disordered phase at the melting temperture T_m. The hexagonal lipid structure of the solid-ordered state (indicated by the yellow hexagon) is lost upon melting, causing an increase in enthalpy H and entropy S (figure adapted from [27]).

membrane the above described order of the carbon chaines is altered cooperatively. Lipid membranes therefore reveal at least two different phases (see figure 2.2)

- **Solid-ordered** phase ($L_{\beta'}$) or often called *gel phase*. Hydrocarbon chains are mostly oriented in the all-*trans* configuration, allowing the formation of a two-dimensional triangular lattice. Therefore, the membrane is rather rigid and unpermeable.

- **Liquid-disordered** phase ($L_{\alpha'}$) or often called *fluid phase*. Lipid chains are mainly arranged in the *gauche*$^{+/-}$ states. Thus, no two-dimensional lattice order can be observed, which causes rather flexible and permeable lipid structures.

Further lipid phases are possible that involve e.g. bending of the membrane and are described in [27]. The transition can be triggered by changes in all thermodynamic

variables influencing the system as e.g. temperature T, lateral pressure π, area A and ionic environment (surface charge density σ). Monolayers display a comparable diversity of morphologies, which are explained more thoroughly in section 2.5.2

2.3. Thermodynamics of lipid structures

> "A theory is the more impressive the greater the simplicity of its premises is, the more different kinds of things it relates, and more extended is its areas of applicability. Therefore, the deep impression, which classical thermodynamics made upon me. It is the only physical theory of universal content concerning which I am convinced that, within the framework of applicability of its concepts, it will never be overthrown." *Albert Einstein* [33].

The macroscopic approach of thermodynamics is particularly designed to describe the behavior of ensembles of many molecules, as lipid membranes are. Thus, the different structures of lipid membranes and the transitions between them can also be described from a thermodynamical point of view. This perspective has the advantage that one can obtain predictions for the system without providing a detailed molecular-mechanical theory. This section will therefore give a short introduction to the thermodynamics of lipid membranes. A more thorough description can be found in [27].

2.3.1. Introduction to thermodynamics

For the description of lipid membranes, the three-dimensional thermodynamic variables pressure p and V need to be reduced to their two-dimensional pendants of surface pressure π and area A. Applied to the principle of energy conservation, yields the first law of thermodynamics in two dimensions:

$$\textbf{1. law of thermodynamics: } \mathrm{d}E = \mathrm{d}Q + \mathrm{d}W = T\mathrm{d}S - \pi\mathrm{d}A\,(+\psi\mathrm{d}q) \tag{2.2}$$

The internal energy $E(T, S, \pi, A)$ is here a function of entropy S, temperature T, surface pressure π and the membrane area A. The additional term identifies the charging of the membrane with charges q, when a surface potential has to be considered. Each state of the system is determined by a set of thermodynamic variables. The difference $\mathrm{d}E$ between two states relies only on the start and end point, not on the particular path chosen in the phase space. In mathematical terms this can be expressed by

$$\oint dZ = 0 \tag{2.3}$$

A function Z obeying equation 2.3 is called a *function of state*. Typical examples are the entropy S, the internal energy E, but also the Helmholtz free energy F, the free enthalpy H and the Gibbs free energy G as written in [6, 27]:

$$\textbf{Helmholtz free energy: } \mathrm{d}F = -S\,\mathrm{d}T - \pi \mathrm{d}A\,(+\psi \mathrm{d}q) \tag{2.4}$$

$$\textbf{Free enthalpy: } \mathrm{d}H = T\mathrm{d}S - A\mathrm{d}\pi\,(+\psi \mathrm{d}q) \tag{2.5}$$

$$\textbf{Gibbs free energy: } \mathrm{d}G = -S\,\mathrm{d}T - A\mathrm{d}\pi\,(+\psi \mathrm{d}q) \tag{2.6}$$

Experimental access is gained through the susceptibilites of the measured system, which can be written as derivatives of the thermodynamic potentials with respect to intrinsic and extrinsic variables. In this thesis, the isothermal compressibility κ_T is mainly used, but also the isobaric heat capacity c_p and the isobaric thermal expansion coefficient α_π are applied:

$$\textbf{Isothermal compressibility: } \kappa_T = \frac{1}{E_T} = -\frac{1}{A}\left(\frac{\partial^2 G}{\partial \pi^2}\right)_T = -\frac{1}{A}\left(\frac{\partial A}{\partial \pi}\right)_T \tag{2.7}$$

$$\textbf{Isobaric heat capacity: } c_p = \left(\frac{\partial Q}{\partial T}\right) = \left(\frac{\partial H}{\partial T}\right)_p = T\left(\frac{\partial S}{\partial T}\right)_P \tag{2.8}$$

$$\textbf{Isobaric thermal expansion coefficient: } \alpha_\pi = \frac{1}{A}\left(\frac{\partial A}{\partial T}\right)_\pi \tag{2.9}$$

E_T in equation 2.7 represents the elasticity; the inverse of the compressibility. In equation 2.8, the three-dimensional pressure is applied. For acoustic phenomena, the adiabatic compressiblity κ_S is important, which can be expressed through κ_T, c_p and the isobaric thermal expansion coefficient α_π [6]

$$\kappa_S = -\frac{1}{A}\left(\frac{\partial A}{\partial \pi}\right)_S = \kappa_T - \frac{TA}{c_p}\alpha_\pi \tag{2.10}$$

A peculiarity of the first order phase transition is the latent heat released or consumed while the system is changing its state. This becomes obvious in the example of a heated mixture of water and ice, where a constant temperature is observed until all ice is molten. The energy invested to change the state from ice to water without increasing the temperature, gives an addtional contribution to the heat capacity at the phase transition temperature. In an ideal system, this contribution yields a delta function. This so-called *excess* heat capacity Δc_π can be seperated from the regular heat capacity of the system, which originates from intramolecular degrees of freedom [27]

$$c_\pi = c_{\pi,0} + \Delta c_\pi = \left(\frac{\partial H_0}{\partial T}\right)_\pi + \left(\frac{\partial\,(\Delta H)}{\partial T}\right)_\pi \tag{2.11}$$

The excess heat capacity is the dominating contribution during the phase transition, so that without the loss of generallity it can be stated $c_\pi \approx \Delta c_\pi$. In the same manner, the excess compressibility $\Delta\kappa_T$, the excess thermal expansion coefficient $\Delta\alpha_\pi$ and the excess electrical capacity ΔC_T can be defined. For lipid membranes it can furthermore be shown that these excess susceptibilities are coupled and directly proportional [34]:

$$\Delta c_\pi \propto \Delta\kappa_T \propto \Delta\alpha_\pi \propto \Delta C_T \tag{2.12}$$

This coupling indicates that whenever one property is changing during the phase transition, the others do as well.

2.3.2. Fluctuation-susceptibility relation

The second law of thermodynamics in addition, is the consequence of the entropy being a function of state:

$$\textbf{2. law of thermodynamics: } \oint \mathrm{d}S = \oint \frac{\mathrm{d}Q}{T} = 0 \tag{2.13}$$

Equation 2.13 indicates that reversible processes are isotropic and no net heat is released. This interpretation of the second law of thermodynamics allows the Taylor expansion of the entropy potential in proximity of the thermodynamic equilibrium:

$$S = \oint dS \approx S_0 + \sum_i \left(\frac{\partial S}{\partial n_i}\right)(\delta n_i) + \sum_{i,j} \frac{1}{2}\left(\frac{\partial^2 S}{\partial n_i \partial n_j}\right)\left(\delta n_i \delta n_j\right) \tag{2.14}$$

Furthermore, the entropy can also be interpreted statistically, as the probability P of a microstate to occur [27]:

$$\textbf{Boltzmann's principle: } S = -k_\mathrm{B} \ln P \tag{2.15}$$

Einstein's approach of *reversing* equation 2.15 allows to start from the macroscopic (phenomenological) behavior instead of starting from an, in most cases incomplete, microscopic or molecular model [35–38]. Additonally combined with the Taylor expanded entropy potential, yields (for simplicity in just one variable):

$$P(x) = \exp\left[\frac{S}{k_\mathrm{B}}\right] \approx \exp\left[\frac{1}{k_\mathrm{B}}\left(S_0 - \frac{\beta}{2}x^2\right)\right] = C_0 \exp\left[-\frac{\beta}{2k_\mathrm{B}}x^2\right] \tag{2.16}$$

$$\beta = -\frac{\partial^2 S}{\partial n^2} \;;\; \frac{\partial^2 S}{\partial n^2} \geq 0 \tag{2.17}$$

Assumption of proximity to the thermodynamic equilibrium allows to omit the first derivative in equation 2.14. Moreover, equation 2.16 is of the same structure as a

Gaussian probability distribution, in which the standard deviation represents the thermodynamic fluctuations in x:

$$\left\langle x^2 \right\rangle = k_\mathrm{B} \left(-\frac{\partial^2 S}{\partial x^2} \right)^{-1} \tag{2.18}$$

Here, the second derivative of the entropy potential with respect to a certain thermodynamic variable is connected to the fluctuations in this variable and thus to a measurable property. This approach has been applied to conductivity fluctuations [39, 40] and relaxation phenomena [41] in lipid bilayers as well as to lipid monolayers more recently [34].
Applied to the isothermal compression of a lipid monolayer (here: $\mathrm{d}E = 0$), the first law of thermodynamics (equation 2.2) yields:

$$\mathrm{d}E = T\mathrm{d}S - \pi \mathrm{d}A = 0 \quad \Rightarrow \quad \left.\frac{\partial S}{\partial A}\right|_T = \frac{\Pi}{T} \quad \Rightarrow \quad \left.\frac{\partial^2 S}{\partial A^2}\right|_T = \frac{1}{T}\frac{\partial \Pi}{\partial A} \tag{2.19}$$

Equation 2.19 can be rewritten using the definition of the isothermal compressibility κ_T (equation 2.7):

$$\frac{1}{A}\left(T\frac{\partial^2 S}{\partial A^2} \right)^{-1} = \frac{1}{A}\frac{\partial A}{\partial \Pi} = -\kappa_T \tag{2.20}$$

By combining 2.18 and 2.20, one arrives at:

$$\langle (\delta A)^2 \rangle = k_\mathrm{B} \left(-\frac{\partial^2 S}{\partial A^2} \right)^{-1} = k_\mathrm{B} \cdot T \cdot A \cdot \kappa_T \tag{2.21}$$

In other words, area fluctuations are directly correlated to the isothermal compressiblity of a lipid monolayer κ_T.

2.4. Electrostatics of charged interfaces

A solid law of electrostatics is that charges of the same kind are repelling each other while opposite charges exerting mutual attractive forces. As any charged object, a membrane immersed in an electrolyte attracts a cloud of oppositely charged counterions, for which the distribution is a result of the competition between electrostatic interaction and thermal movement [42, 43]. The resulting diffuse layer or *Gouy-Chapman layer* of ions shields the electric field produced from the surface charges, influencing the membrane properties as well as its interaction with the environment [42]. For phospholipids, the surface charge normally originates from protons, dissociating from the polar head group according to the bulk water pH or arises from ions (e.g. Ca^{2+}) binding to the membrane [42].

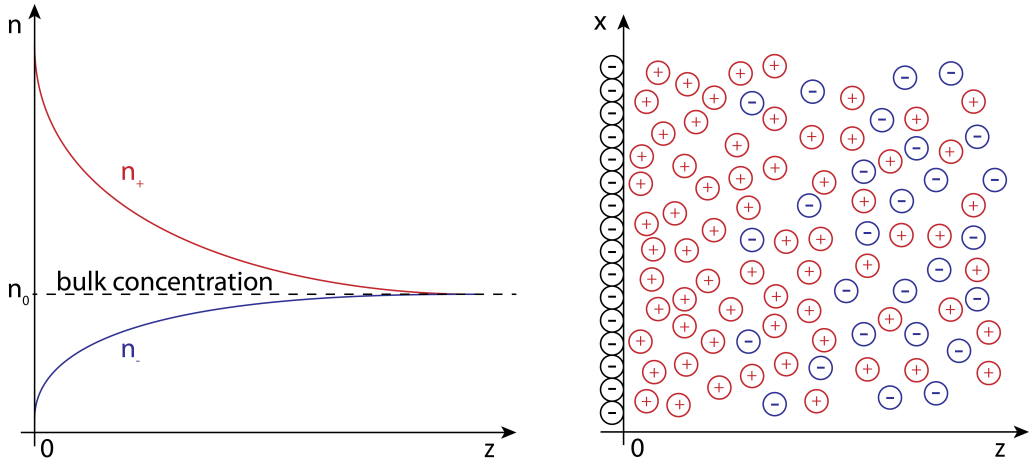

Figure 2.3.: Left: Ion distribution in proximity to a negatively charged surface, located at $z = 0$. Concentration of positively charged ions is strongly augmented at the interface, which is screening the electric potential of the charges fixed on the surface. This depicts the situation described by Poisson-Boltzmann equation 2.22. **Right:** Schematic drawing of the ion distribution in an electrolyte solution.

The distribution of ions near the surface is described by the Poisson Boltzmann equation (derived in section A.1):

$$\nabla^2\psi\left(\vec{r}\right) = -\frac{4\pi e}{\epsilon_W}\left[z_+ n_+ \exp\left(\frac{-ez_+\psi\left(\vec{r}\right)}{kT}\right) + z_- n_- \exp\left(\frac{-ez_-\psi\left(\vec{r}\right)}{kT}\right)\right] \tag{2.22}$$

Here, ϵ_W is the dielectric constant of water and k_B the Boltzmann constant. The elementary charge is represented by e, while $z_{+/-}$ and $n_{+/-}$ symbolize the valency and the bulk concentration of dissolved ions, respectively. For small surface potentials ($\psi \leq 25\,\mathrm{mV}$), equation 2.22 can be linearized and analytically solved, yielding the screening constant for a symmetric, monovalent electrolyte (NaCl case) [42, 44, 45]:

$$\lambda_D = \left(\frac{8\pi e^2 n_0}{\epsilon_W k_B T}\right)^{-1/2} \propto n_0^{-1/2} \tag{2.23}$$

λ_D is called the *Debye-Hückel screening length* and as can be seen in equation 2.23, a increasing salt concentration "compresses" the diffuse layer or accumulates the counter ions closer at the surface [44]. For a symmetric, monovalent electrolyte of $100\,\mu$mol concentration at room temperature the screening length is about 300 Å [44].

This situation becomes mathematically more challenging, when instead of a monovalent ion solution an electrolyte is considered, which is consisting of several salts of different valency. Here, every ion type contributes to the Poisson Boltzmann

equation with its ionic strength I, which is a product of the ion's valency z_i and concentration n_i. For the ionic strength of the entire electrolyte, one can thus write:

$$I = \frac{1}{2} \sum_{i=1}^{n} c_i z_i^2 \tag{2.24}$$

Furthermore it has been shown that in multivalent solutions, the highest valencies are attracted the most by the membrane, according to Coulomb's law. As a consequence, these highly valent ions populate the layer closest to the membrane, which is called a *Stern-layer*, screening the membrane potential and suppressing the interaction of the other ions in solution with the membrane. The interaction is described to be so intense that in the case of two- or threefoldly charged ions, a binding constant to the membrane can be definded [42]. This behavior has been simulated for solutions of Ca^{2+}, K^+ and Na^+ ions in the vicinity of an anionic lipid bilayer [46]. But also the internal membrane properties are altered as a consequence of the sur-

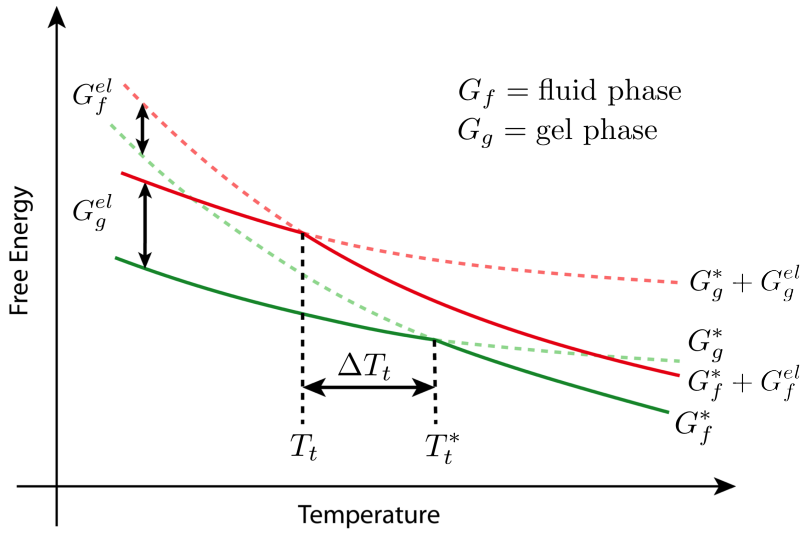

Figure 2.4.: Dependence of free energy on temperature for neutral and charged lipid membranes at the transition from the solid-ordered (g) to the liquid-disordered (f) state. Phase transitions occur at intersections, since the energetically lower and thereby more stable state is always occupied. Addition of surface charges adds an unsymmetric contribution to the free energies of the ordered and disordered state, thus shifting the transition temperature to lower values (figure adapted from [44]).

face charge density and the screening of the resulting surface potential due to the ionic environment. Among others, the elastic properties [42], but also the phase transition of the lipids are affected [44, 45]. For the latter case, the shift in the conditions required to induce a phase transition, according to screened surface charges, can be derived by assuming that the molar free energies of the two thermodynamic

states are composed of additive non-electrostatic and electrostatic terms [44]. For the phase transition temperture of a charged lipid membranes it can thus be found [44, 45]:

$$T_t = T_t^* + \frac{\Delta G^{el}}{\Delta S^*} = T_t^* + \Delta T_t \tag{2.25}$$

This equation is graphically demonstrated in 2.4. Here it can be seen, that additional surface charges are shifting the phase transition towards higher temperatures, because of the additional contribution to the free energy. When immersed in an ionic background, as described above, the surface potential is screened, consequently diminishing the effect of the surface charges. Thus, at high ion concentrations and low surface potentials, the membrane behaves as its uncharged pendant.

2.5. Investigations of monolayers with the film balance technique

The ability of surface active materials to lower the surface tension of the bulk phase, in which it is dissolved, was described by Gibbs in 1878. Irving Langmuir further employed this principle in the construction of a film balance, which enables the determination of the surface tension σ of a fluid interface and moreover the changes $\Delta\sigma$ occuring through the adsorption of surface active films [47]. The Langmuir trough is the central tool used in this thesis and therefore the basics of this measurement technique will here be introduced [28].

2.5.1. Working principle of the Langmuir film balance

The *surface film balance* or *Langmuir trough* consists of a shallow trough manufactured from hydrophobic material to prevent water spilling (here: PTFE[1]) and a force sensor used for the surface tension measurement. The trough is slightly overfilled with ultrapure water ($18\ \frac{M\Omega}{cm}$) or a defined salt solution and equipped with a barrier, lying across the trough, dividing the surface and is used to restrict the area of a monolayer spread on the interface. A schematic drawing of the film balance applied in this thesis is presented in figure 2.5. Lipids are delivered to the clean surface by a measured volume V of chloroform solution of known concentration c. This allows to calculate the average area per lipid $\bar{A}$ by deviding the absolute area A, defined by the position of the barrier, divided by the number of lipids applied to the surface:

$$\bar{A} = \frac{A \cdot M}{N_A \cdot c \cdot V} \tag{2.26}$$

[1]Polytetrafluoroethylene

The surface tension σ is determined by the vertical pull on a wetted Wilhelmy plate hanging through the surface. The use of filter paper as probe enables perfect wetting and allows to neglect buoyancy effects. Thus, the measured force F simply scales by the length l of the perimeter of the wetted plate:

$$\sigma = \frac{F}{l} \tag{2.27}$$

The surface tension of the air-water interface at room temperature is about $\sigma_0 = 72\,\mathrm{mN/m}$ [28], which decreases during the compression of the monlayer accordingly to the respective rise in lipid surface density. The surface pressure π of the monolayer is thus defined as

$$\pi = \sigma_0 - \sigma \tag{2.28}$$

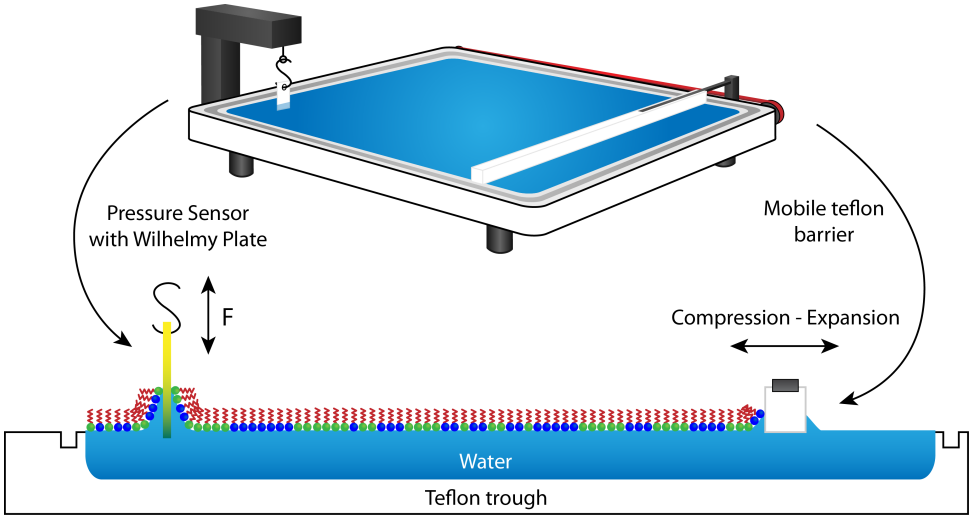

Figure 2.5.: Drawing of the film balance arrangement. Lipids are spread from a chlorofrom solution onto the clean water surface. The mobile barrier is used to confine the accessible area, defining an average area per lipid. Through compression or expansion, π-A-isotherms of the lipids under investigation can be obtained. The Wilhelmy plate allows the extraction of the membrane pressure π by measuring the reduction of the pure water surface tension σ_0. Teflon is used as trough and barrier material according to its dirt-repelling properties and its inertness, minimizing possible contaminations (bottom figure adapted from [6]).

As the overall amount of lipids used for one monolayer is tiny ($\approx 5{\cdot}10^{16} \approx 80\,\mathrm{nmol}$), even smallest amounts of impurities can drastically alter the result of an experiment. This is another reason, why PTFE is used as trough material. The film balance employed in this thesis (*NIMA, type 611D, Coventry, England*) was equipped with surface tension sensors (*NIMA, type PS4, Coventry, England*), a temperature

probe (*NIMA, type temperature sensor, Coventry, England*) and a dipper mechanism (*NIMA, type D1L, Coventry, England*), normally used for Langmuir Blodgett transitions to create solid supported lipid membranes [48]. The different arrangements for each experiment are described in detail in the respective chapters.

The temperture during one experiment is kept constant using a heat bath connected to the film balance, allowing to measure a π-A-isotherm during a compression-expansion cycle. The barrier is moved at slowest possible speed to allow thermodynamic equillibration. This value depends on the physical and geometric properties of the used film balance. All isotherms presented in this thesis are compressed with roughly $2,5\,\frac{\text{Å}}{\text{min}}$. Characteristics of the resulting phospholipid isotherms are the emphasis of section 2.5.2.

2.5.2. Polymorphism of phospholipid monolayers

In contrast to the compression of a harmonic spring, a lipid monolayer reacts highly non-linear when compressed. This non-linear behavior results from the polymorphism of the compressed lipids, which are able to display multiple phases and phase transitions [49]. A schematic example of a π-A-isotherm is given in figure 2.6.

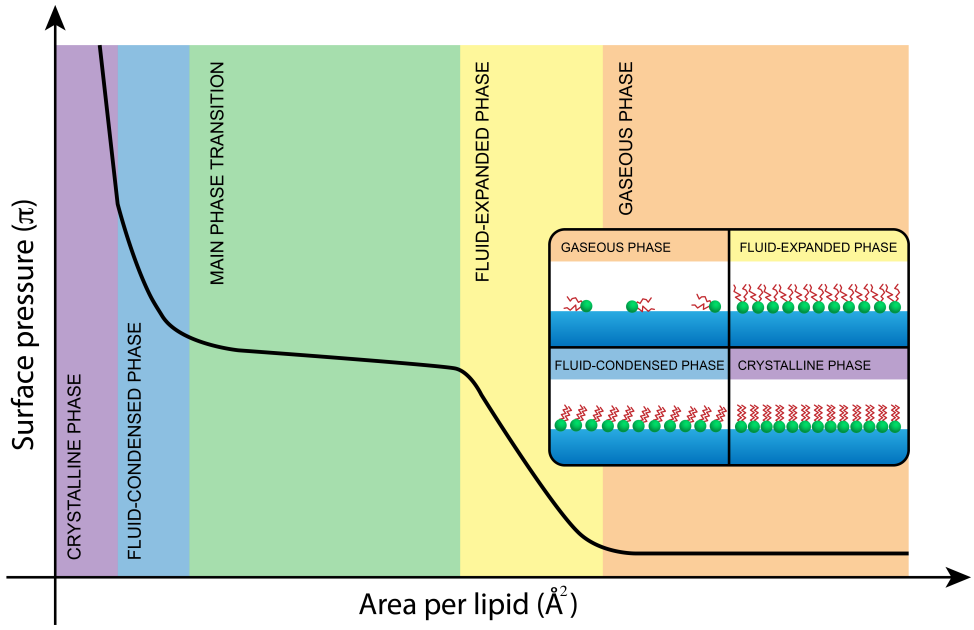

Figure 2.6.: Schematic drawing of a π-A-isotherm depicting the polymorphism of a phospholipid monolayer. Lipid phases are color-coded, which is maintained within the *inset* of the figure. Here, the molecular characteristics are visualized for each individual phases, indicating an increase in order upon increasing lateral pressure.

- **Gaseous phase:** *(orange part in figure 2.6)* This phase occurs at very low lipid density and membrane pressures. According to the large areas per molecule, the lipids are widely seperated and interaction forces can be neglected. Thus, the lipids act as a two-dimensional ideal gas: $\pi A = NkT$. Normally, this phase is not resolved, because of building vibrations or other experimental flaws.

- **Fluid-expanded phase:** *(yellow part in figure 2.6)* This phase is entered after a first order phase transition from the gaseous phase. The lipids form a complete monolayer and interact with each other, which increases the membrane tension. The hydrophobic tails remain mostly in the *gauche*-conformation or disordered state. In contrast to the gaseous phase a increased viscosity can be observed. This phase is the counterpart to the bilayers L_α phase from section 2.2.

- **Phase transition:** *(green part in figure 2.6)* At the main transition, the density and symmetry of the lateral molecular packing will change simultaneously and cooperatively [49]. As indicated in figure 2.6, a finite slope in the transition region remains, what is in contrast to three-dimensional systems. This was first attributed to impurities in the membrane, but couldn't be improved beyond a certain degree. The finite slope thus appears to be a result of the limited size of the cooperatively transforming units [49] and seems to be an intrinsic property of the monolayer.

- **Fluid-condensed phase:** *(blue part in figure 2.6)* The hydrocarbon chains of the lipids are mostly compressed to the *trans*-conformation, increasing the lattice order and enabling the formation of the hexagonal structure (compare figure 2.2). All lipids remain slightly tilted with respect normal vector of the membrane. In this phase, the viscosity is highly increased as is the resistance towards compression. This phase is the counterpart to the bilayers L_β phase from section 2.2.

- **Crystalline phase:** *(purple part in figure 2.6)* After a phase transition of second order, the hexagonal structure is completely developed, resulting in a steep increase of the isotherm. The hydrocarbon chains are all in the *trans*-conformation without any tilt. The accordingly low compressibility and highly ordered structure are the reasons why this phase is often referred to as the solid phase.

- **Monolayer collapse:** *(not shown in figure 2.6)* When compressed beyond a certain membrane pressure, parts of the monolayer are forced out of the surface into the aqueous subphase and consequently forms three-dimensional

structures as multilayers or vesicles. This pressure depends on the lipid type, but also on the subphase composition.

The behavior, indicated by the exemplary isotherm in figure 2.6, does depend strongly on the temperature of the system, as can be seen in the temperature scan of DPPC monolayer presented in figure 2.7. While for the isotherm at 3°C the fluid-expanded phase cannot be observed, the fluid condensed phase vanishes for temperatures beyond the critical point in the phase diagram (indicated with the isotherm at 42°C). This behavior can be explained accordingly to the three-dimensional case of phase diagrams. The coexistence region can only be observed in a certain range of temperatures, while the shift of the phase transition point can be described by the Clausius-Clapeyron equation, here for the two dimensional case [25, 34, 49]:

$$\frac{\mathrm{d}\pi_M}{\mathrm{T}} = \frac{\Delta S}{\Delta A} \tag{2.29}$$

ΔS represents the entropy difference between the fluid-expanded and fluid-condensed phase, while ΔA corresponds to the change in area per lipid, when compressed through the phase transition. Analyzing this behavior thoroughly, one finds a linear correlation between phase transion pressure and system temperature [34]. But also other thermodynamic variables, as the surface charge density σ have impact on the phase transition behavior of phospholipids, what will be the emphasis of the next chapter.

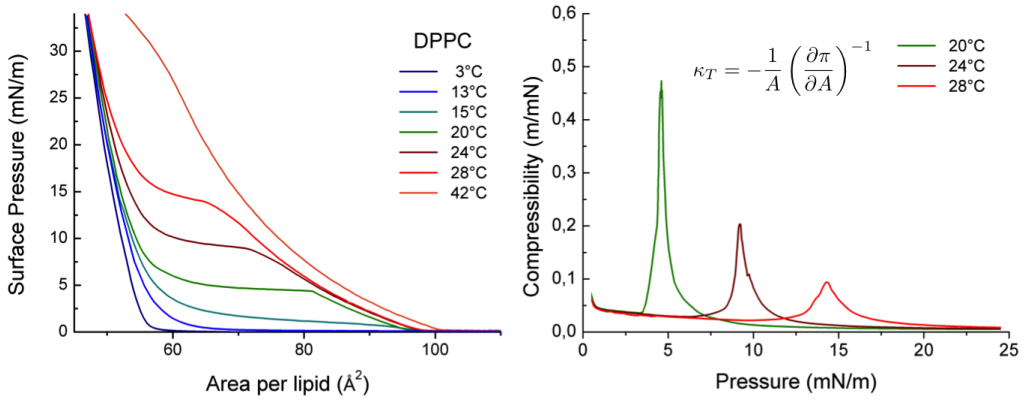

Figure 2.7.: Left: Set of DPPC monolayer isotherms at different temperature (3°C, 13°C, 15°C, 20°C, 24°C, 28°C, 42°C). The phase transition plateau is shifting towards higher pressures, while the temperature is increased. For 3°C and 42°C, the pure fluid-condensed phase and fluid-expanded phase respectively can be observed **Right:** Compressibility profiles calculated from isotherms displayed in the left part of this figure (20°C, 24°C, 28°C) by means of equation 2.7. Maximum in compressibility corresponds to the plateau region in the isotherm, thus indicating the monolayer phase transition (figures replotted from [6]).

2.5.3. Fluorescence measurements of monolayers

The transition between lipid phases can be studied more thoroughly with the incorporation of fluorescent dye molecules into the lipid membrane and the consecutive measurement of the dye distribution. Contrast in the images can be obtained through the utilization of different dye solubilities, fluorescence quantum yields or molecular densities of coexisting phases. Figure 2.8 represents a picture of a fluorescently labeled DPPC monolayer, where the dye distribution is governed by the solubility within the different phases. Since the dye has a tendency to dissolve within the fluid expanded phase, the dark spots observed in figure 2.8 are referred to as the fluid-condensed phase. The observation of a coexistence region in the lipid monolayer implies the first order of the phase transition. Upon compression of the monolayer, a certain number of domains are formed at a distinct pressure π_c. Further compression leaves the number of domains unaltered, but increases the total area covered by the fluid-condensed phase. For the domain shapes it has been found that the interplay between the dipolar repulsion of lipids and the line tension of domains is decisive [50]. Thus, the shape can be altered by screening the dipoles with salts added to the water or cholesterol, changing the line tension [51]. Since lipids are chiral molecules, the hand of rotation of the domains is affected by the chirality of the lipids. Mixtures of both left and right handed lipids don't show macroscopically chiral domains.

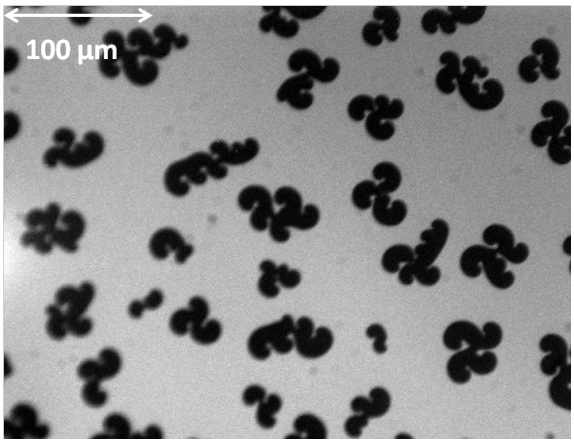

Figure 2.8.: DPPC monolayer fluorescently labeled with NBD-HC (0,5 mol%) at 24°C. Contrast is obtained by differing dye solubilities in the liquid expanded and condensed phase. In the plateau region of the isotherm, chiral domains can be observed, indicating a coexistence region and thereby the first order of the phase transition (picture provided by Shamit Shrivastava)

Chapter 3: Properties of Lipid Monolayer Waves

Distortion of a planar water surface normally results in a transversal wave motion. According to the wave length λ, different forces dominate the behavior of the wave. Long wave lengths ($\lambda \geq 2\,\mathrm{cm}$) cause gravitational waves, where the weight of the deflected water forces the surface back to its equilibrium position, while for short $\lambda \leq 2\,\mathrm{cm}$, the surface tension is the main contribution [52]. The presence of a surface active film tends to lower the surface tension and thus decreases its influence on the wave. Moreover, additional compression and expansion of the film due to the wave motion results in a localized decrease and increase of surface tension [28]. This gradient of interfacial forces induces flow within the subjacent bulk water layer, which is calming the surface according to the augmented viscous forces exerted on the surface. The resulting energy dissipation additionally attenuates the capillary water wave [53].

In this thesis, the aqueous interfaces are covered by a monomolecular film of lipids, so that capillary water waves are strongly impeded. From another point of view, the measureable viscous [54, 55] and elastic [49, 56] properties of the film itself, implies the understanding of the lipid monolayer as a visco-elastic fluid, floating on water. The elastic properties can be directly observed by compression and expansion isotherms of lipid monolayers (see chapter 2.5.2). As for its three-dimensional pendant, the membrane's elasticity implies the capability of conducting an acoustic, longitudinal wave mode. These acoustic, interfacial waves were investigated theoretically and experimentally. There, different excitation methods were employed as e.g. an ultra-thin platinum wire [57, 58], an oscillating Teflon barrier [19, 20, 59] or light-triggered conformational changes of polymers [60]. In all cases, a local change in average area per molecule provokes a pulse, spreading over the surface as a measureable surface density pulse. This chapter will give an introduction to theory and experiments done on longitudinal lipid monolayer waves and mainly focus on the solvent excitation described in [23, 24], which is further applied in this thesis. It is summarized in [6], which also is used as foundation for this chapter.

3.1. Theory of Monolayer Waves

Acoustic waves are a type of longitudinal waves that propagate by means of adiabatic compression or expansion of the conducting media. Thus, the elastic properties of this medium intrinsically control the properties of the wave, like its velocity. In this section, a theory for two-dimensional, acoustic monolayer waves is developed, which is based on the hydrodynamic theory of sound of a three-dimensional compressible fluid [61]

3.1.1. Theory of acoustic waves in lipid monolayers

Density oscillations of small amplitude in an infinitely thin layer of a compressible fluid are considered two-dimensional, acoustic waves. Variations in the monolayer area density $\rho(x, y, t)$ and membrane pressure $\pi(x, y, t)$ due to the passage of a wave are written in the form:

$$\pi = \pi_0 + \pi' \qquad \rho = \rho_0 + \rho' \tag{3.1}$$

π_0 and ρ_0 are the equilibrium density and pressure of the monolayer, while π' and ρ' are the respective variations resulting from the wave. The velocity of single particles in the membrane is $\vec{v}(x, y, t) = v_x(x, y, t), v_y(x, y, t)$, so that the continuity equation reads:

$$\frac{\partial \rho}{\partial t} + \operatorname{div}(\rho \vec{v}) = 0 \tag{3.2}$$

In fluid dynamics, Newton's second law of motion is written in its differential form, yielding the Euler equation:

$$\frac{\partial \vec{v}}{\partial t} + (\vec{v}\nabla)\,\vec{v} = -\frac{1}{\rho}\nabla\pi \tag{3.3}$$

Without loss of generality, it is sufficient to consider simply one direction of propagation (along the x-axis), so that in the following only functions like $\pi(x, t)$, $\rho(x, t)$ and $\vec{v} = (v_{mx}(x, t), 0)$ need to be considered. The index m specifies the movement of the monolayer molecules. The small amplitude of the membrane waves additionally allows to omit terms of second order ($\vec{v}\nabla\vec{v}$, $\vec{v}\rho'$, etc.), transforming equation 3.2 and 3.3 into:

$$\textbf{Continuity equation:}\quad \frac{\partial \rho'}{\partial t} = -\rho_0 \frac{\partial v_{mx}}{\partial x} \tag{3.4}$$

$$\textbf{Euler equation:}\quad \rho_0 \frac{\partial v_{mx}}{\partial t} = -\frac{\partial \pi'}{\partial x} \tag{3.5}$$

Equations 3.4 and 3.5 can be applied to the propagation of acoustic waves under the assumption that the particle velocity is small against the wave velocity $\vec{v} \ll c$

and implies thereby that oscillations in density are small as well ($\rho' \ll \rho_0$). Due to the adiabatic nature (index S) we further can find a direct correlation between small changes in membrane pressure and the density oscillations $\rho' = \left(\frac{\partial\pi_0}{\partial\rho_0}\right)_S^{-1}\pi'$. Moreover it is assumed, that the correlation factor $\left(\frac{\partial\pi_0}{\partial\rho_0}\right)_S^{-1}$ is amplitude and frequency independent. Combined with $\rho_0 = \frac{m}{A_0}$, the correlation factor can be rewritten with its average area A_0 dependency:

$$\begin{aligned}\left(\frac{\partial\pi_0}{\partial\rho_0}\right)_S^{-1} &= m\left(\frac{\partial\frac{1}{A_0}}{\partial\pi_0}\right)_S = -\frac{m}{A_0^2}\left(\frac{\partial A_0}{\partial\pi_0}\right)_S \\ \Leftrightarrow \rho' &= -\frac{m}{A_0^2}\left(\frac{\partial A_0}{\partial\pi_0}\right)_S\pi' = \rho_0\kappa_S\pi'\end{aligned} \tag{3.6}$$

The definition of the adiabatic compressibility $\kappa_S = -\frac{1}{A_0}\left(\frac{\partial A_0}{\partial\pi_0}\right)_S$ was used in equation 3.6. Furthermore, equation 3.5 can now be transformed with the result of equation 3.6. Subsequent differentiation with respect to x, yields:

$$\begin{aligned}\frac{\partial\pi'}{\partial t} &= -\frac{1}{\kappa_S}\frac{\partial v_{mx}}{\partial x} \\ \overset{\frac{\partial}{\partial x}}{\Longrightarrow} \frac{\partial\pi'}{\partial t\partial x} &= -\frac{1}{\kappa_S}\frac{\partial^2 v_{mx}}{\partial x^2}\end{aligned} \tag{3.7}$$

Agitation of the lipid monolayer causes additional movement of the subjacent water phase, which induces shear flow opposing the motion of the monolayer. This can be explained by the similar picture of two plates moving relative to each other (here the monolayer and bottom of the trough), separated by a viscous medium (here water). The resulting shear flow induced within the medium can be determined through Newton's law of viscosity $\tau = \eta\frac{v}{d}$, where τ is the shear stress and d the distance between the upper and lower plate. The dynamic viscosity η is an intrinsic property of the connecting medium, defining the resistance against shear stress. The coupling of the monolayer to the subjacent water phase is introduced to the Euler equation 3.5 through an additional tension term ξv_{mx}, with the coupling constant ξ.

$$\begin{aligned}\rho_0\frac{\partial v_{mx}}{\partial t} &= -\frac{\partial\pi'}{\partial x} - \xi v_{mx} \\ \Longrightarrow \frac{\partial\pi'}{\partial t\partial x} &= -\rho_0\frac{\partial^2 v_{mx}}{\partial t^2} - \xi\frac{\partial v_{mx}}{\partial t}\end{aligned} \tag{3.8}$$

Combining equation 3.7 and 3.8 yields the wave equation for a viscously coupled monolayer:

$$\frac{\partial^2 v_{mx}}{\partial t^2} + \frac{1}{\rho_0}\xi\frac{\partial v_{mx}}{\partial t} - c_0^2\frac{\partial^2 v_{mx}}{\partial x^2} = 0 \text{ with } c_0 = \sqrt{\frac{1}{\rho_0\kappa_S}} \tag{3.9}$$

Here, c_0 is the velocity of a purely acoustic wave. For $\xi = 0$, equation 3.9 simplifies to an undamped differential wave equation which can be solved by the approach

$v_{mx} = Ae^{i(\omega t - kx)}$. This ansatz can also be applied to the damped case, yielding the dispersion relation, which connects the wave vector k and frequency ω:

$$\begin{aligned} &-\omega^2 + i\omega\xi\frac{1}{\rho_0} + c_0^2 k^2 = 0 \\ \Longrightarrow\ &k^2 = \frac{\omega^2}{c_0^2}\left(1 - \frac{1}{\rho_0}\frac{i\xi}{\omega}\right) \end{aligned} \tag{3.10}$$

The complex part of the wave vector k displays the attenuation of the wave due to the viscous coupling to the water phase and again, $\xi = 0$ represents the undamped case, where the dispersion relation yields $c_0^2 = \frac{\omega^2}{k^2}$. In order to evaluate equation 3.10 completely, the constant ξ needs to be determined.

The considered acoustic wave motion changes the local lipid density and thereby creates patches of decreased and increased surface tension. The emerging, equilibrating Marangoni flow firstly opposes the wave motion, dissipating its energy, and secondly evokes movement of subjacent water layers. This movement of the water sub phase shall be accounted here as the main contribution to ξ and is in general described by the Navier-Stokes-equation:

$$\rho_w\left(\frac{\partial\vec{v}}{\partial t} + (\vec{v}\nabla)\,\vec{v}\right) = -\nabla p + \eta_w\nabla^2\vec{v} \tag{3.11}$$

Here, ρ_w and η_w describes the density and the viscosity of water, respectively. As in the Euler equation above (3.5), we further neglect terms of second order $(\vec{v}\nabla\vec{v})$ and only consider one direction of motion (x-axis). For small amplitudes of the wave, it is additionally sufficient to depict the incompressible case ($\nabla p = 0$). Thus we obtain for the velocity v_{wx} of the subjacent water layers:

$$\frac{\partial v_{wx}}{\partial t} = \frac{\eta_w}{\rho_w}\frac{\partial^2 v_{wx}}{\partial z^2} \tag{3.12}$$

At the monolayer-water interface, the velocities must match due to the no-slip boundary condition $v_{mx} = v_{wx}$. This implies the ansatz $v_{wx} = Ae^{i(\omega t - kx)}e^{mz}$ as solution for equation 3.12, yielding:

$$i\omega = \frac{\eta_w}{\rho_w}m^2 \quad \overset{z\leq 0 \Rightarrow m \geq 0}{\Longrightarrow} \quad m = \sqrt{\frac{i\omega\rho_w}{\eta_w}} = e^{i\frac{\pi}{4}}\sqrt{\frac{\omega\rho_w}{\eta_w}} = \sqrt{\frac{\omega\rho_w}{2\eta_w}} + i\sqrt{\frac{\omega\rho_w}{2\eta_w}} \tag{3.13}$$

The resulting solution m for the motion of the water is a complex number, where the real part determines the viscous penetration depth $\delta = \frac{1}{\Re(m)}$, while the imaginary part describes the oscillatory movement of the water molecules. Thus, the water undergoes viscously coupled movement with respect to the oscillations of the monolayer, whose amplitude decays exponentially with the penetration depth. According

to the no-slip condition, the viscous forces at the film-water interface must be equal so that we can determine the beforehand introduced force term ξv_{mx} with help of equation 3.13:

$$\xi v_{mx} = \eta_w \left[\frac{\partial v_{mx}}{\partial y}\right]_{z_0} = \eta_w m v_{mx} \Rightarrow \xi = \eta_w m = e^{i\frac{\pi}{4}} \sqrt{\omega \rho_w \eta_w} \tag{3.14}$$

Thus, the dispersion relation 3.10 can be reformulated for an acoustic monolayer wave, which is viscously coupled to the subjacent water layers.

$$k^2 = \frac{\omega^2}{c_0^2}\left(1 - \frac{1}{\rho_0} e^{i\frac{3\pi}{4}} \sqrt{\frac{\rho_w \eta_w}{\omega}}\right) \tag{3.15}$$

3.1.2. Discussion of the dispersion relation

The real part of the wave vector k can be used to calculate the propagation velocity $c = \frac{\omega}{\Re(k)}$ of the wave as well as the damping constant from the imaginary part $\beta = -\Im(k)$. Therefore, equation 3.15 needs to be solved explicitly:

$$\begin{aligned}
\Re(k) &= \frac{\omega}{c_0}\frac{1}{2}\sqrt{\sqrt{4\left(1 + \frac{1}{2}\frac{\sqrt{\frac{2\rho_w\eta_w}{\omega}}}{\rho_0}\right)^2 + \frac{2\rho_w\eta_w}{\omega\rho_0^2}} + 2 + \frac{\sqrt{\frac{2\rho_w\eta_w}{\omega}}}{\rho_0}} \\
\Im(k) &= -\frac{\omega}{c_0}\frac{1}{2}\sqrt{\sqrt{4\left(1 + \frac{1}{2}\frac{\sqrt{\frac{2\rho_w\eta_w}{\omega}}}{\rho_0}\right)^2 + \frac{2\rho_w\eta_w}{\omega\rho_0^2}} - 2 - \frac{\sqrt{\frac{2\rho_w\eta_w}{\omega}}}{\rho_0}}
\end{aligned} \tag{3.16}$$

The results of equation 3.16 can be evaluated by plotting the frequency course of both parts of the complex wave vector $\Re(k)$ and $\Im(k)$ (see figure 3.1). For the calculation, the velocity for the purely acoustic wave was assumed to be $c_0 \approx 100\,\frac{\mathrm{m}}{\mathrm{s}}$ [62], the area density of the monolayer $\rho_0 \approx 2 \cdot 10^{-6}\,\frac{\mathrm{kg}}{\mathrm{m}^2}$, the bulk density of water $\rho_w \approx 1000\,\frac{\mathrm{kg}}{\mathrm{m}^3}$ and the dynamic viscosity of water $\eta_w \approx 1 \cdot 10^{-3}\,\mathrm{Pas}$. For better comparability, also the relative attenuation per wave length $(1 - e^{\Im(k)\frac{2\pi}{\Re(k)}})$ is calculated. The wave velocity is increasing almost linearly over a wide frequency range to approximate the pure acoustic wave velocity for frequencies $\geq 10^{12}\,\frac{1}{\mathrm{s}}$. Additionally the relative damping per wave length decreases to almost 10% in the high frequency limit. The velocity range of waves excited within this thesis is indicated by the green area in figure 3.1. Within the expected frequency range, the relative damping is rather high ($\approx 90\%$), so that the amplitude of the wave should be highly attenuated over one wave length ($\approx 1\,\mathrm{m}$). The Fourier transform of the found wave phenomena displayed a frequency spectra around $0.1\,\mathrm{Hz} - 1\,\mathrm{Hz}$. Thus, a low frequency approximation of equation 3.10 will be further discussed.

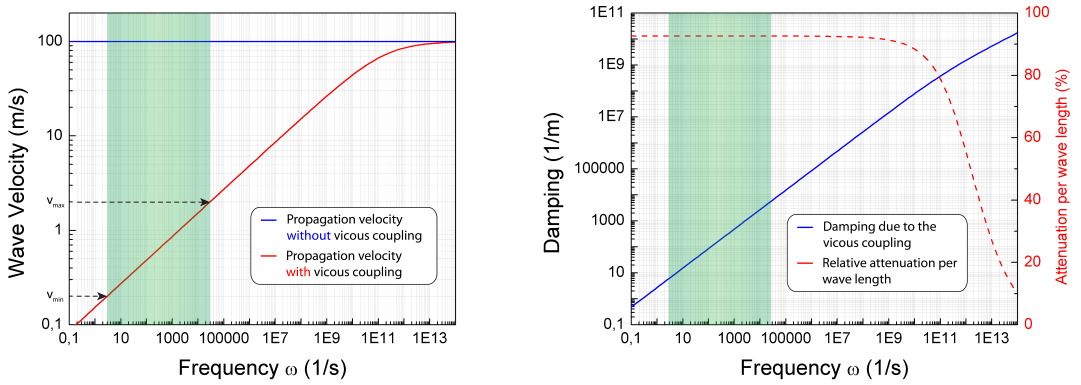

Figure 3.1.: Frequency course of the velocity (**right**) and damping (**left**) of the viscously coupled, acoustic wave as calculated from the dispersion relation displayed in equation 3.16. Values used for calculation are $c_0 \approx 100\,\frac{\mathrm{m}}{\mathrm{s}}$, $\rho_0 \approx 2 \cdot 10^{-6}\,\frac{\mathrm{kg}}{\mathrm{m}^2}$, $\rho_w \approx 1000\,\frac{\mathrm{kg}}{\mathrm{m}^3}$ and $\eta_w \approx 1 \cdot 10^{-3}\,\mathrm{Pas}$. Green areas indicate the frequency range of the investigated wave phenomenon.

3.1.3. Low frequency approximation

The experimental finding of low frequency membrane waves enforces the discussion of a low frequency approximation of equation 3.15. Here we assume that $\frac{\rho_w \eta_w}{\omega} \approx 1\,\frac{\mathrm{kg}}{\mathrm{m}^2}$ and $\rho_0 \approx 2 \cdot 10^{-6}\,\frac{\mathrm{kg}}{\mathrm{m}^2}$ and can thus neglect the first summand in equation 3.15:

$$k^2 = -\frac{1}{c_0^2}\frac{1}{\rho_0} e^{i\frac{3\pi}{4}} \sqrt{\rho_w \eta_w \omega^3} = e^{i\frac{\pi}{4}} \kappa_S \sqrt{\rho_w \eta_w \omega^3} \tag{3.17}$$

The definition of the adiabatic compressibility $\kappa_S = \left(c_0^2 \rho_0\right)^{-\frac{1}{2}}$ is used to simplify. Separating the real and imaginary part of the simplified complex wave number (equation 3.17) yields:

$$\begin{aligned} c &= \frac{\omega}{\Re\,(k)} = \frac{1}{\cos\left(\frac{\pi}{8}\right)} \sqrt{\frac{1}{\kappa_S}} \sqrt{\frac{\omega}{\rho_w \eta_w}} \\ \beta &= -\Im\,(k) = \sin\left(\frac{\pi}{8}\right) \sqrt{\kappa_S \sqrt{\rho_w \eta_w \omega^3}} \end{aligned} \tag{3.18}$$

This represents also the results obtained in [19, 22, 59, 63], where longitudinal capillary waves along an aqueous interface of a lipid monolayer are described. There, the mass of the lipids is neglected, allowing to omit the inertia term $\frac{\partial^2 v_{mx}}{\partial t^2}$ in equation 3.9. The resulting equation is introduced in [19] as boundary condition at the air-water interface.

The results displayed in equation 3.18 are further evaluated and discussed within

this thesis. While the correlation of the wave velocity c with the isothermal compressibility κ_T of the monolayer will be described in the following section 3.4 and can also be found in [6, 23], the wave attenuation factor β will be further discussed in section 8.

3.2. Experimental Arrangements

For the excitation of monolayer waves, a variety of substances can be applied to the air-water interface that are able to provoke a pressure pulse propagating in the lipid membrane. In this section, the experimental setup is introduced, which is employed in [6, 23, 24] and moreover in this thesis to investigate the lipid monolayer waves theoretically described in section 3.1. The excitation mechanism itself is more thoroughly illustrated in section 4.
In order to enable the proper excitation of lipid monolayer waves, a regular film balance (*NIMA, type 611D, Coventry, England*), introduced in section 2.5.1, is used and additionally equipped. A sketch of the setup and procedure is presented in figure 3.2. The substances investigated are applied to the lipid monolayer via a

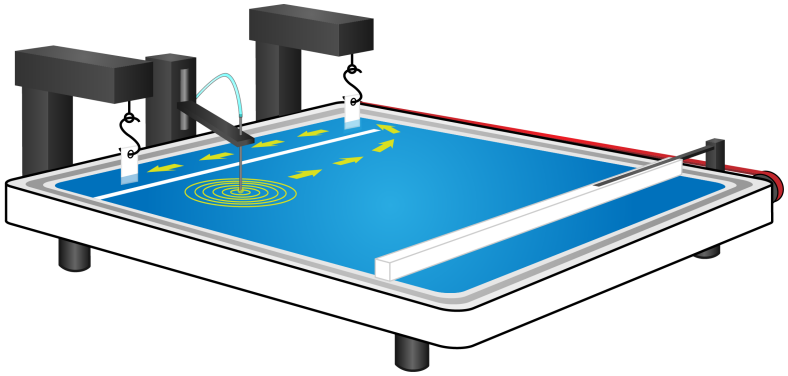

Figure 3.2.: Setup and process for excitation measurements is illustrated. A regular film balance is equipped with an additional pressure sensor to allow the measurement of wave velocities. Exact recording of the pulse's shape is arranged by a high sensor read out *(10000 samples/second, 0,01 mN/m resolution)*. The additional barrier suppresses secondary water waves and creates an exact wave path.

dipper/needle arrangement, which enables best reproducibility of approaching speed and contact angle. The needle itself is connected via a Teflon hose to a micro syringe, minimizing the possibility of interface contamination and improving the accuracy of the amount of substances applied for a singular excitation. An additional Teflon barrier is placed inside the water to divide the trough into an excitation and detection compartment. This represses secondary water waves, stimulated on the excitation site and interfering with the measurement, but in particular defines an accurate wave

path. At the entrance of the detection site, according to the Huygens principle, the arbitrary wave motion is transformed into a point wave. Thus, reproducible wave fronts are established, which are subsequently investigated by means of the Wilhelmy plate method (compare section 2.5.1). This technique allows the direct observation of changes in lateral lipid density in the monolayer. A rapid sensor read out *(10000 samples/second, 0,01 mN/m resolution)* assures the high time resolution needed to elucidate the exact shape of the pulses observed. Due to a second sensor, placed within the channel in a known distance to the first, the propagation dynamics of the pulses can be examined by extracting its arrival times. In order to apply an objective criterion as condition for an arriving wave front, the derivative of the pressure course π' was chosen to exceed a value of $\pi' = 0,04\,\frac{\mathrm{mN}}{\mathrm{ms}}$. The run time $\Delta t = t_1 - t_2$ is then directly translated into the velocity of the wave. The compression barrier in the back part of the trough is used to set the equilibrium membrane pressure π_0, tuning the membranes phase state. Thereby, the propagation properties of excited pressure pulses can be investigated in dependence of the membrane phase state. Studies done on the excitability of lipid membranes by solvents and acids are described in the next section.

3.3. Solvent Excitation of Lipid Monolayer Waves

In order to be able to study a wide variety of substances able to excite a membrane pressure pulse, a defined amount of the pure substance or solution was applied. It was revealed that not only the absolute amplitude, but also the shape of the pressure pulse depends strongly on the properties of the substances used for excitation. Alcohols like methanol and ethanol [23], but also carbonic acids as acetic acid [24] are able to penetrate the lipid core of the membrane and thus provoke a pressure pulse. Due to the additional good solubility within the water sub phase, these solvent molecules can exit the lipid membrane quickly, resulting in a fast excitation and relaxation of the pressure pulse [6] (compare 3.3 left). Solvents as chloroform and pentane, which are more hydrophobic and less soluble in water maintain for longer times within the membrane, before evaporation. Thus, the time course of the excitation is extended compared to alcohols and the relaxation times are highly increased [6, 23] (compare 3.3 left).

Also the amplitude of the excited wave can be investigated more thoroughly. In the right part of figure 3.3 the maximum amplitudes are displayed with respect to the basic pressure of the membrane. Two general trends can be observed:

- Pronounced minima of pulse amplitudes at the maximum compressibility
- Decreasing amplitude at higher pressures

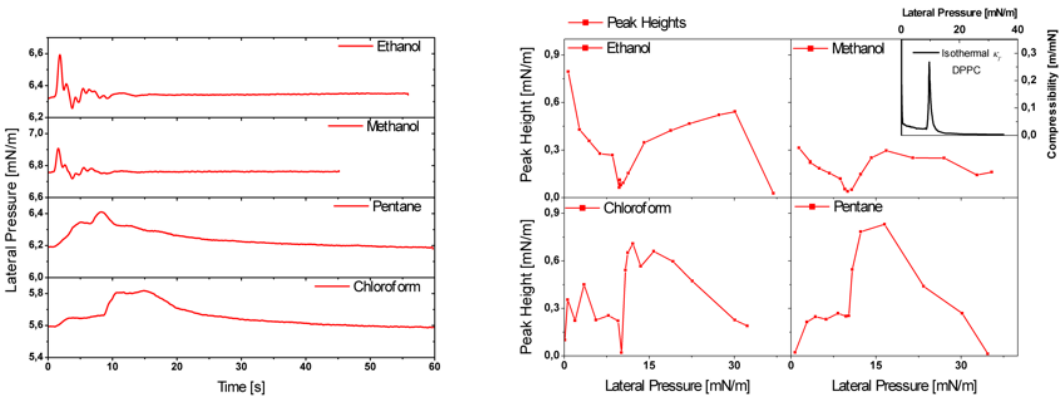

Figure 3.3.: Left: Shapes of excited pressure pulses due to different solvents. While ethanol and methanol exhibit sharp excitation forms, because they rapidly solve in the sub phase after excitation, pentane and chloroform remain for several ten seconds in the monolayer, due to their long evaporation time and bad solubility in the sub phase. Multiple reflection waves can be recognized for methanol and ethanol excitation, which indicate the fast excitation behavior of the alcohols. **Right:** Peak heights of excitation pulses for different solvents of ethanol, methanol, pentane and chloroform. For all solvent types a minimum in the phase transition regime around 10 mN/m (DPPC 24°C) is shown, which is explained by a maximum in compressibility at these pressures. Also for all solvents, the excitability at high pressures decreases as a result of the lower solubility at these pressures. (Figures copied from [6])

Since the excitation of the monolayer resembles a compression by area reduction, the minima in amplitude at the transition region can be explained by employing the equation for the isothermal compressibility (equation 2.7). Considering a constant, relative area reduction $\frac{\Delta A}{A}$ through the incorporation of solvent molecules, this yields:

$$\Delta\pi = -\frac{1}{\kappa_T}\frac{\Delta A}{A} \tag{3.19}$$

Application of the isothermal, instead of the adiabatic compressibility, can be justified by the assumption that for both susceptibilities maximum values are obtained at the plateau region of the isotherm. The minima in wave amplitude upon a constant amount of excitation solvent are thus a consequence of the maximum in compressibility. Furthermore, the overall decrease in amplitude at higher membrane pressures can be explained by the decreased solubility of solvent molecules within the membrane. This affects the distribution of the solvent molecules, which are more likely at higher membrane pressures to enter the aqueous sub phase. In the next section it will be shown that also the velocity of the pulses correlates to the compressibility of the membrane.

3.4. Velocity Profile of Lipid Monolayer Waves

The experimental arrangement with two pressure sensors, laterally displaced by $\Delta x = 14,5\,\text{cm}$, allows the measurement of the wave's velocity profile by determination of the delay time of the signal between the two sensors $c = \frac{\Delta x}{\Delta t}$. In the left part of figure 3.4 the procedure to extract the pulse's arrival times is depicted. In order to neglect baseline shifts, the derivative of the pressure-time course was calculated with *Origin* and compared to a straight line at $\pi' = 0,04\,\frac{\text{mN}}{\text{ms}}$. The intersection points were then elected by hand and further used for the calculation of the delay time and velocity of the pulse. Through consequent application of the standard-

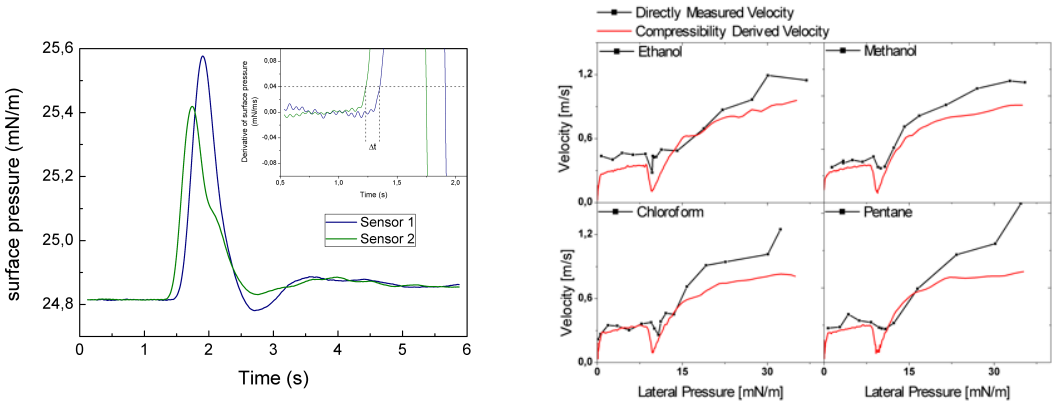

Figure 3.4.: Left: Procedure for the extraction of delay times. Pressure curves of a DPPC monolayer at 24°C, excited with ethanol. *Inset:* Time-derivative of the pressure curves. Intersection points with straight line at $\pi' = 0,04\,\frac{\text{mN}}{\text{ms}}$ are used for the extraction of the delay time Δt. **Right:** Velocity profiles of a DPPC monolayer (24°C) excited with methanol, ethanol, chloroform and pentane. Red curves display the theoretically predicted velocity profile $c = \frac{1}{\cos\left(\frac{\pi}{8}\right)} \sqrt{\frac{1}{\kappa_S}} \sqrt{\frac{\omega}{\eta_w \rho_w}}$ (equation 3.18), calculated from the isothermal compressibility of the respective DPPC monolayer. (Values used: $\omega \approx 2\pi \cdot 1\,\text{Hz}$, $\rho_w \approx 1000\,\frac{\text{kg}}{\text{m}^3}$ and $\eta_w \approx 1 \cdot 10^{-3}\,\text{Pas}$. (Figures adapted from [6])

ized method for monolayer excitation, explained in section 3.2, the whole surface pressure spectra can be probed. The right part of figure 3.4 illustrates the obtained results for different solvents (methanol, ethanol, chloroform and pentane) [23]. All substances display the same quantitative range ($0,2\,\frac{\text{m}}{\text{s}} - 1,2\,\frac{\text{m}}{\text{s}}$) and qualitative trend with a minimum at the phase transition regime and maximum values towards the highest surface pressures in the liquid-condensed phase of the investigated DPPC monolayer.

Comparison to the predicted velocity profile of an acoustic monolayer wave, as being derived in section 3.1, is displayed in the right part of figure 3.4. For the calculation of the red curves the low frequency approximation of equation 3.18 is applied, since Fourier transformation of the measured wave indicated a frequency spectra of

$\approx 0,2-3\,\mathrm{Hz}$. Thus, $c = \frac{1}{\cos\left(\frac{\pi}{8}\right)}\sqrt{\frac{1}{\kappa_S}\sqrt{\frac{\omega}{\eta_w\rho_w}}}$ is computed using the isothermal compressibility and $\omega \approx 2\pi \cdot 1\,\mathrm{Hz}$, $\rho_w \approx 1000\,\frac{\mathrm{kg}}{\mathrm{m}^3}$ and $\eta_w \approx 1 \cdot 10^{-3}\mathrm{Pas}$. The discrepancy between the calculated and measured velocities, especially during the phase transition, might be attributed to the approximation of the adiabatic compressibility κ_S with its isothermal pendant κ_T. A comparison between both susceptibilities allows a reversion of equation 3.18, which enables the calculation of κ_S:

$$\kappa_S = \frac{1}{\cos\left(\frac{\pi}{8}\right)} \cdot \frac{1}{c^2} \cdot \sqrt{\frac{\omega}{\eta_w\rho_w}} \tag{3.20}$$

The resulting graph of a DPPC monolayer at 24°C is displayed in figure 3.5, together with the isothermal compressibility, derived from the slope of a π-A-isotherm. As a general trend one can state that the relation $\kappa_T > \kappa_S$ is true over the entire lateral pressure accessible. This effect is most pronounced during the phase transition, indicated by the maxima, and thus might give a possible explanation for the divergence between the measured and calculated velocity profiles.

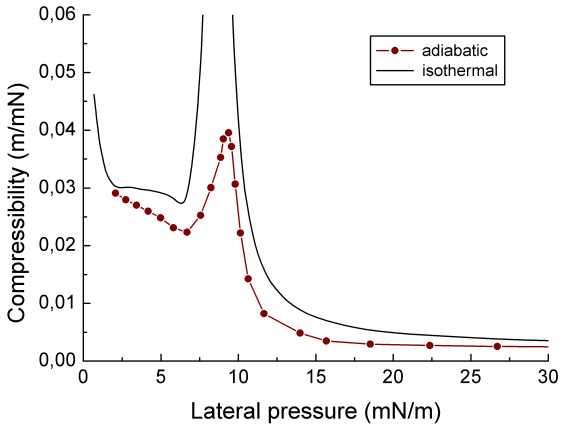

Figure 3.5.: Comparison between the isothermal κ_T and adiabatic κ_S compressibility of a DPPC monolayer at 24°C. While the first is derived from the slope of the π-A-isotherm, equation 3.20 is employed to calculate the latter.

Chapter 4: Excitation of Lipid Monolayer Waves

The previous section gave an introduction to lipid monolayer waves and described the basic excitation mechanisms as well as the pulse velocities, which are found to depend on the membrane state. Also the pulse's amplitude has been monitored and displayed a correlation to the state of the membrane. In this section the excitation process will be investigated more comprehensively. First, a further study of the direct excitation method will be presented, where the influence of the solvent's hydrophobicity as well as the absolute number of solvent molecules applied, is investigated. This will be supplemented in the second part, which is dedicated to the new indirect excitation of lipid monolayer waves by solvent vapors. Eventually, an auto-oscillation phenomenon is presented, which can additionally be induced by solvent vapor.

4.1. Direct solvent excitation

In the following, the results displayed in section 3.3 are extended by a comprehensive study of the properties of the direct solvent excitation. A correlation exists between the wave amplitude and the partition coefficient of the solvent as well as the number of solvent molecules applied to the surface. These findings indicate that the external force responsible for excitation of the wave can be completely controlled and predicted. The results will be applied further within the range of this thesis.

4.1.1. Influence of the solvent hydrophobicity

The empirical finding that the wave amplitude varies accordingly to the phase state of the lipid membrane, but moreover is also affected by solubility of the solvent within the lipid membrane (compare section 3.3), requires a more detailed investigation. Therefore, a homologous series of hydrocarbons with two different functional groups (alcohol & carbon acid) were selected to probe their efficacy of exciting lipid monolayer waves.
The experimental setup applied for this study has been described in section 3.2.

To enable best comparability, the solutions used for excitation were standardized to a molar concentration of $10\,\frac{\mathrm{mol}}{\ell}$. Excited pulse shapes are recorded subsequently after fusion of a $2\mu\ell$ solvent drop with the monolayer interface. The equilibrium membrane pressure π_0 and the maximal pressure π_{max}, measured during one compression pulse were identified. The wave amplitude was calculated according to $\pi_{\mathrm{amp}} = \pi_{\mathrm{max}} - \pi_0$.
Results obtained at an equilibrium pressure of $\pi_0 = 5\,\mathrm{mN/m}$ and averaged over at least 10 measurements are displayed in the left part of figure 4.1. Obviously, the influence of the functional group is minor, as indicated by similar wave amplitude for the first three carbon atoms. The difference in amplitude between butanol and butyric acid can be explained by the relatively increased aqueous solubility of butyric acid over butanol, as can be seen in table 4.1. The additional, collective

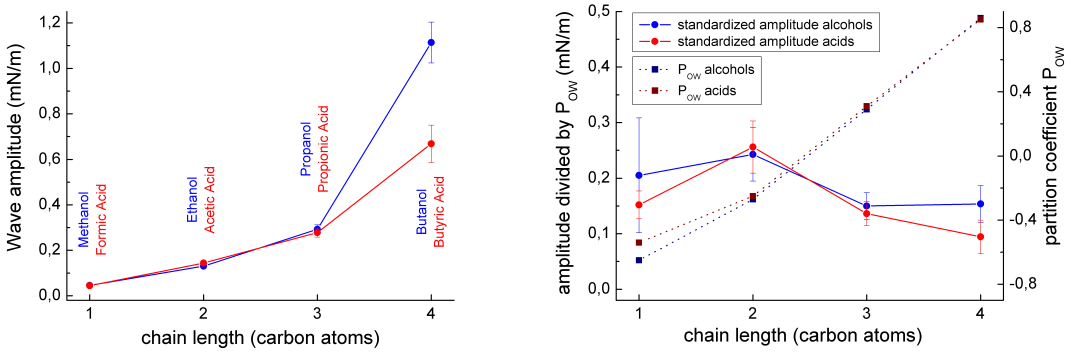

Figure 4.1.: Left: Dependence of wave amplitude on solvent chain length. DPPC monolayer, compressed to an equilibrium pressure $\pi_0 = 5\,\mathrm{mN/m}$ at 24°C, were excited with $2\,\mu\ell$ droplets of aqueous solutions of the respective alcohols and acids ($10\,\frac{\mathrm{mol}}{\ell}$). Decreasing water solubility (compare table 4.1) increases incorporation into the lipid membrane and thereby enhances the wave amplitude. **Right:** Partition coefficients of alcohols and acids (dashed lines) as displayed in table 4.1 are used to normalize the wave amplitude. For this purpose, the measured amplitudes, displayed in the right part of this figure, are divided by the partition coefficient. The resulting amplitudes exhibit a linear behavior within range of error.

increase in amplitude upon extension of the carbon chain, indicates a correlation to the overall hydrophobicity of the solvent molecule. Here, the carbon tail acts as the hydrophobic anchor, which determines the probability of the solvent to adsorb to the lipid interface. This property is analytically expressed by the partition coefficient P_{OW} (water - octanol), which represents the tendency of a compound to accumulate

solvent	**molar mass**	**density**	**solubility**	**molar concentration**	**partition coefficient**
	g/mol	g/cm^3	in water	mol/ℓ	$\log(P_{oct/wat})$
Methanol	32,04	0,79	100%	24,66	-0,65
Ethanol	46,07	0,79	100%	17,15	-0,27
Propanol	60,10	0,80	100%	13,31	0,29
Butanol	74,12	0,81	7,9%	10,93	0,86
Formic Acid	46,03	1,22	100%	26,50	-0,54
Acetic Acid	60,05	1,05	100%	17,49	-0,25
Propionic Acid	74,08	0,99	100%	13,36	0,31
Butyric Acid	88,11	0,96	100%	10,90	0,85

Table 4.1.: Properties of the investigated solvents. Molar mass, density, solubility from the respective Sigma Aldrich data sheets and controlled with [65]. Molar concentration calculated from molar mass and density: $n = \frac{\rho}{M_{\text{mol}}}$. Averaged partition coefficients adapted from multiple references (see [64]

within one phase between two immiscible fluids. This can be introduced to equation 3.19, which we found as a measure for the wave amplitude in section 3.3:

$$\Delta\pi = -\frac{1}{\kappa_T}\frac{\Delta A}{A} \quad \overset{\Delta A \to \Delta A \cdot P_{OW}}{\Longrightarrow} \quad \Delta\pi = -\frac{1}{\kappa_T}\left(\frac{\Delta A}{A}\right)P_{OW} \tag{4.1}$$

Here, we augmented the area term ΔA, which represents the area occupied by the solvent molecules upon fusion with the monolayer, by the partition coefficient. This would compensate the enhanced tendency of more hydrophobic molecules to accumulate stronger on the surface and thus require more area. This augmentation of equation 4.1 is justified in the right part of figure 4.1. Normalization of the wave amplitude by the partition coefficient of the respective solvent results in a straight line within the range of error. The large error bars follow from the relatively disperse numbers for the partition coefficient acquired from multiple references summarized on [64]. Values used in this thesis are averaged over all surveys. Another source of error might also result from neglecting the increase in occupied average surface area per solvent molecule, according to the increasing length of the aliphatic carbon chain. However, the partition coefficient seems to be an important factor which influences the amplitude of the excited pressure pulse.

4.1.2. Linearity of excitation

In a continuation of the experiments to study the process of pulse excitation by solvents comprehensively, the influence of the molar concentration c of the excitation solution as well as the absolute volume V of the drop on the wave amplitude were analyzed. For this purpose, series of aqueous solutions of ethanol with increasing molar concentrations (0.01, 0.1, 1, 2, 4, 8, 16 $\frac{\text{mol}}{\ell}$) were employed (process described in B.4). As depicted in the left part of figure 4.2, the amplitude of monolayer waves was amplified with increasing ethanol concentration. It also can be seen that below $c = 0.01\ \frac{\text{mol}}{\ell}$ no longitudinal pressure wave can be excited. This lower limit is further investigated in the next section 4.1.3.

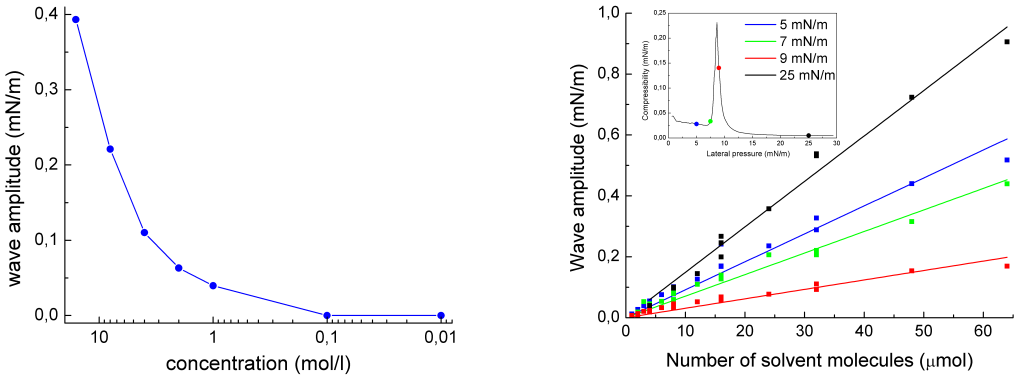

Figure 4.2.: Left: Ethanol excitation sweep executed on a DPPC monolayer at 5 mN/m and 24°C. Potency for wave excitation increases with increasing ethanol concentration. Aqueous solutions of ethanol made by dilution of pure ethanol with ultrapure water to the respective concentrations (0.01, 0.1, 1, 2, 4, 8, 16 $\frac{\text{mol}}{\ell}$). Also visible: Excitation of lipid monolayer waves is not possible with pure water or ethanol concentration $\leq 0,1\ \frac{\text{mol}}{\ell}$ **Right:** Linear correlation found between the absolute amount of solvent molecules applied to the monolayer and the amplitude of the excited wave. Absolute numbers are varied by alteration of the drop volume as well as solvent concentration, while N is calculated by $N = c \cdot V$. The slope of the linear correlation is found to depend inversely on the monolayer compressibility, which is displayed in the *inlay* for a DPPC monolayer at 24°C. Color coded dots indicate the phase state and the compressibility for each respective set of excitation measurement.

Additionally variation the volume of the droplet used for excitation $(1 - 4\,\mu\ell)$ gives access to the absolute number of solvent molecules N applied to the lipid interface, which can be calculated by $N = c \cdot V$. When the respective wave amplitude is plotted against N, as is depicted right part of figure 4.2, a linear correlation can be found. The slope of each straight line depends on the inverse of the compressibility, as is indicated by equation 4.1. The additional variables, which alter the amplitude lin-

early, can be introduced to equation 4.1 by expanding again the term for the required lipid area. Thus, one can state that the absolute area displaced ΔA consists of the area occupied per solvent molecule ΔA_{mol} times the absolute number of molecules applied to the membrane N. Equation 4.1 can therefore be rewritten as:

$$\Delta\pi = -\frac{1}{\kappa_T} \cdot P_{OW} \cdot \left(\frac{\Delta A}{A}\right) \overset{\Delta A \to c \cdot V \cdot \Delta A_{\mathrm{mol}}}{\Longrightarrow} \quad \Delta\pi = -\frac{1}{\kappa_T} \cdot P_{OW} \cdot c \cdot V \cdot \left(\frac{\Delta A_{\mathrm{mol}}}{A}\right) \tag{4.2}$$

This equation allows to calculate precisely the wave amplitude excited under the respective condition. Moreover it is worth mentioning that despite the fact of a non-linear compressibility, within the range of amplitudes probed, the pressure pulse response of the membrane remains a linear phenomena, as indicated by the amplitudes shown in the right part of figure 4.2.

4.1.3. Threshold of excitation

This section is dedicated to the already mentioned onset of excitation, at low solvent concentrations of the excitation solution. In the following, the linear correlation between number of molecules and pulse amplitude is described in more detail. The slope is employed as a measure of the excitability, since the derivative amplifies any deviations from the linear behavior. For this purpose, all pressures illustrated in the right part of figure 4.2 are directly derivated and depicted in the left part of figure 4.3. For each membrane pressure a more or less constant value is obtained, justifying the assumption of the linear fit, conducted in figure 4.2. Besides, in the liquid expanded phase (5 mN/m and 7 mN/m) as well as in the transition region (9 mN/m), a small non-linear effect is observed towards the onset of excitation. Exceptional behavior is found in the liquid condensed phase (here: 25 mN/m and represented by the black curve in the left part of figure 4.3), which reveals a strong non-linear effect at low numbers of solvent molecules. A detailed and closer look at the excitation with low numbers of solvent molecules allows the right part of figure 4.3. Here, a threshold can be observed, located between 2 mol/ℓ and 4 mol/ℓ. While at a concentration of 4 mol/ℓ, a quantity of 4 μmol of ethanol is already sufficient to excite a longitudinal wave (squares in figure 4.3), a concentration of 2 mol/ℓ is not capable of excitation, even with the four-fold amount of molecules. A similar threshold was observed for the excitation with acetic acid.
This non-linear behavior might be explainable by the concentration dependency of the partition coefficient P_{OW}, which was introduced to the equations in section 4.1.1. As is shown for two different chemicals in [66, 67], the partition found in the hydrophobic phase increases with the overall concentration of the chemical in

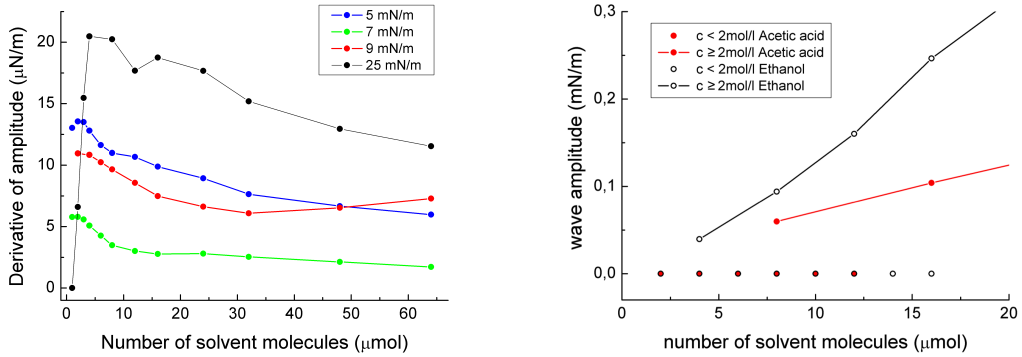

Figure 4.3.: Left: Direct derivation of the curves in the right part of figure 4.2. The ethanol excitation displays almost constant values, justifying the linear fit, with small non-linear effects at low numbers of solvent molecules. Exceptional behavior is found for the excitation in the liquid condensed phase, with a strong non-linearity at the onset of excitation **Right:** Excitation threshold of ethanol and acetic acid concentration c on a DPPC monolayer at 25 mN/m and 24°C. For $c \leq 2\,\mathrm{mol}/\ell$, no excitation occurs, even at high numbers of solvent molcules. For $c > 2\,\mathrm{mol}/\ell$, regular linear excitation is obtained.

the solution. Thus, one can conclude that a decreasing solvent concentration in the excitation solution induces a higher solubility of the solvent within the sub phase water. As a consequence, below a certain threshold concentration, the majority of the solvent molecules preferentially dissolves directly into the subphase, thus rendering the lipid monolayer unexcited.

4.2. Indirect vapor exctitation

The first part of this chapter described the direct excitation process in detail. In order to fuse the solvent drop with the lipid membrane, one has to approach the latter very closely with a drop present at the tip of the needle. While carrying out this procedure it was found that evaporating solvent molecules from the droplet surface are capable of exciting longitudinal monolayer waves. This empirical finding is the basis for the studies that will be presented in the second part of this chapter, where in the following the necessary adaptations of the experimental setup will be described. Furthermore, a concise theory for the vapor excitation of monolayer waves by solvent vapors will be introduced and completed by the experimental results.

4.2.1. Experimental Arrangements

The setup as introduced in section 3.2 was slightly altered in order to create a more stable and reproducible experimental arrangement. A plastic cone was fitted around

the needle (compare left part of figure 4.4) since this was expected to ensure a constant evaporation rate and area. Additionally, the vapor pressure is stabilized, since the restricted volume inside the cone saturates fast. This better defined vapor phase is accompanied by a geometric restriction of the area accessible by the solvent vapor. In order to systematically test these adaptations to the experimental setup, three

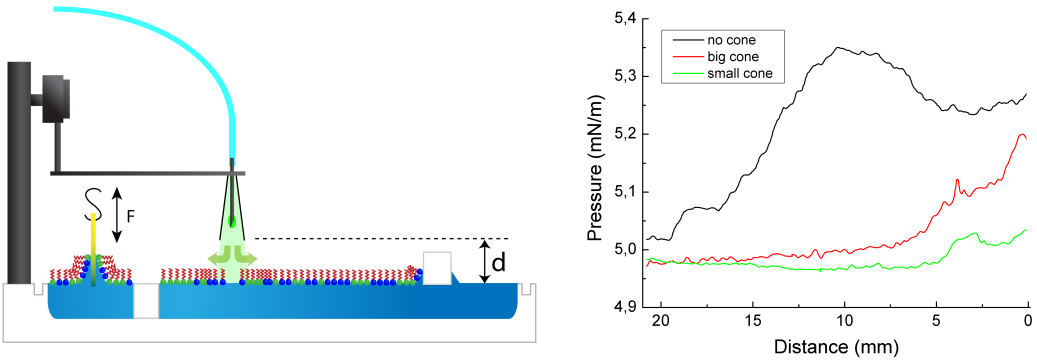

Figure 4.4.: Left: Experimental setup employed to investigate the lipid monolayer - vapor interaction. A cone, fitted around the needle, prevents irregular evaporation of the drop and creates a defined vapor pressure inside the cone. This allows slower dipper velocities and enables better reproducibility. **Right:** Increase in surface pressure of the lipid monolayer upon progressive approaching of the vapor-saturated cone. Surface pressure - distance curves are displayed for three different cone arrangements. Reduction of the cone opening diameter (no cone, large cone ($r = 3.5\,\mathrm{mm}$), small cone ($r = 2\,\mathrm{mm}$)) constrains the area exposed to the vapor.

different arrangements (no cone, large cone ($r = 3.5\,\mathrm{mm}$), small cone($r = 2\,\mathrm{mm}$)) were investigated (compare right part of figure 4.4). The optimum in reproducibility and intensity of the phenomenon was aquired with the large cone attached to the needle, which was the setup employed for all further measurements.
Due to the intense scent of multiple solvents, it was expected to find a correlation to the olfactory perception, since several studies have proposed that lipids might be involved in odor recognition and discrimination. Odorous substances have been shown to increase membrane permeability [68, 69], to increase the surface pressure of a lipid monolayer, when added to the sub phase [70] or to dissolve into lipid bilayers when applied from the vapor phase [71, 72]. All these effects have been found to scale with the partition coefficient of the respective odor. A double-log plot of these effects versus the minimum concentration in air required for human perception results in a straight with the slope of minus one. This resembles the Meyer-Overton rule, which correlates the potency of an anesthetic drug by its solubility in olive oil (lipophilic phase). These findings couldn't be reproduced with our setup. Among multiple odors tested, only the group of carboxylate esters displayed the capability

of increasing the surface tension when approached to the interface and within this group, ethyl butyrate showed the most pronounced effects and highest amplitudes. It is therefore used throughout the following sections to probe the interaction of solvent vapors with lipid monolayers.

4.2.2. Vapor Excitation of Lipid Monolayer Waves

The previous section gave an introduction to the lipid monolayer-solvent vapor interaction and to the experimental arrangement employed for the investigation. In the following, the interaction is studied in detail and in particular concerning the following question: Is the entire membrane simultaneously elevated in surface pressure or is the pressure increased locally, succeeded by a spreading pulse?

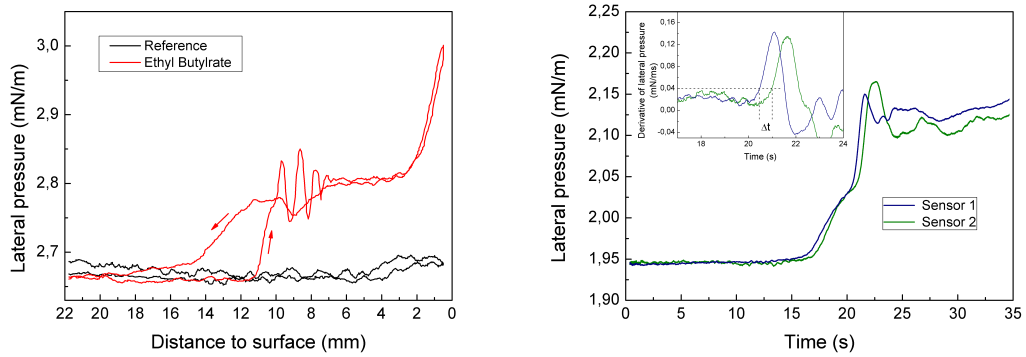

Figure 4.5.: Left: Effect of ethyl butyrate vapor on a DPPC monolayer at 24°C during a full dipper cycle. At certain distance, sudden increase in membrane pressure can be observed. Except for the small hysteresis at the pressure onset on the baseline, the phenomenon is completely reversible. Reference measurement without a solvent drop at the needle tip displays no alteration of the membrane pressure during one complete dipper cycle. **Right:** Time-resolved approach of the ethyl butyrate vapor at two laterally displaced (14,5cm) pressure sensors. The increase in pressure at the distal sensor is delayed, indicating propagation of a longitudinal wave. *Inset:* Derivation of the pressure course as measured at both pressure sensors. Application of the same criteria as explained in 3.4 allows extraction of the delay time and thus the calculation of the propagation velocity.

For this purpose, in the left part of figure 4.5, the response of the monolayer during a complete *up-down* cycle of the dipper is displayed. The approach and return path are indicated by arrows close to the graph. In a comparison to the reference graph, obtained by running one entire cycle with no solvent drop at the tip of the needle, a marked increase in membrane pressure at a certain distance to the interface is observed. This points towards a threshold in vapor concentration necessary to penetrate the membrane. When comparing the approach and return path it is found

that the transition is almost completely reversible within a certain amount of time. By recording the membrane pressure during the approach of the vapor phase with two laterally displaced pressure sensors (setup as described in section 3.2), potential spreading of the localized excitation can be detected. In the right part of figure 4.5, the time-resolved approach of the vapor is displayed, while in the inset the time derivative of the pressure is given. The delayed response of the second pressure sensor indicates the propagation of a pulse and by applying the same criteria as in section 3.4, the velocity of the pressure spread can be extracted. The velocities obtained are in the range of $c \approx 0,3\,\mathrm{m/s}$, which is comparable with the velocities obtained by direct solvent excitation. It therefore can be assumed that the indirect, as the direct, application of solvents results in the localized displacement of lipid molecules, which is further conducted as a pressure pulse through the entire membrane. This consideration clearly separates the excitation from the propagation process.

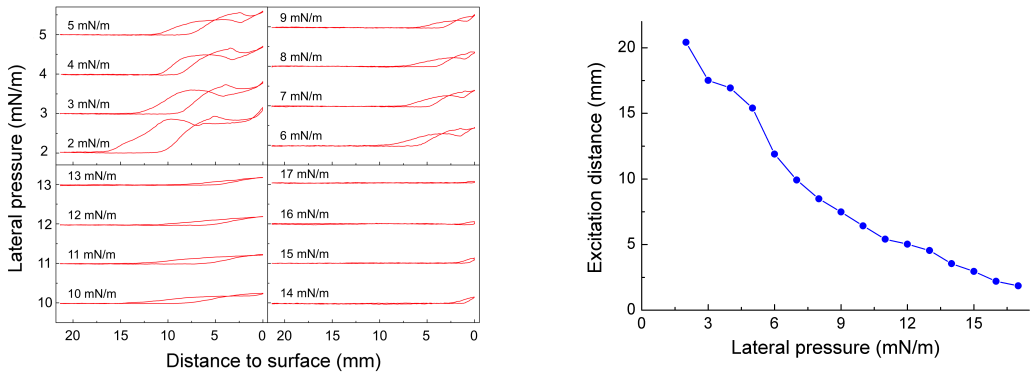

Figure 4.6.: Left: Effect of ethyl butyrate vapor on a DSPC membrane measured for different surface pressures at 24°C. Distance taken as difference between cone opening and lipid interface. With increasing membrane pressure, the distance of the dipper necessary for excitation is reduced (compare right figure). Additionally, the absolute rise in pressure and the observed hysteresis are decreased. **Right:** Excitation distance versus lateral membrane pressure as extracted from the data displayed in the left figure. Data points are extracted from the intersection of the pressure course derivative with a straight line at $\pi'(d) = 0.05\,\mathrm{mN/m^2}$. Towards higher pressures, the solvent drop needs to be approached closer to the membrane in order to excite a longitudinal pulse. No excitation can be observed anymore beyond a certain pressure (Here: $\approx 18\,\mathrm{mN}$).

It therefore remains unanswered, which property of the ethyl butyrate vapor is crucial to excite a pressure wave within a lipid membrane. For this purpose, complete dipper cycles are recorded for varying lateral membrane pressures to investigate the threshold concentration elucidated in figure 4.5. The results recorded on a DSPC membrane are illustrated in the left part of figure 4.6. By variation of the lateral

membrane pressure, changes in the minimum distance necessary to excite a membrane pulse can be observed. This is summarized in the right part of figure 4.6, where the excitation distance is displayed as a function of the lateral pressure of the membrane. An almost linear correlation is found which slightly saturates for high membrane pressures. Since the concentration of vapor molecules in air is decaying with increasing distance from the cone opening, it can be concluded that for higher monolayer pressures, a higher concentration of solvent molecules is required for the pulse excitation.

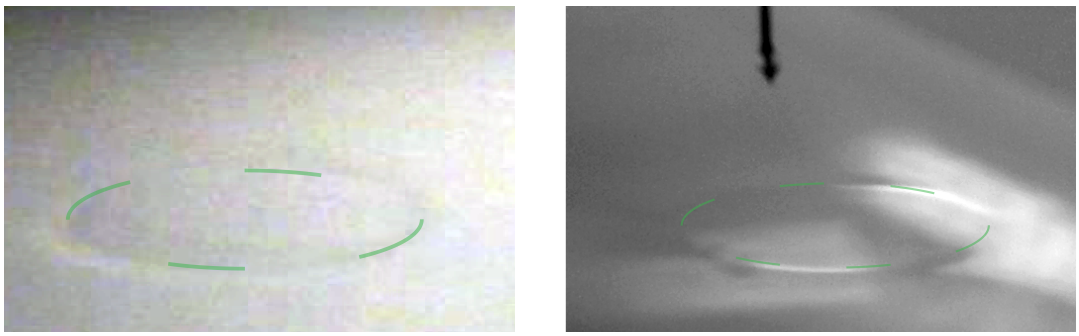

Figure 4.7.: Left & right: Pictures of a faint ring appearing at the air/water interface during vapor excitation. Structure establishes directly underneath the solvent drop, whenever an increase in pressure indicates the excitation of a monolayer wave. Differences in surface tension, discriminating the solvent rich patch from the lipid rich membrane, might be responsible for the observed phenomenon. The introduced, dashed green lines serve as a guide to the eye.

The advantageous position of studying the vapor excitation of monolayer waves is that one can examine quasi-static situations of the direct solvent excitation. This is due to the fact that the force exerted by the vapor can be kept constant by maintaining a certain distance to the surface. It therefore can be observed that whenever an increase in pressure indicates the excitation of a monolayer wave, a faint ring appears on the aqueous surface (figure 4.7). This might be the result of a difference in optical density between the solvent enriched patch in the middle and the lipid membrane covering the outside region, but could also arise from a difference in surface pressure. Overall it can be stated that the solvent excitation process, direct or indirect, creates a solvent enriched patch, which disappears as soon as the vapor vanishes or its concentration falls below a certain threshold. Preliminary fluorescent measurements on the vapor excitation (not shown) are even pointing towards a complete depletion of lipids within the excitation center.

4.2.3. Excitation of Auto-Oscillations

When the vapor phase of a solvent is approached to a lipid monolayer, auto-oscillations of the membrane pressure can occur. This behavior was already noticed and displayed in figure 4.5 and is comprehensively investigated and discussed in the following.

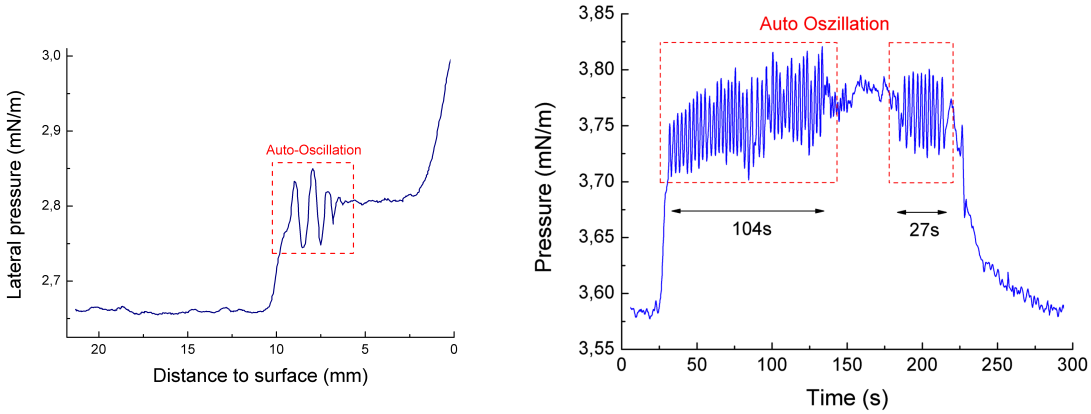

Figure 4.8.: Left: Approach of ethyl butyrate vapor to a DPPC membrane at 24°C. Auto-oscillations in membrane tension occur, when the dipper is within a certain range of distance to the interface. **Right:** Sustained auto-oscillation induced by "clamping" the distance to the surface. The ethyl butyrate drop is produced at $t \approx 25\,\mathrm{s}$, causing a marked increase in surface pressure. Auto-oscillations vanish at $t \approx 120\,\mathrm{s}$, reappear at $t \approx 180\,\mathrm{s}$ and finally are stopped when the drop is retracted into the needle.

During an approach cycle of an ethyl butyrate drop, oscillation of the surface pressure was observed once the drop passed a certain distance to the surface. These oscillations can be sustained by keeping the dipper fixed at this distance, while extruding a solvent droplet (right part of figure 4.8). A subsequent steep increase in membrane pressure ensures the interaction with the membrane and indicates the excitation of a monolayer wave. As a requirement for the onset of auto-oscillations it was found that the drop needs to be within a certain range of distance to the surface $\Delta d \pm 1.5\,\mathrm{mm}$. It is assumed that as long as the drop is present at the needle tip, the vapor pressure is kept constant, which consequently sustains the auto-oscillations. Under these circumstances, maximal oscillation life times up to $150\,\mathrm{s}$ have been observed. Typically, the oscillations last between $30 - 150\,\mathrm{s}$. Termination of the oscillation process might be due to variations in external conditions such as convection, which disturbs the sensitive equilibrium between membrane and vapor pressure. Moreover, retraction of the ethyl butyrate drop into the needle interrupts the oscillation and causes a typical relaxation process, indicating progressive desorption of solvent molecules from the interface (depicted for $t \geq 220\,\mathrm{s}$ in the right

part of figure 4.8).
In order to elucidate further the underlying mechanism of the auto-oscillations, the advanced film balance setup (two sensors, high time resolution (*(10000 samples/second, 0,01 mN/m)*) was employed to investigate the exact shape. An exem-

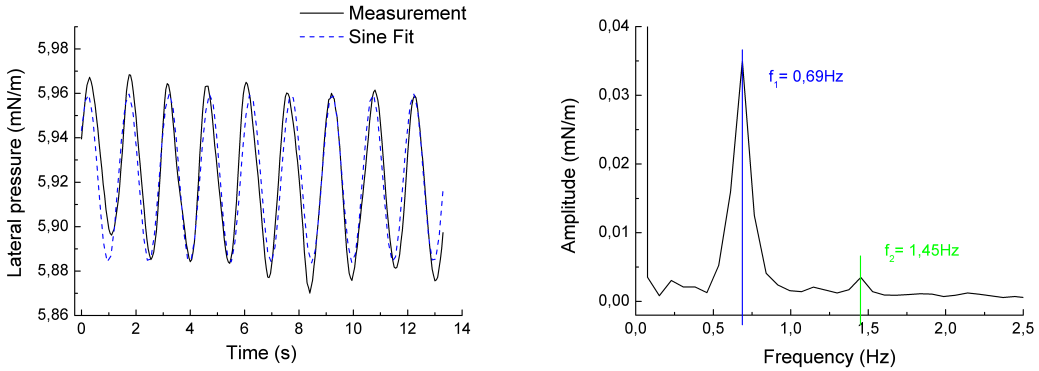

Figure 4.9.: Left: Recording of auto-oscillation with high time-resolution (*(10000 samples/second, 0,01 mN/m)* and fit of the data with a sine function. Good agreement with the fit indicates almost symmetrical oscillations. **Right:** Fourier transformation of the sine wave yields a main frequency ($f = 0,69$ Hz) and a low amplitude for the first harmonic ($f = 1,45$ Hz).

plary recording is displayed in the left part of figure 4.9, where the superposition of a sine wave was fitted to the pressure data recorded with the proximal sensor. This indicates a highly symmetric, sinusoidal oscillation of the surface. When compared to the pressure recording of the distal sensor, a delay angle can be extracted. According to the known distance between the sensors, the velocity of the spreading phenomenon is calculated to $c = 0,29\frac{\mathrm{m}}{\mathrm{s}}$, which is again in the range for a DPPC membrane at 6mN/m and 24°C (compare figure 3.4 & [6, 23]. Moreover, a Fourier transform of the sine wave (right part in figure 4.9) allows to study the frequency behavior. The obvious maximum at $f = 0,69$ Hz is the main frequency, supplemented by a small peak of the first harmonic at $f = 1,45$ Hz. Thus, the results obtained for velocity as well as for frequency of the auto-oscillations, can be compared with good agreement to the previously presented results (see chapter 3). This again draws the line of an excitation independent propagation phenomenon.
A surprising result of the experiments on lipid membrane auto-oscillations is the stability of the phenomena against external changes as temperature and membrane pressure. As can be seen in left part of figure 4.10, alteration of the temperature doesn't change the distance necessary to induce auto-oscillation, even though the DPPC membrane undergoes a phase transition in this temperature and lateral pressure range (compare figure 2.7). The frequency of the oscillations is slightly

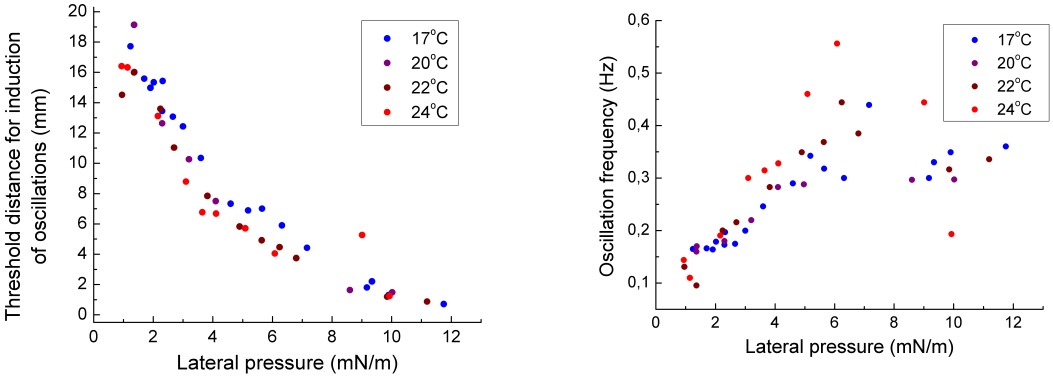

Figure 4.10.: Left: Drop distance necessary to induce auto-oscillations as a function of the lateral pressure of the lipid membrane. The threshold distance for the induction of oscillations approaches asymptotically towards zero for higher lateral pressures, indicating the experimental limit at $\approx$ 12 mN/m. **Right:** Frequency of oscillation as a function of the lateral membrane pressure. Linear behavior can be observed at low lateral pressures, while an increasingly dispersive character manifests at $\approx$ 5 mN.

decreased towards lower surface pressure and is rather disperse at high pressures. Assuming the lipid membrane as driven harmonic oscillator, a correlation between oscillation frequency and membrane compressibility would be expected. This is due to the dependence of the restoring force on the compressibility of the membrane, since the monolayer acts in this picture as a Hookean spring. Since no minimum in oscillation frequency can be observed at the compressibility maximum for the different temperatures, further investigations are required in order to obtain an entire picture of this phenomenon.

4.3. Summary excitation

From the results presented in this chapter it was concluded that the direct excitation process of longitudinal monolayer waves by fusion of a solvent drop with the lipid monolayer depends among others on the accumulation of solvent molecules at the aqueous interface. Incorporation into the lipid membrane requires additional lateral space, which causes a displacement of lipids. This displacement is subsequently conducted over the entire interface area as a lateral pressure pulse. The magnitude of the observed pressure pulse depends on the hydrophobicity of the solvent. This was accounted for by introducing the partition coefficient P_{OW} of the solvent into equation 4.2. Furthermore, the amplitude can be scaled linearly by the number of solvent molecules applied, defined by drop volume times solvent concentration.

In the liquid crystalline phase state of the membrane, a concentration threshold is found, rendering wave excitation impossible below $c \leq 2\frac{\text{mol}}{\ell}$. This effect is explained by the concentration dependence of the P_{OW}.
Additionally an indirect method of inducing lipid monolayer waves has been demonstrated. For this purpose, the vapor phase of a solvent drop is approached to the surface, which results in a sudden increase in membrane tension, indicating excitation of a longitudinal wave. The wave propagation velocities extracted under these conditions are similar to those with direct excitation. This finding indicates that the propagation process is independent from the type of excitation and thus exclusively depends on the membrane properties. Moreover, these results were confirmed for auto-oscillations induced by solvent vapors. As illustrated by experiments conducted at different temperatures, the phase state of the lipid membrane surprisingly does not influence the appearance and properties of the oscillations.

Chapter 5: Relaxation of Lipid Monolayer Waves

The relaxation characteristic upon external perturbation is a crucial feature of lipid membranes since it determines, among other things, the passive and active transport behavior according to the life time of pores. This was e.g. observed in the case of sodium ion conductivity across a lipid bilayer [39, 40, 73, 74]. A variety of methods have been applied to lipid bilayers in order to create an artificial disequilibrium, allowing the investigation of the subsequent relaxation process. Among others, temperature [75] and pressure jumps [41, 76–80] have been applied to vesicle solutions, but also dielectric [81] and ultrasonic techniques [82] have been used to excite lipid membranes. Besides, different tools and properties of the membrane were employed for the experimental read out, e.g. fluorescent probes [75], membrane turbidity [78, 79], infrared spectra [77] or calorimetry [41, 76]. The common result in all these studies is a significant increase of relaxation time during the phase transition of lipid bilayers. Even multiple relaxation processes, measured simultaneously over time scales ranging from μs to s, displayed this typical relaxation characteristic. In most cases, this behavior is related to the maximum in the excess heat capacity of the membrane under consideration [41, 77–79]. Those experiments are supported by the theoretical work by Kanehisa and Tsong [83], which predicted a multiple exponential decaying process of the membrane with a pronounced maxima during it's phase transition. Boehm at al. [76] proofed that the correlation between relaxation time and excess heat capacity even holds for the pretransition in lipid vesicle systems.

In a continuation of the work about bilayer relaxation, this chapter will focus on the relaxation characteristic of lipid monolayers and is based on [84]. The pressure pulse, introduced and discussed in the preceding chapters, will in this context be considered as a 2-dimensional perturbation, which causes a local deflection of the monolayer followed by a relaxation process. Monitoring the exact shape of the wave form allows furthermore the extraction of the respective relaxation time by an exponential interpretation of the 2-dimensional pressure pulse. The time scales obtained correlate with the macroscopic compressibility of the monolayer and are in agreement with microscopic observations [51]. This empirical section will be preceded by the derivation of a theoretical model, based on Albert Einstein's approach to

thermodynamics and combined with an Onsager type ansatz, predicting the found correlation between κ_T and τ correctly.

5.1. Theory of Relaxation Processes

In section 2.3.2 it is derived that the area fluctuations of a lipid monolayer are directly correlated to its isothermal compressibility κ_T. This was accomplished by following Einstein's approach to thermodynamics, who *reversed* the Boltzmann principle $P = \exp(S/k_B)$ in order to start from a macroscopic (phenomenological) behavior:

$$\langle(\delta A)^2\rangle = k_B\left(-\frac{\partial^2 S}{\partial A^2}\right)^{-1} = k_B \cdot T \cdot A \cdot \kappa_T \tag{5.1}$$

Equation 5.1 summarizes the so far purely thermodynamic and thus statistical approach. This will be expanded by the introduction of time in an Onsager type relation, which states that the changes of a thermodynamic variable α_i in time (thermodynamic flux) are proportional to the derivative of the entropy with respect to the conjugated thermodynamic variable (thermodynamic force) [85, 86].

$$\frac{\partial \alpha_i}{\partial t} = L_{ik}\frac{\partial S}{\partial \alpha_k} \tag{5.2}$$

L_{ik} is a phenomenological parameter called transport coefficient, which must be determined experimentally. By following an identical line of arguments, a direct correlation between relaxation time τ and excess heat capacity c_p of a lipid bilayer is found [41, 80]:

$$\tau = \frac{T^2}{L}c_p \tag{5.3}$$

Here, T is the system temperature although usually measured in the bulk.
Application of equation 5.2 to lipid monolayer waves requires that all α_i, changing during the passage of a density pulse, have to be included. This comprises among others the area A, enthalpy H and surface charge density σ. The resulting set of equations can be simplified by considering that these variables are tightly coupled for sufficiently small deviations from equilibrium, leaving only one independent variable [27, 41, 87]. Hence, it is sufficient to employ the deviation from the equilibrium area per molecule $A' = A - A_0$, caused by the passing wave, to describe the system:

$$\frac{\partial A'}{\partial t} = L\frac{\partial S}{\partial A'} \tag{5.4}$$

Taylor expansion of the first derivative on the right side of equation 5.4

$$\frac{\partial S}{\partial A'} \approx \frac{\partial^2 S}{\partial A^2}\cdot A' \quad \Rightarrow \quad \frac{\partial A'}{\partial t} = L\left(\frac{\partial^2 S}{\partial A^2}\right)_{A_0} A' \tag{5.5}$$

leads to the solution of the evolving differential equation, which is solved by an exponential function $A' = A'_0 \exp(-t/\tau)$:

$$-\frac{1}{\tau} = L\left(\frac{\partial^2 S}{\partial A^2}\right)_{A_0} \tag{5.6}$$

This result reflects the direct connection of area fluctuations and relaxation times in a lipid monolayer. Combined with equation 5.1 one arrives at the relation between isothermal compressibility κ_T and relaxation time τ:

$$\tau = \frac{1}{k_B L}\left\langle (\delta A)^2 \right\rangle = \frac{T \cdot A}{L} \cdot \kappa_T \tag{5.7}$$

It should be noted that in general the entropy potential is a function of *all* thermodynamic variables ($S(H, A, N, \dots)$), which allows deriving similar relationships as equation 5.7 for fluctuations in all these variables and their respective susceptibilities to the relaxation time of the system. The resulting coupling of all excess susceptibilities is experimentally further supported by [34, 87] and allows to conclude:

$$\Delta c_\pi \propto \Delta \kappa_T \propto \Delta \alpha_\pi \propto \Delta C_T \propto \tau \tag{5.8}$$

It is therefore predicted that relaxation times are directly correlated with the compressibility of a monolayer i.e. with the thermodynamic state of the membrane. Comparison with Einstein's fluctuation-dissipation theorem [88] demonstrates that equation 5.7 is in its essence a fluctuation-dissipation relation for the membrane area. Along the same lines, the relation between τ and c_p (equation 5.3) was derived by studying the fluctuations in enthalpy of lipid systems [41]. This relation was experimentally verified by observing the relaxation c_p profiles following 3-dimensional pressure jumps applied to large unilamellar vesicles.
Moreover, equation 5.7 can be solved for the transport coefficient L:

$$L = A \cdot T \cdot \frac{\kappa_T}{\tau} \tag{5.9}$$

, enabling its calculation. As a consequence, the assumption of a linearized correlation between thermodynamic fluxes and forces can be tested in the experimental section by the assumption of a constant transport coefficient.

5.2. Measurement of the Relaxation Process

The evaluation of pulse velocities and amplitudes have been thoroughly discussed. Here, we observe the decaying wave form subsequently after the solvent excitation in order to extract the relaxation time needed for pressure equilibration. For this purpose, an exponential function was fitted to the envelope of the pressure pulse:

$$\pi(x) = \pi_0 + \pi_{\text{Pulse}} \cdot \exp\left(-(t - t_0)/\tau\right) \tag{5.10}$$

Equilibrium pressure π_0, peak center t_0 and the initial amplitude of the pulse π_{Pulse} are all experimentally determined, leaving the relaxation time t as the only fitting parameter. In figure 5.2, a typical time-resolved example for a propagating pressure pulse is displayed (blue graph). The peak tips are fitted by equation 5.10 to obtain the envelope of the oscillation (purple graph). The characteristic time constant τ of the decay is further used for evaluation.

To compare relaxation time and thermodynamic state of the interface, isotherms were measured prior to the solvent excitation experiments. The corresponding lateral compressibility was calculated using equation 2.7:

$$\kappa_T = -\frac{1}{A}\left(\frac{\partial \pi}{\partial A}\right)^{-1} \tag{5.11}$$

In the plateau region of a π-A isotherm, the compressibility shows a distinct maximum, which indicates the transition pressure π_t. As can been seen in figure 2.7, π_t can be sensitively altered by changes in temperature, but also strongly depends on the lipid type. In the following, both of these variables are used to vary π_t in order to investigate, if the maximum in relaxation time is shifting accordingly to the maximum in isothermal compressibility and thus verifying the correlation between κ_T and τ.

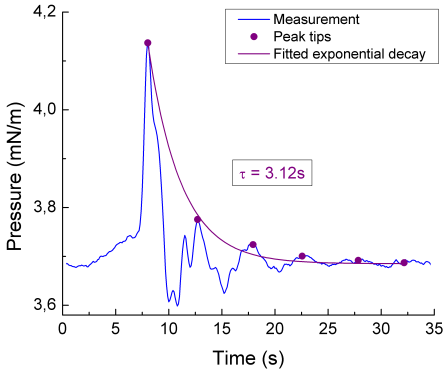

Figure 5.1.: Example for a typical time-resolved pressure pulse propagating in a DPPC membrane at 24°C and recorded by the right sensor in figure 3.2. Peak tips are selected by hand and fitted with an exponential decay function (equation 5.10)

5.3. Conservation of the relaxation time - compressibility relation

Plotting the extracted relaxation times versus the lateral equilibrium pressure π_0 allows the comparison to the previously measured isothermal compressibility κ_T. As is demonstrated in figure 5.2 for a DPPC monolayer at 24°C, τ and κ_T are directly correlated. Both functions display a distinct maximum at the transition pressure $\pi_t \approx 10\,\text{mN/m}$ and also the relative decrease from liquid-expanded to liquid-condensed phase is of the same order. These results are confirmed when compared to relaxation time measurements on a monolayer comprised of D15PC lipids, as presented in figure 5.3. Here, the monolayer is cooled to 16°C in order to observe a plateau within a measureable π-A range. The resulting maximum

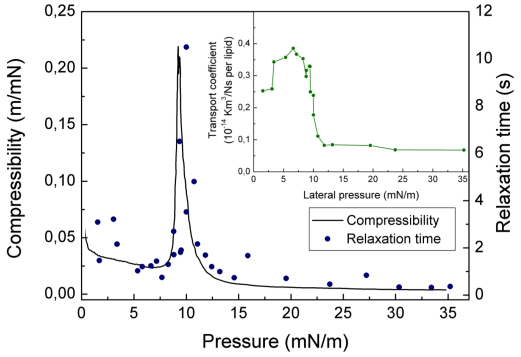

Figure 5.2.: Correlation between monolayer compressibility of DPPC at 24°C and the measured relaxation times are shown. Pressure pulses are excited with $2\mu\ell$ droplets of ethanol. Relaxation times follow directly the compressibility of the lipid monolayer. *Inset:* Transport coefficient L versus lateral membrane pressure. Values are calculated accordingly to equation 5.9. Additionally, the adiabatic compressibility κ_S, extracted from pulse velocity measurements, is employed for calculation.

in compressibility at the transition pressure π_t was again accompanied by a maximum in relaxation time, indicating the predicted coupling. Thus, neither a change of lipid type nor the change in temperature affected the correlation. Moreover it

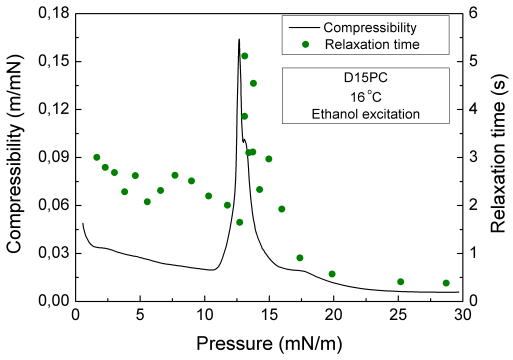

Figure 5.3.: Invariance of the compressibility-relaxation time correlation with respect to membrane composition. Exchange of lipid type to D15PC as well as the variation in bulk temperature to 16°C does not alter the correlation indicated by the coinciding maxima.

can be shown that the found correlation is not a consequence of the excitation. Indeed, the same correlation is observed when exciting with chloroform or pentane instead of ethanol (see section B.5). Since the hydrophobicity of these solvents is increased compared to ethanol, the wave from is altered towards longer

extended pulses, as studied in [23]. Although this will affect the absolute numbers of the relaxation time, the predicted correlation between τ and κ_T is conserved.

The conservation of the correlation between relaxation times and compressibility under temperature variation is comprehensively demonstrated in figure 5.4. During a sweep from 20 to 28°C the phase transition pressure and thereby the maximum in compressibility of the probed DPPC membrane is shifted from around 4 to 14mN/m, in accordance to figure 2.7. By using ethanol as excitation solvent it can be shown that the relaxation time maximum follows the maximum in compressibility for each temperature.

Thus, one can state that our results demonstrate that relaxation times and interface state (expressed in terms of compressibility) are directly correlated. This correlation is conserved under thermodynamic (Π, T), excitation (Ethanol, Chloroform) and molecular (lipids) variations.

Using ethanol as probing agent, the relaxation time cumulates at $\tau_{le} = 2\,\mathrm{s}$ in the liquid expanded phase for all lipids and temperatures investigated. This value increases by a factor of 2-5 towards the phase transition, depending on the position within the coexistence region of the respective lipid type. This difference in relaxation time actually increases with temperature (compare Fig. 5.4), what could point towards the approach of a critical point in the monolayer's phase diagram.

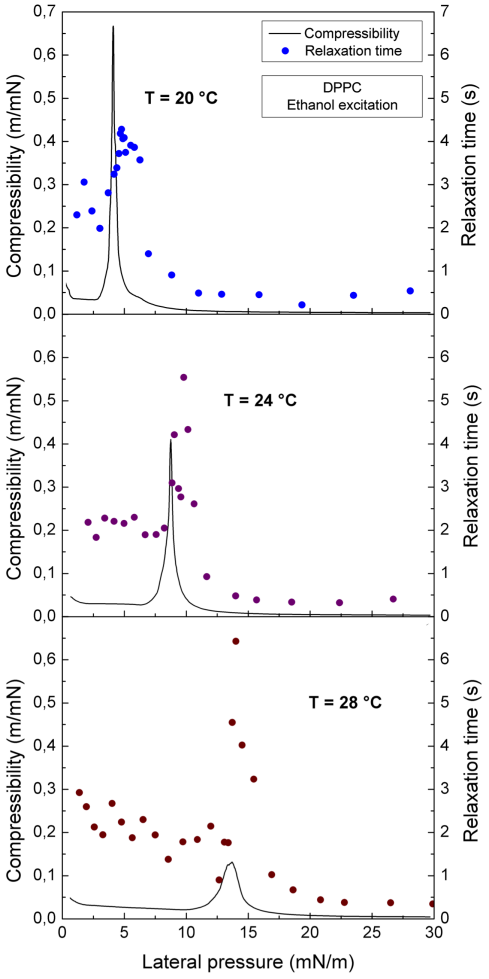

Figure 5.4.: Invariance of the compressibility-relaxation time correlation with respect to changes in bulk water temperature, which is indicated by coinciding maxima for each temperature probed (20°C, 24°C, 28°C). Increasing absolute numbers of the relaxation time during the transition may indicate the approach of a critical point.

5.3.1. Discussion of the transport coefficient

As mentioned in section 5.1, the resolved correlation of relaxation time and compressibility (equation 5.7), allows the calculation of the transport coefficient L. This phenomenological parameter can only be accessed experimentally and is specific for each lipid system. The inset of figure 5.2 therefore displays the transport coefficient, calculated from equation 5.9, for the respective relaxation time measurement. Due to the adiabatic nature of the described pressure pulses, the adiabatic compressibility κ_S is employed for calculation (instead of κ_T), which is extracted from the respective pulse velocities, as is described in section 3.4. The reversion of equation 3.18, yields a correlation for the adiabatic compressibility:

$$c = \frac{1}{\cos\left(\frac{\pi}{8}\right)} \sqrt{\frac{1}{\kappa_S} \sqrt{\frac{\omega}{\eta_w \rho_w}}} \quad \Longrightarrow \quad \kappa_S = \frac{1}{\cos\left(\frac{\pi}{8}\right)} \cdot \frac{1}{c^2} \cdot \sqrt{\frac{\omega}{\eta_w \rho_w}} \tag{5.12}$$

Here, ρ_w and η_w denote as well the density and viscosity of the sub phase (here: water) and ω the frequency evaluated by a Fourier transform of the according wave. The described behavior is also found in the temperature variation measurements. The calculated transport coefficient for each temperature is shown in figure 5.5, where apart from the qualitative curve progression also the quantitative values of L for the liquid-expanded and liquid-condensed phases are reproduced. Notice that

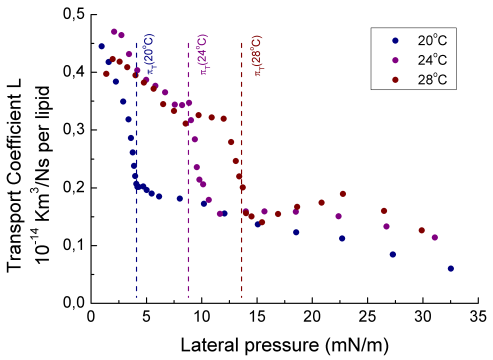

Figure 5.5.: Transport coefficient L calculated from the temperature variation experiment presented in figure 5.4. The adiabatic compressibility κ_S, extracted from pulse velocity measurements, is employed for calculation. Within experimental error, constant values for each membrane state are obtained, accompanied by a non-linear behavior at the transition pressure, indicated by the dashed lines for the respective temperatures.

the values for the transport coefficient vary for the respective membrane states, indicating the limitations of the assumptions made in the theoretical section B.

While in the liquid-expanded phase, the values for L accumulate around $L_{le} \approx 0,4 \cdot 10 - 14 \frac{\mathrm{Km}^3}{\mathrm{Ns}}$ per lipid, the transition coefficient decreases sharply during the phase transition, reducing the average value to $L_{lc} \approx 0,15 \cdot 10 - 14 \frac{\mathrm{Km}^3}{\mathrm{Ns}}$ per lipid in the liquid-condensed phase. These results indicate that the transport coefficient is membrane state dependent and imply augmented thermodynamic fluxes to occur in the liquid-expanded phase. Moreover, the constant value of L in each phase, verifies the validity of the linearization used in the Onsager approach, at least for the individual phases (equation 5.4).

5.3.2. Comparison to timescales of current fluctuations

To outline the potential of the presented theoretical approach, some additional predictions are derived. It has been demonstrated that quantized current fluctuations are present in pure lipid bilayers, in particular in the range of the phase transition regime [39, 40, 89]. The time scales of these currents have been shown to correlate directly with the state of the bilayer, what was explained on the base of an increased curvature of the entropy potential [39, 41]. In those studies, the fluctuation in enthalpy is correlated with the relaxation time scales, resulting in a similar expression as equation 5.7, with the excess heat capacity as material susceptibility (compare equation 5.3).
The relative change in relaxation time between liquid-expanded phase and transition region is extracted from our experiments of propagating interfacial waves and predicts an increase in time scales in the order of 4, depending on the system temperature. In earlier studies we have demonstrated that the average channel opening times in lipid bilayers of DOPC/D15PC mixtures increase by a factor of 7 when comparing the fluid phase with the region of maximum heat capacity [39]. Considering the various differences between monolayer and bilayer as well as the lipid composition, these numbers indicate that the physical origin of these opening times is the thermodynamic state of the system.

5.4. Summary Relaxation

In this chapter, the local relaxation of pressure pulses, propagating in monomolecular lipid films, is studied. First, a correlation between relaxation time τ and lateral compressibility κ_T is predicted, based on Einstein's approach to thermodynamics, which centerpiece is the reversion of the Boltzmann principle. In the second part, this correlation is experimentally confirmed by demonstrating its invariance with respect to physical (π, T), chemical (ethanol, chloroform) and molecular (lipid type) variations. At last, the derived correlation is resolved for the transport coefficient

L and thus reviewed by calculation of L from experimental data. The temperature independent, constant value found for each thermodynamical membrane state justifies the linearization used in the Onsager theorem, while the non-linearity at the lipid phase transition indicates the limitations of this theoretical approach.

Chapter 6: Influence of the Lipid Headgroup Size on Lipid Monolayer Waves

The cytoplasm is surrounded by the cell membrane which thus separates the intracellular from the extracellular environment. The membrane consists of two lipid monolayer leaflets in which proteins are embedded. The glycocalyx [90]; a layer of oligo- and polysaccharide chains covalently attached to lipids and proteins covers the extracellular side of the cell membrane [91]. The carbohydrate residues stabilize the structure of the cell membrane by a combination of physical forces (e.g. hydrogen bonds) [91]. This effect has also been observed with artificial lipid vesicles [92]. Additionally, the glycocalyx protects the plasma membrane from chemical degradation and plays a vital role in the interaction of cells with the immune system [90].

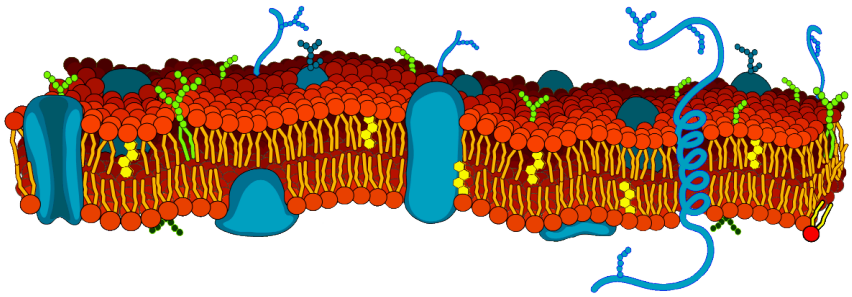

Figure 6.1.: Schematic drawing of a cell membrane comprised of the lipid bilayer with embedded proteins. Covalently attached oligo- and polysaccharide chains form the glycocalyx (figure adapted from [93]).

In order to study the effect of such a carbohydrate coating on the propagation of waves in lipid monolayers, polyethylene glycol-lipids (PEG-lipids) were employed to form the lipid monolayer. These lipids are characterized by a PEG-chain that is covalently coupled to the headgroup. In this particular study, DSPE[1]-PEG was used.

[1] 1,2-dioctadecanoyl-sn-glycero-3-phosphoethanolamine

In an aqueous environment, the PEG-chain is highly hydrated. This is expected to clearly increase the extension of the interfacial hydration layer of the lipid monolayer into the aqueous sub phase. Thus, when lipids are displaced by the passage of a longitudinal wave, more interfacial water has to be dragged along and therefore viscous forces are expected to be increased. The influence of the hydration layer has already been included in the monolayer wave equation in chapter 3 and will be more thoroughly discussed below.
The emphasis of this chapter is to elucidate the impact of glycolipids on the properties of monolayer waves. In particular, the impact of the PEG-chain length on the propagation of pressure pulses will be studied. A discussion about its possible role for biology in the context of lipid monolayer waves will conclude this chapter.

6.1. Polyethylene Glycol Lipids

The ability of poly(ethylen glycol) to dissolve in polar and nonpolar solvents displays the amphiphilic nature of this molecule [94] and explains its tendency to form a monolayer at the air-water interface at moderate film pressures ($\pi < 10\,\mathrm{mN/m}$) [94]. At higher surface pressures the polymers exceedingly dissolve into the bulk water phase. In addition, PEG molecules are classified according to their average molecular weight, which is indicated in the respective polymer name (e.g. PEG 350). The

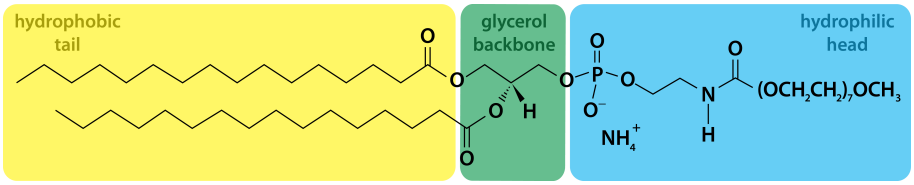

Figure 6.2.: Chemical structure of DSPE PEG 350.

number of monomers in the molecule N can simply be calculated from this average molecular weight by dividing it by the weight of a single monomer (44 Da). Thus, a polymer with the average molecular weight of 350 Da is comprised of 7 monomers, while a PEG chain weighing 2000 Da corresponds to $N = 45$. Considering the PEG chain as a non-ideal polymer allows to calculate its Flory radius [95]:

$$R_F = a \cdot N^{3/5} \tag{6.1}$$

Here, a is the persistence length of one PEG monomer ($a = 3.5\,\text{Å}$) [95]. Consequently the Flory radius of the two PEG derivatives that will be employed in the subsequent studies are calculated to $R_F(\text{PEG 350}) = 11.2\,\text{Å}$, and $R_F(\text{PEG 2000}) = 34.4\,\text{Å}$. This value represents the lateral extension of the coiled polymer. As representative for the

lipopolymers used in this study, figure 6.2 depicts DSPE PEG 350. When covalently bound via an ester bonding to the head group of a lipid, the properties of the entire compound differ from the single polymer. The resulting behavior is described by the Alexander-de Gennes theory of grafted polymers [96, 97], which is graphically summarized in the right part of figure 6.3.

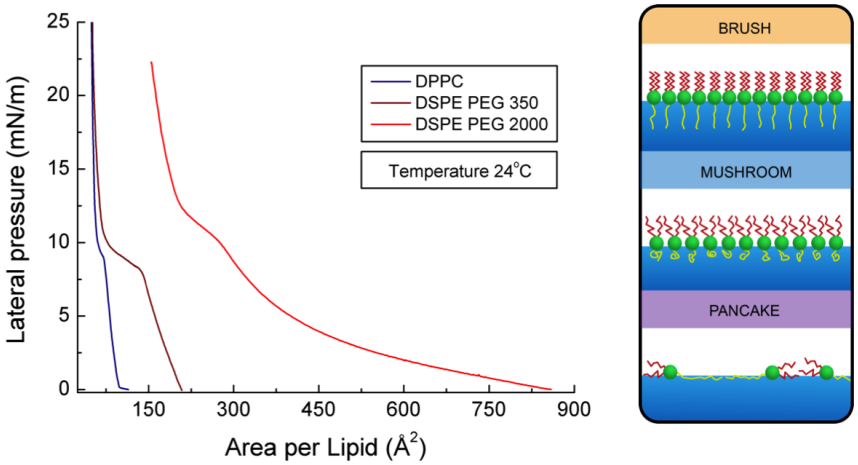

Figure 6.3.: Left: Comparison of π-A-isotherms of DPPC, DSPE-PEG 350, DSPE-PEG 2000 at 24°C. An overall increase of average area per molecule as observed for PEG-conjugated lipids indicates that the polymer chains require additional area at the interface **Right:** Schematic drawing of the most likely molecular conformations of PEG-lipids during compression as predicted by the Alexander-de Gennes theory of grafted polymers [96, 97]. After desorption of the PEG chains from the interface, indicated by the phase transition at $\pi \approx 10\,\mathrm{mN/m}$ in the lipopolymer isotherm, the mushroom state is dominant. In a further transition at higher film pressures (not resolved in isotherms), the brush state is mainly occupied.

Sprited on a pure water surface, the PEG polymer chains are floating up and covering the surface, together with its lipid anchor [98]. Upon compression of the film, the polymers act as soft "springs" in between the lipids. The behavior for this so-called *pancake-like* conformation is demonstrated in the π-A-isotherm depicted in figure 6.3. The membrane pressure for lipopolymers is already increasing for very large areas per molecule, which complicates the recording of a baseline pressure [92, 99]. An overall increase in average area per molecule can be observed due to the additional space required by the hydrocarbon chains [98]. As above for a collapsing monolayer of pure PEG [94], the polymer chains desorb from the interface at about $\pi_{\mathrm{low}} = 10\,\mathrm{mN/m}$ [92, 99]. Here, the attached lipid anchor ensures that the PEG stays in the vicinity of the air/water interface. The emerging free space can be observed in the isotherm (figure 6.3) by a phase transition occurring for both PEG lipids at roughly the same lateral pressure. Deviations from π_{low} result from the

imprecise definition of the pressure baseline. Beyond this transition pressure, the PEG chain is supposed to in the so-called *mushroom-like* conformation (see left side of figure 6.3) [92, 98, 99]. Although the polymers did desorb from the interface, they maintain in their coiled conformation. At an additional transition, which occurs at $\pi_{\text{high}} = 20{-}40\,\text{mN/m}$ and is not resolved in figure 6.3, it is predicted that the polymer transfers into a stretched, so-called *brush-like* conformation [92, 98, 99]. Here, the polymer is elongated to reach almost its contour length L_c, which can be calculated by $L_c = a{\cdot}N$. The exposed oxygen atoms of the PEG chains can now intercalate water molecules via hydrogen bonds to other polymers, thus forming a gel [92, 99]. This behavior was elucidated from rheological measurements, which showed that beyond the high-pressure transition the storage modulus is the dominating component while below the loss modulus mainly contributes to the monolayers viscoelasiticity.
As a consequence of the hydrophilic carbohydrate tail, the interaction of lipopolymer with the subjacent water is increased, in comparison to regular lipids. This is mediated by an augmented number of hydrogen bonds, amplifying the coupling to the viscous water phase.

6.2. Impact of Lipopolymers on Lipid Monolayer Waves

The local displacement of lipids during a longitudinal monolayer wave, induces streaming of water in superficial layers of the aqueous sub phase. This results from the ability of the lipid headgroup to engage hydrogen bonds, which mediate the movement further into the bulk. The affected region of water is referred to as the hydration layer of a lipid monolayer. An additionally attached hydrophilic polymer increases the number of possible hydrogen bonds with the water, which increases the coupling. As a consequence, the attached polymer expands the thickness of the hydration layer, which is a term for water that needs to be dragged along with a longitudinal pulse. This is expected to amplify the viscous forces experienced by the wave. The central subject of this section is to demonstrate the implications of the hydration layer for lipid monolayer waves. It is composed of a first part that majorly focuses on the damping of pulses propagating in glycolipid monolayers, supplemented by a second part, investigating variations of the velocity profile of the wave.

6.2.1. Hydration layer determines viscous forces

In order to determine the impact of a lipid-bound carbohydrate on the properties of a longitudinal, interfacial wave, a monolayer of the respective PEG-lipid is spread on

a water surface in a Langmuir trough and investigated with the same experimental arrangement as described in chapter 3. Pressure pulses are therefore evoked by fusion of a solvent drop with the air/water interface that consisted of PEG-conjugated lipids. Table 6.1 presents the influence of the polymer in general and its length in particular on the monolayer wave. A strong reduction in pulse amplitude was observed for all solvent types probed. Moreover, it was found that the pulse amplitude is clearly decreasing with increasing length of the PEG-chain.

Lipid	3 $\mu\ell$ Ethanol	3 $\mu\ell$ 1-Propanol	3 $\mu\ell$ 1-Pentanol
DPPC	0,91mN/m	1,89mN/m	4,4mN/m
DSPE PEG 350	0,12mN/m	0,98mN/m	1,6mN/m
DSPE PEG 2000	0,03mN/m	0,18mN/m	0,5mN/m

Table 6.1.: Pulse amplitudes at a surface pressure of $\pi \approx 20\,\mathrm{mN/m}$ on the respective lipid systems at 24°C.

Since the amplitudes of pulses excited by means of ethanol are too small for a thorough analysis of the properties of the wave, 1-propanol was chosen instead to probe the entire pressure range accessible (compare section 4.1.1). The left part of figure 6.4 displays the amplitudes of pulses excited by 1-propanol in a DSPE PEG 350 monolayer and illustrates their correlation with the isothermal compressibility. In accordance with equation 4.2, the amplitudes are related to the inverse of the

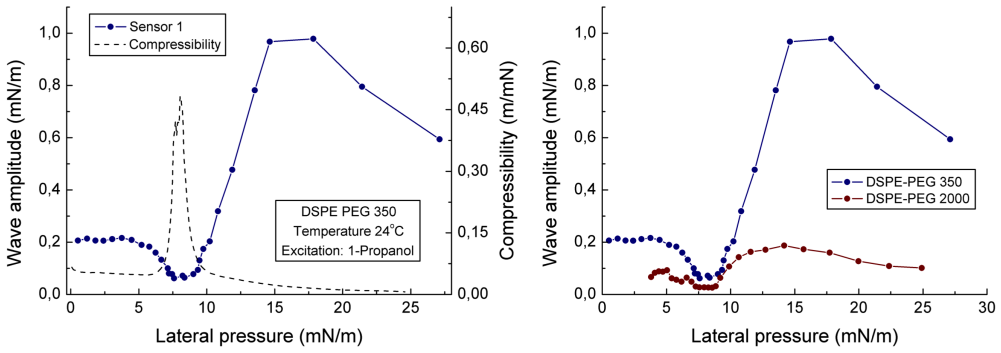

Figure 6.4.: Left: Amplitude of pulses excited in monolayers consisting of DSPE PEG 350 at 24°C. The minimum in amplitude coincides with the compressibility maximum. **Right:** Comparison of pulse amplitudes for monolayers of DSPE-PEG 350 or DSPE-PEG 2000.

compressibility, with a pronounced minimum in the phase transition region. The decreasing excitability at high pressures is again interpreted by the reduced solvent solubility within the lipid matrix at these membrane pressures. Qualitatively, the

same behavior was observed for the longer PEG-chain, as illustrated in the right part of figure 6.4. Despite the overall reduction of pulse amplitudes due to the increased number of monomers, the compressibility-amplitude correlation is conserved.
The reduction of the pulse amplitudes, which depends on the number of ethylen glycol monomers attached to the lipid head, is a consequence of the increased interaction with the bulk water and the additional weight of the lipopolymer. This results on the one hand from the polymer chain itself and on the other from the water bound to it. At a constant force applied to the interface ($3\mu\ell$ of 1-propanol), the acceleration of lipids is expected to scale with its weight according to Newton's second law $a = F/m$. This consideration enters the monolayer wave equation via the inertia term used in the Euler equation. However, this initial explanation is not sufficient for the observed amplitude reduction, since the entire lipid mass is only increased by a factor of $f_{\text{Lipid}} = \frac{M(\text{DPPC})}{M(\text{DSPE PEG 2000})} \approx 4$, while the amplitude diminishes by a factor of $f \approx 10$ (compare table 6.1). Generally, a major factor contributing to the decrease in amplitude seems to be the extension of the interfacial water layer due to the presence of PEG-chains. This might be particularly important beyond the transition pressure of $\pi \approx 10\,\text{mN/m}$. The increased hydration layer thickness amplify the viscous force exerted by the water on the monolayer and thereby not only affect the amplitude of the wave, but also its velocity, which is the emphasis of the next section.

6.2.2. Alteration of the velocity profile

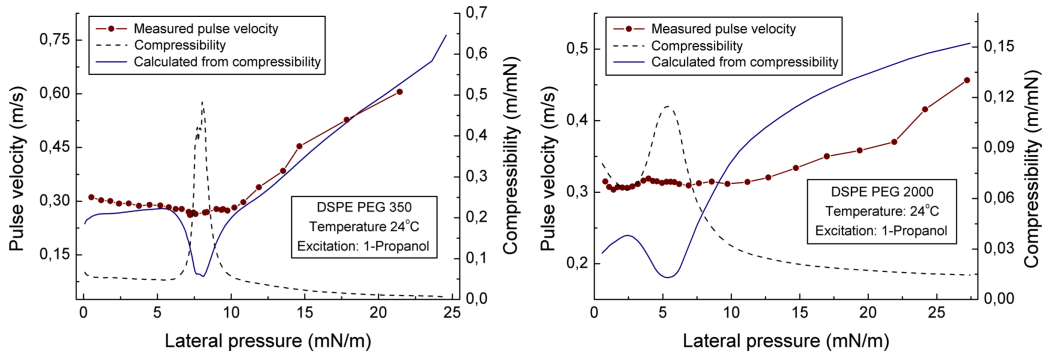

Figure 6.5.: Velocity of pulses excited in PEG-lipid membranes in comparison to values calculated from the monolayer compressibility by means of equation 3.18 **Left:** Velocity profile for a monolayer consisting of DSPE PEG 350 at 24°C. **Right:** Velocity profile for a membrane consisting of DSPE PEG 2000 at 24°C.

As mentioned above, the application of 1-propanol as excitation solvent ensures sufficiently large pulse amplitudes for a full analysis of the velocity profile. The

arrival times of the pulses at the laterally separated pressure sensors are extracted in the same manner as has been explained in section 3.4.
Figure 6.5 displays the results obtained for two different polymer chain lengths. A widely constant pulse velocity was observed for DSPE-PEG 350 monolayers at low membrane pressures. After the maximum in compressibility an steady increase of the velocity was obtained. When compared to velocities that were calculated from the isothermal compressibility by means of the lipid monolayer wave equation 3.18, a relatively good correlation with the experimental results is obtained; except for the predicted minimum at the transition pressure (here: $\pi_{\text{trans}} \approx 8\,\text{mN/m}$). This correlation between calculated and experimentally obtained velocities is clearly worse for DSPE-PEG 2000 monolayers. Here, the velocity spectrum seems linearized over almost the entire range of pressures probed, with a slight increase for large lateral pressures. A comparison of measured and calculated velocities no longer shows any correlation.

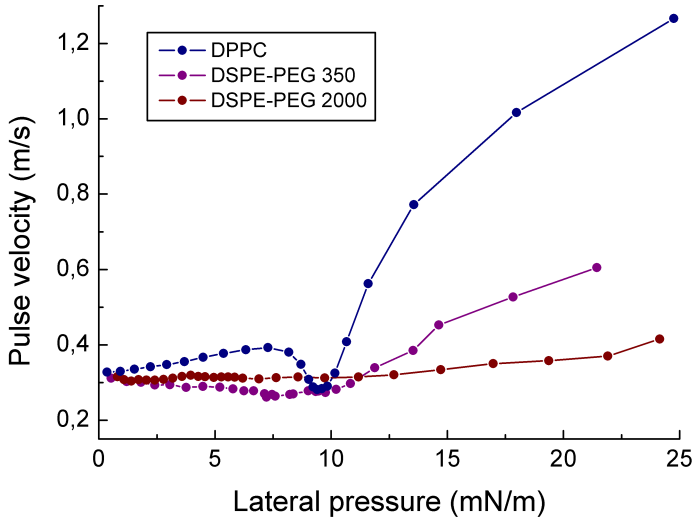

Figure 6.6.: Comparison of the velocity profile for lipid and PEG-lipid membranes. With increasing chain length of the PEG-moiety the pulse velocity approaches an almost constant value ($c \approx 0.3\,\text{m/s}$ for the longest chain probed (PEG 2000)).

The pulse velocities for PEG-lipid monolayers are summarized in figure 6.6 and furthermore compared to the velocity profile of a DPPC membrane. While the differences between the three systems are only minor at low membrane pressures ($\pi < 10\,\text{mN/m}$) two characteristics were observed for higher lateral pressures:

1. A reduction of pulse velocities in PEG-lipid as compared to DPPC monolayers

2. The longer the PEG-chain, the more drastic the reduction in pulse velocity.

These trends can be explained by taking the atomic structure of the PEG lipid into consideration.
As described in chapter 3, the lateral displacement of a regular lipid in course of a longitudinal wave induces flow within the subjacent bulk water which in return exerts a viscous force on the lipid monolayer. Within the realm of the monolayer wave equation 3.18, this effect is expected to cause a slowing down of pulses. When a lipopolymer is employed, additional hydrogen bonds can be engaged, according to the hydrophilic nature of the attached hydrocarbon chain. This basically leads to an enlargement of the hydration layer and amplifies the viscous force experienced by the monolayer. Moreover, the interaction with the bulk water alters accordingly to the conformation of the polymer, which was shown to depend on the lateral membrane pressure and area (see Alexander - de Gennes theory of grafted polymers [96, 97] or section 6.1). Thus, each polymer conformation needs to be discussed:

- **Pancake-like conformation:** At low membrane pressures ($\pi < 10\,\mathrm{mN/m}$), the polymer chains are floating up, mainly laying on the aqueous interface [98]. The resulting hydration layer is rather thin. The PEG chains therefore only interact with surface water and display only a minor impact on the amplitudes and velocities of solvent-excited waves.

- **Mushroom-like conformation:** At intermediate pressures of the PEG-lipid membrane ($10\,\mathrm{mN/m} < \pi < 20\,\mathrm{mN/m}$), the hydrocarbon chains are increasingly submerged into the sub phase and maintain a coiled conformation. This structural arrangement is mainly due to entropic forces. The thickness of the hydration layer depends on the number of monomers and can be estimated from the Flory radius (compare section 6.1: $R_F(\mathrm{PEG\ 350}) = 11.2\,\text{Å}$ and $R_F(\mathrm{PEG\ 2000}) = 34.4\,\text{Å}$). These considerations underline that a higher viscous drag is exerted by the longer PEG chain. In agreement with the monolayer wave equation 3.18, higher viscous forces lead to a decrease in pulse velocity (see figure 6.6).

- **Brush-like conformation:** At high membrane pressures ($\pi < 20\,\mathrm{mN/m}$), the polyethylene glycol chain is in a stretched state and probably reaches its complete contour length L_c which exceeds the Flory radius by far. Thus, more oxygen atoms are exposed which increases the potential for forming hydrogen bonds. This amplifies the viscous forces and results in an additional reduction of the pulse velocity.

6.3. Possible impact for biology

The glycocalyx is an essential characteristic of eukaryotic cells. This allows to speculate about the possible impact of the presented effects of lipopolymers on longitudinal monolayer waves in the framework of cell-cell communication. As was shown, the increased interaction with the bulk water phase, according to the hydrophilic nature of the hydrocarbon chains, decreases the amplitude upon a constant excitation force. This was explained by an amplification of viscous forces that consequently hampers the propagation of longitudinal waves. Pressure pulses conducted within a cell membrane would thus experience an increase of damping according to the presence of glycolipids and -proteins. The overall amount of the amplitude reduction should thereby depend on the fraction of glycolipids to regular lipids and the average length of the polymer chains.
The velocity profile of the longitudinal waves was also found to be affected. Here, the presence of the hydrocarbon chain reduced the influence of the monolayer compressibility and linearizes the velocity profile to a constant value of $c \approx 0.3\,\mathrm{m/s}$. Thus, the glycocalyx would not only be responsible for the mechanical protection and stabilization of the cell, but also would diminish influences from lateral membrane pressure variations onto the pulse velocity. This would in general improve the conditions for signal conduction, since the time required for propagating a certain distance becomes more or less fixated.
In conclusion, the reduction in amplitude diminishes the effects described so far for the lateral density pulses, which propagate within cell membranes. Nevertheless, pressure pulses are still observable over macroscopic distances ($d = 30\,\mathrm{cm}$), indicating a decreasing, but not abolishing effect of the hydrocarbon layer.

6.4. Summary Lipopolymers

The effects of lipid-bound hydrocarbon chains on longitudinal lipid monolayer waves were investigated. A decrease of amplitude and velocity of solvent excited pressure pulses was observed and attributed to additional viscous drag. The latter is a result of the hydrophilic nature of the PEG moiety, which increases the interaction with the bulk water phase. The chain length of the polymer determines the thickness of the hydration layer and consequently the magnitude of the viscous forces. The hydration layer thickness was also found to correlate with the PEG molecule conformation, which differs depending on the lateral membrane pressure. Moreover, the introduction of PEG-lipids leads to a linearization of the wave velocity over the entire range of surface pressures.

Chapter 7: Blockage of Lipid Monolayer Waves by Lanthanides

The effects of lanthanide ions such as Gadolinium (Gd^{+3}) and Lanthanum (La^{+3}) on the static properties of lipid membranes have been studied extensively. As a result of their high charge density, the threefold charged lanthanides dominate when introduced to an ionic background of mono- and divalent salts. In the vicinity of a charged membrane, mono- and divalent ions form a diffusive layer, which compensates and screens surface charges. Lanthanides, on the contrary, are able to approach the membrane completely according to the strong electrostatic interaction. This already indicates the potency of lanthanides to establish an ionic bond to the membrane. It has also been found that they are capable of displacing e.g. Ca^{+2} from its lipid binding sites [100]. Phospholipids are characterized by a particularly high tendency to bind lanthanides. This is probably due to the complexation potential of phosphoric acid [101, 102]. As a consequence, lanthanides are known to influence and shift phase transitions of phospholipids [103–107], to induce domains [101, 105, 108] and pores [108, 109], to strongly affect the surface potential [110] and furthermore to causes shape changes [111] and leakage of vesicles [100].
In physiology, lanthanides and in particular Gadolinium are known to non-specifically block stretch-activated ion channels at submillimolar concentrations [112]. Considering the diversity of channels (Na^+, K^+, Ca^{2+}) sensitive to Gadolinium [113], a common lipid-based mechanism was proposed to underlie this blocks. Recently this hypothesis was supported by the finding that mechanosensitive channels can be effectively blocked by Gd^{3+} *only* when they are constituted in a negatively charged lipid membrane [114]. This effect was attributed to the ability of Gadolinium ions to reduce membrane fluidity by inducing lipid compaction. Molecularly, this compaction of the lipid matrix is thought to compress the protein ion channel at its trans-membrane site, thus favoring its closed state. Theoretically, this view has been supported by calculations which indicate that changes in the lateral membrane pressure profile can alter the open probability of ion channels [115, 116].
This chapter investigates the effects of lanthanides on lipid monolayer waves. By starting to elucidate the impact of lanthanides on the static properties of membranes

established from mixtures of DPPC and DPPG, the interpretation of subsequent dynamic wave experiments will be facilitated. The effect of lanthanides on monolayer structure and phase behavior will primarily be studied with isotherms and fluorescence microscopy. Subsequently, a comprehensive study about the impact of Gadolinium on the dynamic properties of the monolayer and on its excitability. Finally, the experimental findings will be discussed regarding their potential relevance for physiological phenomena (i.e. ion channel blockage).

7.1. Impact of Lanthanides on charged lipid monolayers

When a charged membrane is immersed into an electrolyte solution, it attracts a cloud of charged counterions which screens the surface potential (see section 2.4). The resulting Debye length is a measure for the average distance of the ion cloud to the membrane and depends on the ionic strength as well as on the valency of the ions; with polyvalent ions being attracted most strongly to the surface. In the case of threefold charged ions, the Debye length is reduced to such a high degree that a binding constant can be assigned [100, 102]. As a consequence, trivalent ions are expected to have a pronounced impact on the phase state and structure of a charged and zwitterionic lipid monolayer. This hypothesis will be tested for a DPPC DPPG (9:1) monolayer.

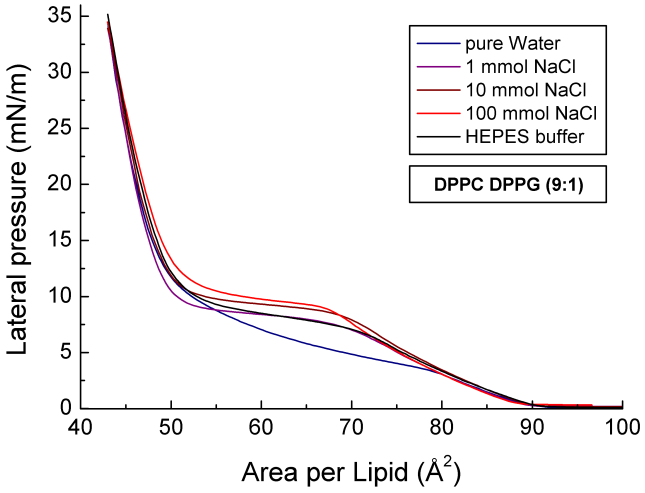

Figure 7.1.: Lateral pressure - area isotherms of a DPPC DPPG (9:1) monolayer with increasing Na^+ concentration. HEPES buffer solution (150 mmol/ℓ NaCl, 10 mmol/ℓ HEPES and pH = 7,4 adjusted with NaOH).

7.1.1. Impact of salts on π-A-Isotherms

Since all consecutive measurements are conducted on an ionic background consisting of a standard HEPES buffer, the influence of monovalent salts on DPPC DPPG (9:1) monolayers was investigated. As has been described in section 2.4, the screening of the membrane surface potential, which evolves from the charged and zwitterionic lipid headgroups, affects the phase behavior of the monolayer. It is important to highlight that the pressure-area isotherms are already altered if HEPES/NaOH (pH = 7,4; + 150mM NaCl) is used as sub phase instead of pure water (figure B.2). When successively increasing the concentration of sodium chloride in an aqueous sub phase of a lipid monolayer, it can be observed that the main impact of the charge screening, induced by monovalent salts, is an upwards shift of the transition pressure. This effect saturates, when all charges are screened. A combination of ions as in the HEPES buffer system therefore displays a similar effect, while the exact charge distribution within the diffusive layer will depend on the specific ions used and their corresponding concentrations. The resulting isotherm of a screened DPPC DPPG (9:1) monolayer resembles the isotherm of a pure DPPC membrane, which bares no net surface charges. It is therefore can be concluded that the influence of the employed ionic background (HEPES buffer) can be reduced to diffusive screening of charges.

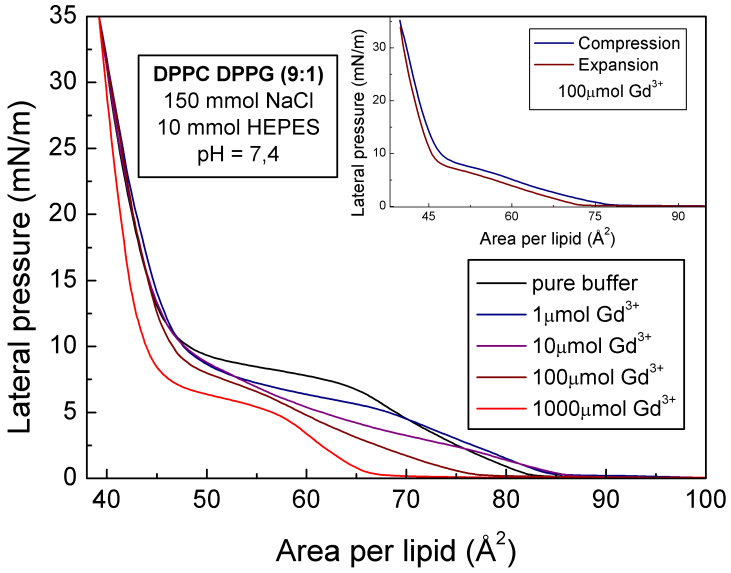

Figure 7.2.: Lateral pressure - area isotherms of a DPPC DPPG (9:1) monolayer with increasing Gd^{+3} concentration in the sub phase (150 mMol NaCl, 10 mMol HEPES and pH = 7,4 adjusted with NaOH +1 μMol, +10 μMol, +100 μMol or +1000 μMol Gd^{+3}) *Inset:* Complete compression and expansion cycle for 100 μMol Gd^{+3}.

When Gadolinium ions are introduced to the described ionic background (HEPES buffer), the polymorphism of the lipid monolayer becomes clearly affected. Even $1\,mu$Molar Gd^{+3} concentration, which is five orders less then the concentration of NaCl in the buffer, displays a significant influence on the monolayer (see figure 7.2). This is in agreement with predictions based on the Poisson-Boltzmann equation that the ion type of the highest valency has the most pronounced impact on a membrane (compare equation A.4). Thus, the set of isotherms displayed in figure 7.2 demonstrates that the phase transition pressure is lowered upon increasing the Gadolinium concentration. Also, between 10-100 μMol of Gd^{+3}, a reduction of the average area per lipid of about $\approx 10\%$ is induced, as can be calculated from the corresponding areas at the pressure onset of the respective isotherms. This effect is continued even more drastically for higher Gd^{+3} concentrations. These observations point towards an overall compression of the lipid monolayer with increasing Gadolinium concentration. This might be due to the formation of ionic bonds between Gd^{+3} and the negatively charged phosphoric acid of the lipid head group. Similar results have been reported for DMPS[1] monolayers [114].
Moreover, the observed compaction of the membrane does not affect the macroscopic elasticity of the monolayer as can be seen in the inset of figure 7.2. The compression and expansion isotherms of a DPPC DPPG (9:1) monolayer on top of a sub phase containing $100\,\mu$Mol Gd^{+3}, display only a small hysteresis. This indicates that the lipid membrane remains elastic and therefore allows the propagation of longitudinal pressure pulses.

7.1.2. Structural changes due to Lathanide-Lipid Interaction

The finding of Gadolinium influence on the polymorphism of charged lipid monolayers in addition to reports in the literature about shifts of the phase transition of phospholipids [103–107], induction of domains [101, 105, 108] and pores [108, 109] as well as shape changes of vesicles [111] point towards a strong impact of this lanthanide ion on the structure of lipid assemblies. Thus, to observe the impact of lanthanide ions on monolayer morphology directly, 2mol% of a phospholipid dye (NBD 16 PC[2]) was added to the membrane. The higher solubility of the dye in the liquid-expanded phase creates a contrast between the two main lipid phases. In the upper left part of figure 7.3, a picture of a fluorescently labeled DPPC DPPG (9:1) monolayer at $\pi \approx 12\,\mathrm{mN/m}$ and $T = 24°\mathrm{C}$ on a standard HEPES buffer (see section B.3) is shown. The regular pattern displays liquid-condensed domains (black spots)

[1] 1,2-dimyristoyl-sn-glycero-3-phospho-L-serine
[2] 1-palmitoyl-2-12-[(7-nitro-2-1,3-benzoxadiazol-4-yl)amino]dodecanoyl-sn-glycero-3-phosphocholine

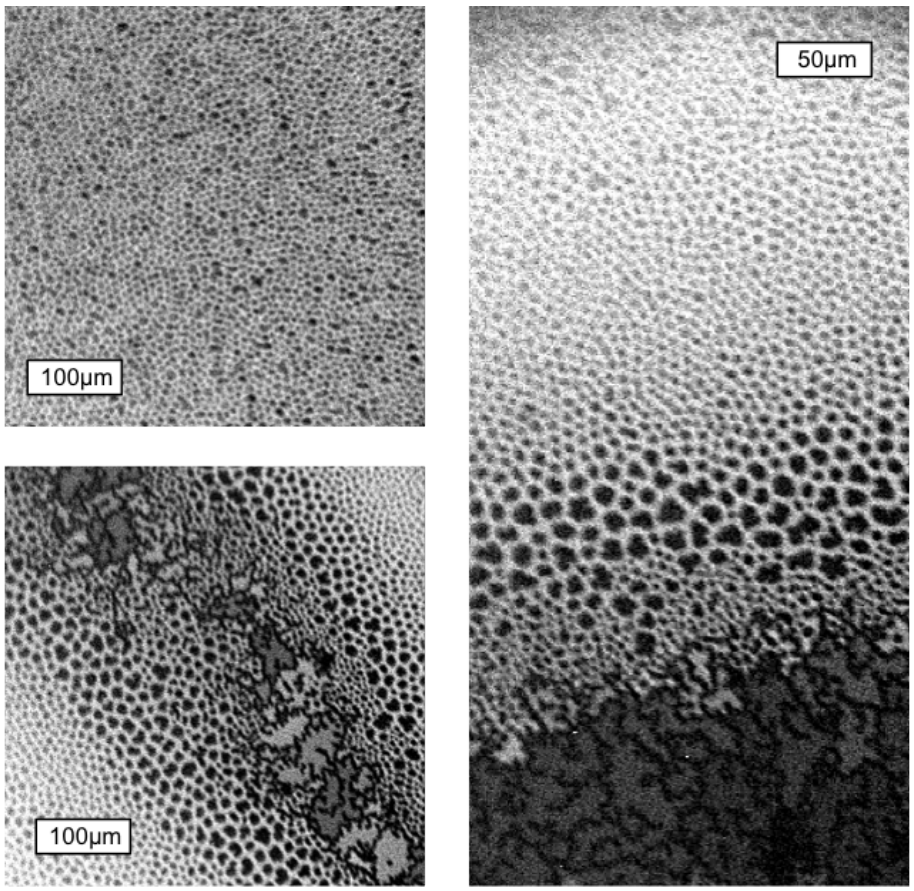

Figure 7.3.: Impact of Gadolinium ions on the structure of a DPPC DPPG (9:1) monolayer. The membrane was labeled with 2mol% NBD 16 PC, which does not alter the respective π-*A*-isotherms. **Upper left:** Membrane at $\pi \approx 12\,\mathrm{mN/m}$ on a standard HEPES buffer solution. The presence of domains indicates a phase seperation. **Lower left:** Injection of Gd^{+3} into the sub phase at a concentration of $100\,\mu\mathrm{mol}/\ell$. Figure taken subsequently after injection and without stirring or incubation. Ruptures over large areas of the monolayer are induced. **Right:** Magnification of the transition region. Beyond a transition region with increased size of liquid-condensed domains, the membrane appears almost unaltered.

of approximately equal size, randomly distributed over the interface. Since domains typically only exist in the coexistence region of the monolayers, this observation indicates that the monolayer was indeed close to the compressibility maximum.
When Gadolinium ions are injected into the sub phase to achieve a final concentration of $100\,\mu$Mol, changes in monolayer structure were observed immediately. Within 2-3 minutes after injection and without additional mixing or stirring strong alterations of the monolayer structure occurred. Regions of domains with uniform size were interrupted by structures showing an entirely different appearance with spiky shaped domains. Moreover, the reduced fluorescence intensity indicates a depletion of dye molecules within this structure and thereby identifies the liquid-condensed as

the main lipid phase. These Gd^{+3} induced structures seemed to spread in a line over macroscopic distances (orders of cm), while being surrounded by mostly circular liquid-condensed domains of increased size. The prevalence of the liquid-condensed phase thus solidifies this region of the membrane, which can also be observed live by the microscope. Here, the reduced fluidity was evaluated by a strongly diminished domain movement. This solidification is in good agreement with literature [117], where it was shown that Gd^{+3} e.g. causes a rigidification of the red blood cell membrane. Beyond the rim of the rupture, the membrane remains almost unaltered and displays again domains of approximately equal size, randomly distributed.
The effects observed can therefore be summarized as that the injection of Gd^{+3} into the aqueous sub phase of a charged lipid monolayer subsequently induces macroscopic structures, where the lipids are mainly in the liquid-condensed phase. This reduces the required average area per molecule, which can be compared to the compaction of the monolayer observed in pressure - area isotherms presented above.

7.2. Influence of Salts on Lipid Monolayer Waves

The impact of Gadolinium ions on the static properties of charged lipid monolayers implies that the addition of these ions to the sub phase will also affect longitudinal lipid monolayer waves.

7.2.1. Influence of Mono- and Bivalent Salts on Lipid Monolayer Waves

The addition of monovalent salts to the aqueous sub phase of a charged lipid monolayer does indeed alter its static properties as *e.g.* the phase transition pressure (figure B.2). In order to elucidate the impact on its dynamic characteristics, longitudinal lipid monolayer waves were excited as described in chapter 3. The introduction of monovalent salts (10 mMol of NaCl or TEA[3]Cl) to the pure aqueous sub phase of a DPPC DPPG (9:1) monolayer does not display strong effects on the properties of the wave as velocity or amplitude. The corresponding velocity profiles range from $c \approx 0.3\,\mathrm{m/s}$ for the liquid-expanded to $c \approx 1\,\mathrm{m/s}$ in the liquid-condensed phase as can be seen in the left part of figure 7.4. The pulse velocities can furthermore be calculated from the respective isothermal compressibility profile, which varies slightly in accordance to the ion type and concentration used for the screening of monolayer surface charges.
Monovalent salts can also affect the dynamic properties of neutrally charged, zwitterionic lipid monolayers. This was demonstrated by excitation of pulses on a DPPC

[3]Tetraethylammonium

membrane with 10 mMol NaCl or 10 mMol TEA Cl in the bulk water phase. When calculating the adiabatic compressibility from the pulse velocities via equation 5.12, a reduction of the adiabatic compressibility maximum results under the influence of monovalent salts. Thus one can state that even the dipole moment of the neutrally charged headgroup allows the interaction with the monovalent ions dissolved in the sub phase.

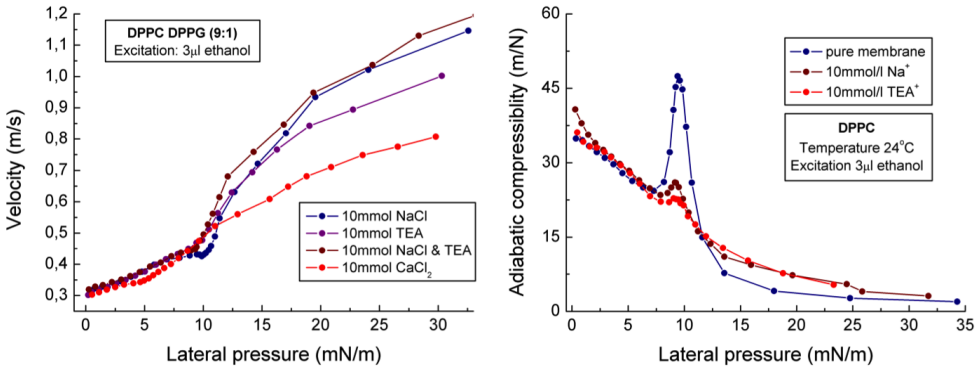

Figure 7.4.: Left: Velocities of ethanol-induced pulses in a DPPC DPPG (9:1) monolayer under the influence of mono/bivalent salts. While monovalent salts only slightly alter the velocity profile, bivalent salts tend to linearize the pressure-velocity relationship by reduction of the pulse velocity in the liquid-condensed phase. **Right:** Adiabatic compressibility of a DPPC monolayer under the influence of monovalent salts calculated from pulse velocity measurements.

While monovalent salts only have a minor influence on the dynamic properties of a DPPC DPPG (9:1) membrane, addition of Ca^{+2} to the sub phase leads to a linearization of the membrane pressure - pulse velocity relationship. This is especially due to a reduction in propagation velocity in the liquid-condensed phase. This result is counterintuitive since the literature describes a reduction in fluidity of the membrane upon interaction with highly charged ions and thus one would rather expect an increase in pulse velocity. Thus, one could speculate about alterations of the interfacial water structure induced by Ca^{+2}, which might improve the interaction with the aqueous sub phase. This would cause the pulse to slow down in accordance to equation 3.18, as was demonstrated in the preceding chapter 6 with PEG-lipids.

7.2.2. Impact of Gadolinium on Lipid Monolayer Waves

As has been shown for the static properties of a DPPC DPPG (9:1) monolayer, the introduction of a submillimolar concentration of Gd^{+3} to the aqueous sub phase does alter the dynamic characteristic of the membrane as well (figure 7.5). While the influence of Gadolinium ions at low membrane pressures ($\pi < 15\,\mathrm{mN/m}$) is negligible,

it becomes strongly amplified with increasing Gd^{+3} concentration and membrane pressure. In both graphs a distinct alteration of pulse velocities and amplitudes can be observed between 1 and 10 μMol Gadolinium, indicating a threshold concentration necessary for the binding of Gd^{+3} to the phospholipid membrane.

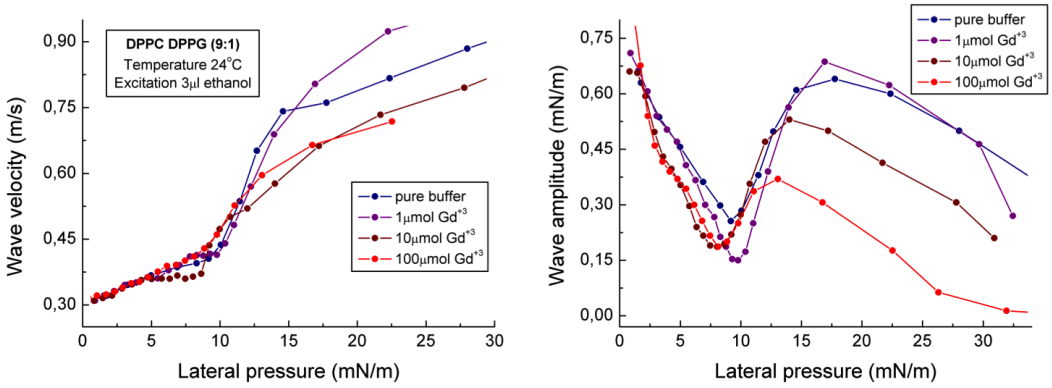

Figure 7.5.: Left: Pulse velocities are increased at higher membrane pressures and only slightly affected by the concentration of Gd^{+3}. **Right:** Characteristic dependency of the wave amplitude on the lateral membrane pressure with a pronounced minima at the monolayer phase transition.

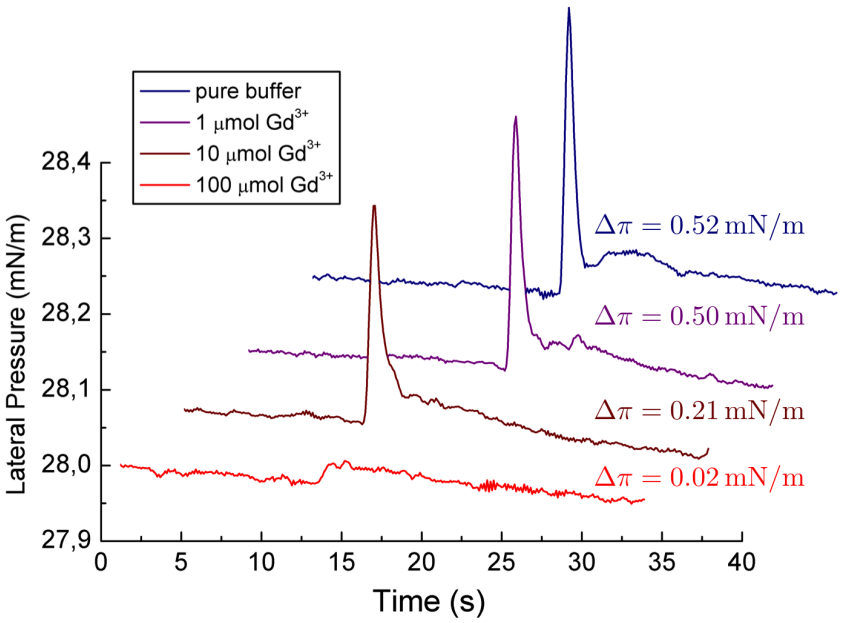

Figure 7.6.: Time-resolved recording of lateral pressure pulses on a DPPC DPPG (9:1) monolayer with different Gd^{+3} concentrations in the aqueous sub phase.

Further indications for a binding threshold are given when the amplitudes of the

pressure pulses are considered (figure 7.5). While the pulse amplitude is relatively independent of the Gd^{+3} concentration in the liquid expanded phase, it is strongly diminished in the liquid-condensed phase with increasing Gd^{+3} concentration. This is most apparent at the monolayer-bilayer equivalence pressure of $\pi \approx 30\,\mathrm{mN/m}$ [114], where the pulse amplitude drops from $\Delta\pi \approx 0,5\,\mathrm{mN/m}$ in the pure buffer case to $\Delta\pi \approx 0\,\mathrm{mN/m}$ for a Gadolinium concentration of $100\,\mu$Mol. Figure 7.6 displays this effect in more detail. Here, the raw data of pressure pulses excited with $3\,\mu\ell$ drops of pure ethanol on a DPPC DPPG (9:1) monolayer at $T = 24°\mathrm{C}$ and $\pi \approx 28\,\mathrm{mN/m}$ with increasing Gadolinium concentration in the sub phase are plotted. At a concentration of $100\,\mu$Mol Gd^{+3} the propagation of a lateral density pulse is strongly impeded and eventually appears as a little shift in baseline pressure. This suggests a concentration threshold between 10 and $100\,\mu$Mol Gd^{+3}.

7.2.3. Reduction of Excitability

The presented result of a threshold concentration of Gadolinium ions, at which the amplitude is strongly reduced, motivated further experiments to investigate the excitability of the lipid monolayer. This was conducted on a similar basis as in chapter 4, where it was shown that the wave amplitude depends linearly on the ethanol concentration of the excitation solution (see equation 4.2). In the following, this effect

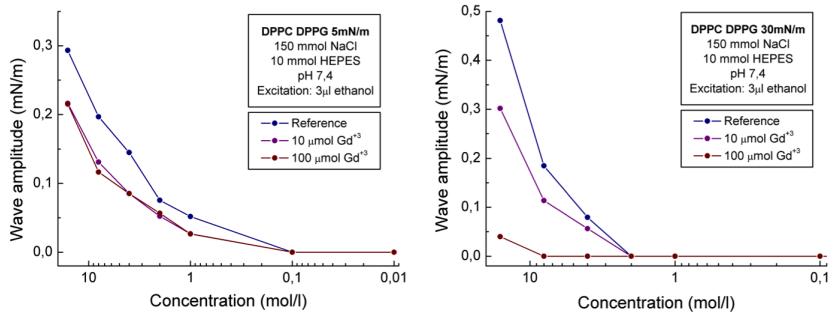

Figure 7.7.: Probing excitability of a DPPC DPPG (9:1) monolayer with and without Gd^{+3} (10 or 100μMol in the sub phase by increasing the concentration of ethanol in the excitation solvent $(0,1; 1; 2; 4; 8; 16\,\mathrm{mol}/\ell)$. **Left:** At low membrane pressures ($\approx 5\,\mathrm{mN/m}$) only a slight reduction of the excited pulse amplitudes was observed with Gd^{+3} in comparison to reference measurements. **Right:** At higher membrane pressures ($\approx 30\,\mathrm{mN/m}$), excitability is strongly reduced up to almost complete inhibition of pulse propagation at $100\,\mu$Mol Gd^{+3}.

is further employed in order to probe the excitability of a DPPC DPPG (9:1) monolayer under the influence of Gd^{+3}. The usage of a logarithmic scale on the abscissa allows thereby to display a wider range of concentrations and transfers the linear

correlation into an exponential curve as can be seen for both reference measurements (on HEPES buffer) in figure 7.7. Here, the left side shows the membrane excitability for the liquid-expanded state ($\pi = 5\,\mathrm{mN/m}$), while on the right the situation in the liquid-condensed phase ($\pi = 30\,\mathrm{mN/m}$) is depicted. The comparison of both reference measurements indicates that a higher minimum concentration of ethanol is required in the liquid-condensed phase in order to excite a pressure pulse. Also, as expected from the inverse correlation between compressibility and wave amplitude given by equation 4.2, the absolute measured amplitude is higher in the liquid-condensed phase.
The addition of Gadolinium ions to the HEPES buffer reduces the excitability of the membrane (figure 7.7). While in the liquid-expanded phase only a slight decrease of the pulse amplitude was detected, the effects were even more pronounced in the liquid-condensed phase. Gd^{+3} almost completely inhibits the pulse excitation at a concentration of $100\,\mu$Mol, which agrees with results presented above. In addition to the reduction in pulse amplitude, the threshold concentration at which a pressure pulse can be detected, is shifted towards higher concentrations of ethanol.

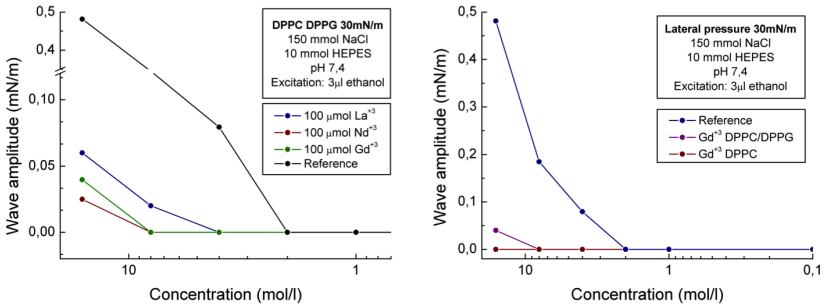

Figure 7.8.: Probing excitability of a DPPC DPPG (9:1) monolayer by increasing the concentration of ethanol in the excitation solvent ($0, 1; 1; 2; 4; 8; 16\,\mathrm{mol}/\ell$). **Left:** Lanthanides are investigated for their pulse inhibition potency at a membrane pressure of $\approx 30\,\mathrm{mN/m}$. Similar behavior is observed for all lanthanides, with a sequence of $La^{+3} > Gd^{+3} > Nd^{+3}$. **Right:** Inhibition of pulses in charged (DPPC DPPG (9:1)) and neutrally charged (DPPC) monolayers.

In most studies in the literature, it has been indicated that Gd^{+3} and other lanthanides have similar effects on lipid membranes. These effects are in general ascribed to the potency of lanthanides to bind to the lipid membrane [100–103]. By following this line of argument, a similar process is considered here for the reduction of excitability. To test this hypothesis, Lanthanum and Neodymium were chosen as representatives to probe the excitation impediment due to lanthanide binding. For this purpose, excitability of a DPPC DPPG (9:1) monolayer was studied at $\pi \approx 30\,\mathrm{mN/m}$ for the three mentioned lanthanides (figure 7.8, left). As expected, excitability was strongly reduced for all three lanthanides as compared to the ref-

erence measurement. Moreover, the resulting amplitudes scale accordingly to the series $La^{+3} > Gd^{+3} > Nd^{+3}$, which might reflect the tendency of the respective lanthanides to bind to the phospholipid monolayer.
As illustrated in figure 7.8 (right), this reduction of excitability is not selective for negatively charged membranes, but also applies to neutrally charged monolayers with a remaining dipole moment. In accordance to literature [102, 107] this might indicate that the phosphoric acid group is the main interaction site of the Gadolinium ion with the phospholipid.

7.3. Discussion

7.3.1. Influence of Gadolinium on lipid membranes

The pronounced influence of Gadolinium and other lanthanide ions on negatively and neutrally charged phospholipid assemblies has been described in the literature [100–111] and was further investigated above. In summary one can state that the strong affinity of a threefold charged rare earth ions to the phosphoric acid group of phospholipids [102] results in the formation of lipid-lanthanide complexes [101]. The resulting stoichiometry of two or three lipids per lanthanide ion [100, 106] leads to crosslinking of lipids and thus to a compaction and solidification of the lipid membrane. Evidence in favor of this interpretation was obtained from the respective π-A-isotherms of DPPC DPPG (9:1) monolayers with increasing Gadolinium concentration in the sub phase. The average area per lipid was clearly reduced as compared to the reference (see figure 7.2). In other lipid systems a similar type of behavior has been observed [114]. Moreover, it was shown by fluorescence microscopy that lanthanide ions did drastically alter the membrane structure by inducing macroscopic patches of the liquid-condensed phase. This would account for the compaction of lipids and the overall reduction in membrane fluidity. These changes in membrane structure might also be a possible explanation for the previously observed increase of leakage of vesicles in the presence of lanthanides [100].
The reduced excitability of lipid monolayers upon ethanol excitation might be explained by the binding of Gadolinium to the lipid head groups. When a lipid membrane is exposed to ethanol molecules, these dissolve within the lipid matrix and mainly remain in the head group region [115]. A deeper penetration is unfavorable due to the relatively polar character of ethanol as compared to the membrane forming lipid. Thus, the strong binding of Gadolinium to the lipid head [102] might limit the interaction of ethanol with the lipid, since both molecules have to compete for the phosphoric acid as the respective binding site.
The compaction of the lipid membrane due to lanthanide binding will also alter its lateral pressure profile. Incorporated molecules as e.g. ion channel proteins would

thus experience an increased lateral pressure around their transmembrane domain, favoring configurations of reduced average size. It was calculated that especially a lateral pressure increase in the region of the lipid head group, compared to the center of the membrane, will cause ion channels to favor their closed state [115, 116]. Since the interaction site of lanthanides with lipids is supposed to be exclusively the phosphoric acid group [102], located at the lipid head, the binding of lanthanides is expected to cause a decreased ion channel conductivity. These assumptions are in agreement with experiments executed on mechanosensitive ion channels, which are particularly influenced by membrane tension [118] and can be blocked by the binding of Gadolinium ions to the lipid membrane [114].

7.3.2. Solubility of channel blocking substances

The experimental application of Gadolinium is limited, due to its strong interaction with anions, which are obviously present in most buffer solutions and blood [113]. Since Gadolinium phosphates and carbonates are characterized by a rather low aqueous solubility, the injection of a $GdCl_3$ solution into buffers containing these anions will cause an immediate precipitation of the respective Gadolinium salts. As a result of this low solubility, the formed Gadolinium precipitates are highly stable and thus considered biocompatible. This and other properties have led to their use as contrast agents in nuclear magnetic resonance tomography [113]. On the other hand, the unexpected depletion of Gadolinium ions, according to simple precipitation, from the buffer solution used in biological experiments could lead to false assumptions about the impact of Gadolinium or other processes. Having these considerations about the ion solubility in mind, it is not surprising anymore that bicarbonates influence the block of ion channels by Gadolinium [119] or that pores in erythrocyte membranes, induced by Gadolinium, can be resealed when washed with EDTA[4] [108], a strong sequester of free metal ions.
But this solubility argument must then, as a consequence, apply to all substances that display toxic influence on tissue *in vivo* or in experimental arrangements. As such, one might conclude that the effects demonstrated in this chapter must be a result of the threefold charge of the ion, leading to a strong binding with negatively charged phospholipids. This hypothesis was tested among others by employing $AlCl_3$ solution, which contains trivalent Aluminum ions. These ions precipitated immediately when injected in the Ringer as well as in the HEPES buffer solution, according to the extremely low solubility of Aluminumhydroxides (AlOH) at neutral pH. Both buffers are adjusted to neutral pH$\approx 7,4$ to simulate *in vivo* conditions. Only other lanthanides display solubilities in the range of Gadolinium (compare table B.4), so that it is not surprising to obtain similar results. As a consequence of

[4]Ethylenediaminetetraacetic acid

these solubility arguments, it can be predicted that Gadolinium effects on neuronal cells or erythrocytes will highly depend on the environment's pH and will decrease with an increase in pH.
Also non-ionic toxins must obey these rules of solubility. For example the solubility of the sodium channel blocker TTX[5] is highly pH dependent. While it is soluble at pH=4,7 in acetic acid buffer, it is almost insoluble at pH=7,4. As a consequence, TTX should have a high tendency to precipitate when injected into neutral standard buffers as used *e.g.* for measurements on neuronal cells. In order to probe for lipid-based effects TTX, the toxin was introduced into the aqueous sub phase of a phospholipid monolayer. Since no obvious interaction site for the TTX within the monolayer is found, in contrast to the phosphoric acid for lanthanide ions, the TTX does not show any influence on the phospholipid membrane, as is depicted in section B.7. This might be an indicator for the requirement for certain proteins that introduce the specificity which might be necessary to explain the effects of various chemicals on neuronal cells.

7.4. Summary Lanthanides

In this chapter, the specific influence of positively charged, trivalent ions on charged and zwitterionic lipid monolayers was studied. The main emphasis was placed on Gadolinium induced blockage of pressure pulses propagating in lipid monolayers. First, the impact of Gadolinium on the static properties of a lipid membrane (DPPC DPPG (9:1)) was investigated. It was found that due to binding of the rare earth ions, a condensation of the monolayer occurred. This compression is accompanied by an induction of macroscopic liquid-condensed domains, as observed directly by fluorescence microscopy images of the lipid monolayer under Gd^{+3} influence. In excitation experiments it was moreover shown that the excitation of pressure pulses with ethanol can be effectively blocked, when the Gadolinium concentration in the aqueous sub phase exceeded $\approx 10\,\mu$Mol. This characteristic behavior was also found for other lanthanides. Since the submillimolar concentration threshold found is in the same range as necessary for the blockage of mechanosensitive ion channels by Gd^{+3}, future measurements on a black lipid membrane setup could identify, if the found influence on membrane polymorphism by Gd^{+3} is indeed responsible for the blockage of conductivity.

[5]Tetrodotoxin

Chapter 8: Collision of Lipid Monolayer Waves

The electric nature of cell-cell communication and here in particular the nervous excitation is widely studied and described by the prominent model of the Hodgkin and Huxley equation [5]. One major feature of action potentials propagating on nerve cells is the cancellation upon collision, as shown e.g. on motor nerve fibers of the toad [120]. This behavior has also been observed in vivo, where it is considered a common occurrence among cardiac cells [121]. Here it enables the homogeneity of the heartbeat through the annihilation of signals send in the backwards direction, thus regulating the harmonic contraction of cells in only one direction. Differences in the regular collision pattern are therefore assumed to induce conditions, where the heart's normal rhythm is disturbed [121]. Moreover, in numerical studies of colliding action potentials, calculated by means of the Hodgkin and Huxley equation or its simplified pendant, the FitzHugh-Nagumo model [122, 123], other regimes besides the total annihilation were found to be possible. Besides the self-oscillation of the system, a soliton-like regime was found, where pulses can penetrate each other without cancelation [124–126].

The solitary wave is furthermore the basis of another, thermodynamic approach to the nerve pulse propagation [16–18]. In this model, localized density waves are propagating as action potentials along the axon membrane of a neuronal cell, thus resembling the type of wave discussed and described so far within this thesis. A soliton is moreover a special type of wave, where nonlinear properties of the conducting media cancel dispersive effects and therefore allow the shape of the pulse to be maintained during propagation. This non-linearity in the elastic properties of the membrane can empirically be found slightly below physiological temperatures [17]. Application of this theory has among others led to a thermodynamic explanation of the Meyer-Overtone rule, describing correctly the potency of anesthesia [17, 40, 127]. Simulation of the head-on collision of these solitary waves showed the penetration of pulses as well as their stability to small amplitude fluctuations or dissipation [18, 128].

All these considerations about the collision of pulses have been carried out theoretically [18, 124–126, 128] or on real axon membranes [120, 121]. To close this gap of a missing experimental model system, this chapter presents studies on the exper-

imental collision of longitudinal density pulses within nanometer thin lipid layers. For this purpose, the excitation of longitudinal lipid monolayer waves is conducted as described earlier in this thesis 3, while a simple geometric alteration of the Langmuir trough enforces the formation of two similar density pulses, in accordance to the Huygens principle. In the following, these pulses approach each other mutually and thus eventually collide. The resulting interference pattern indicates the penetration of colliding pulses in lipid layers and thus a classical wave behavior, which is expected from the linear stress-strain relationship, described in section 4.1.2.

8.1. Experimental Arrangements

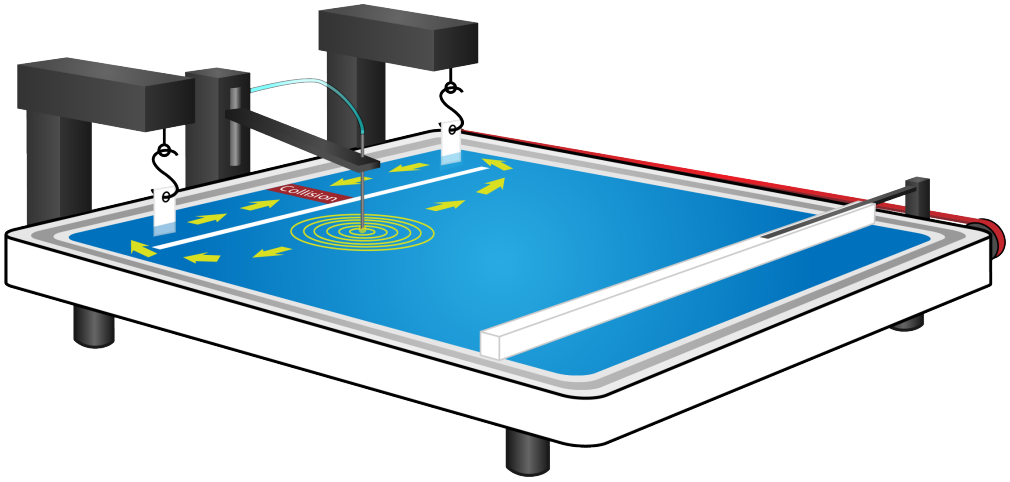

Figure 8.1.: Experimental arrangement employed for the investigation of the monolayer-pressure-pulse-collision. The film balance is equipped with two laterally separated pressure sensors to enable time resolved observation of the two approaching wave fronts. A Teflon barrier is used to separate the excitation and detection compartment, thus repressing secondary water waves and additionally to create two wave paths upon singular excitation. The delay time between the two pulses can be adjusted by lateral variation of the excitation spot. Reference measurements are executed by means of a third Teflon barrier (shown in figure 8.3), placed perpendicularly to the barriers displayed, to prohibit the second pathway.

The experimental setup employed here resembles the arrangement used so far, which is comprehensively described in chapter 3. In order to investigate the collision of lipid monolayer waves, a slight variation of the setup is introduced by the shortening of the additional barrier. This new arrangement creates an additional entrance to the detection compartment, allowing a second pathway for the excited pressure pulse. According to the Huygens principle, two identical waves are established at the entrances to the detection site (compare figure 8.1). In the following, both density pulses are approaching each other, yielding their collision within the

channel, indicated by the red dots in figure 8.1. Based on the lateral displacement of the pressure sensors, located at each end of the channel, the recording of the pulses displays the signal before and after the collision, which enables an interpretation of the occurred interference.

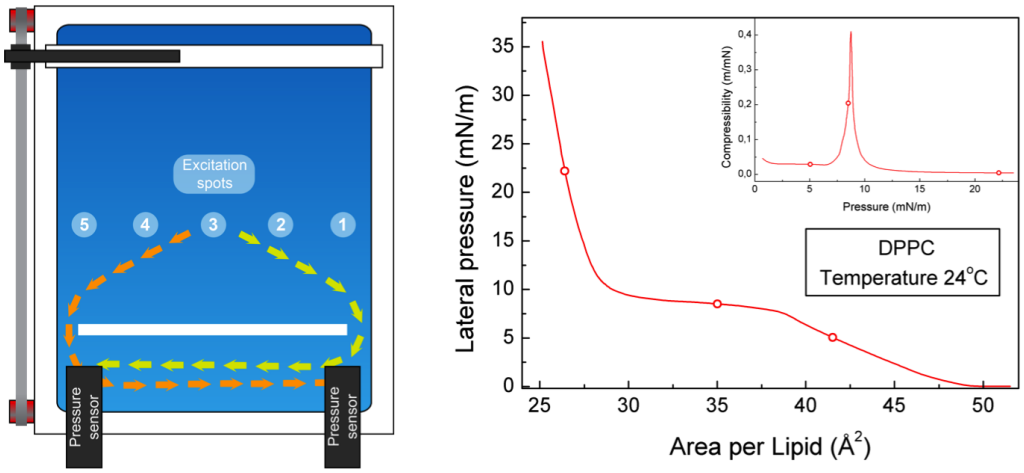

Figure 8.2.: Left: Top view of the Langmuir trough arrangement employed for monolayer wave collision. Both pulse pathways are shown, supplemented with the indication of the laterally varying excitation spots **Right:** Isotherm of a DPPC monolayer, measured prior to the collision experiment. Dots indicate the measurement points used. The inlay displays the compressibility, calculated from the slope of the isotherm.

The situation is more thoroughly depicted in the left part of figure 8.2. Here, in the top view of the Langmuir trough, both possible wave paths are shown. In addition, the variation of the excitation spot is indicated, which allows the alteration of the path difference between the two pulses and by shifting the collision spot to the left or right. As a consequence, the expected interference pattern should change coherently.

In this study about monolayer wave collision only ethanol is used as an excitation solvent, since it displays the least influence as a solvent onto the created waveform (see section 3.3). All experiments presented in this chapter are conducted on a DPPC membrane kept at 24°C, for which an exemplary isotherm is depicted alongside with its resulting compressibility in the right part of figure 8.2. The red dots, integrated into the isotherm, indicate the equilibrium pressures π_0 chosen for the various collision experiments.

Reference measurements are executed by the introduction of a third Teflon barrier, placed perpendicular to the two barriers already present (compare left part of figure 8.3). This setting prohibits the second pathway of the wave upon excitation, leading to a singular density wave passing through the detection channel. Thus, only a single pulse is detected at both pressure sensors, as can be seen in the right part

of figure 8.3 and allows to interpret subsequently appearing alterations of the pulse shape as a consequence of the collision.

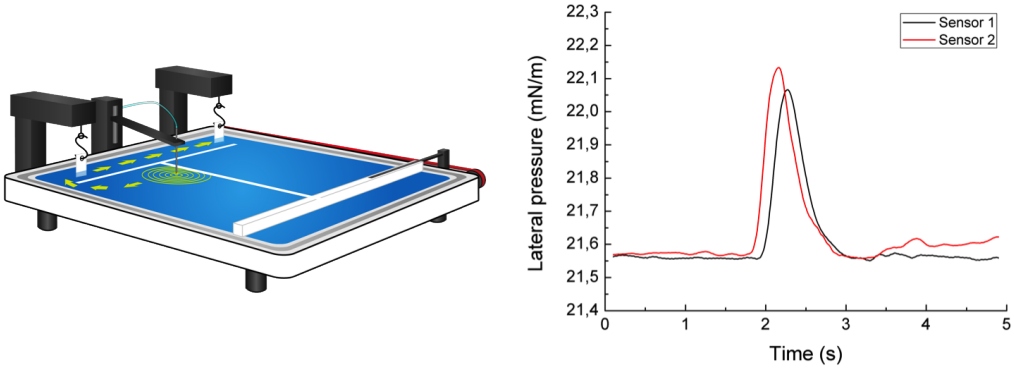

Figure 8.3.: Left: Langmuir trough arrangement used for reference measurements. An additional Teflon barrier is placed orthogonal to the other barriers, which prohibits the second pathway of the wave. **Right:** Pressure sensor reading for a reference measurement executed on a DPPC monolayer at 24°C. An equilibrium pressure of $\pi_0 = 21.6$mN/m indicates the liquid condensed phase. Only a single peak is observed at both pressure sensors upon passing of the wave.

8.2. Colliding Interfacial Waves

The annihilation of colliding pulses [120, 121] displays a distinct feature of action potentials propagating on the axon membrane. Since longitudinal monolayer waves are suggested as a possible model for cell-cell communication [23], their behavior upon collision needs to be evaluated. This is executed and presented in the following section. While the emphasis of the first part is on pulse collisions in different thermodynamic states of the membrane (red spots in figure 8.2), the second part focuses on the alteration of the interference pattern, resulting from the lateral shift of the excitation spot. The elucidated classical wave behavior will be discussed in the subsequent section.

8.2.1. Linear Superposition of Pulses

Fusion of an ethanol drop with the air/water interface of a lipid monolayer evokes a pressure pulse, which spreads over the entire area. Thus, introduction of two laterally separated entrances to the detection compartment, as demonstrated in figure 8.1, produces two mutually approaching pulses, which will consequently collide. According to the time-resolved observation of the lateral membrane pressure, the result of the colliding lipid monolayer waves can be displayed directly (left panel of figure

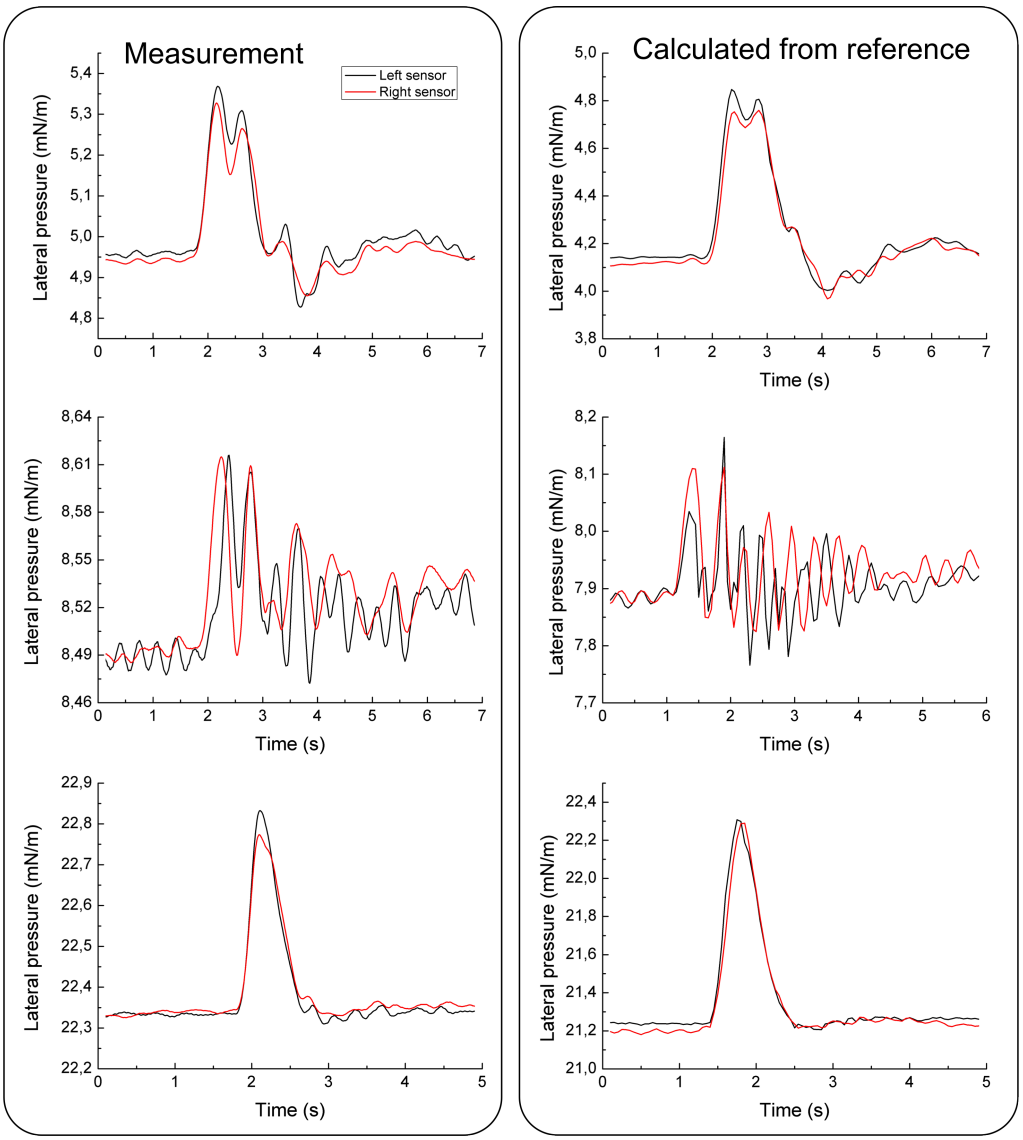

Figure 8.4.: Left panel: Collision of monolayer waves excited from the central position (3). The corresponding membrane pressures are 5, 8.5 and 22 mN/m, representing the liquid-expanded (*le*), the plateau region (*p*) and the liquid-condensed (*lc*) phase of the lipid monolayer respectively. **Right panel:** Calculation of the interference pattern through linear superposition of two reference waves. Aligned with panel on the left from top to bottom, the le, p and lc phases are displayed.

8.4). Here, measured traces of lateral pressure for all membrane states and both sensors (black & red) are displayed. Due to the excitation from the central position, which is illustrated as position 3 in the left part of figure 8.2, two symmetric wave paths are created, yielding a collision spot in the middle of the detection channel (compare figure 8.1). The penetration of the pulses upon collision is indicated by the double peak, as can be seen for the liquid-expanded state and the plateau region. According to the increased pulse velocity of the liquid-condensed phase (see figure

3.4), the two pulses are completely superimposed, thus rendering the resolution of the double peak impossible.
The empiric result of penetrating pressure pulses upon collision of longitudinal monolayer waves is additionally supported by the simple superposition of reference measurements (reference of liquid-condensed phase in the right part of figure 8.3). For this purpose, a third Teflon barrier is introduced to the experimental arrangement, which is depicted in the left part of figure 8.3. This divides the excitation compartment into two sections and thereby is prohibiting the second pathway of the wave. Excitation of a pressure pulse on each side of the additional barrier generates the two reference traces used for the linear superposition, which is displayed in the right panel of figure 8.4 for each membrane state. The extraordinary good agreement between measured and calculated pressure traces confirms the penetration of pulses and thus a classical behavior of the observed wave phenomenon.

8.2.2. Variation of the Excitation Spot

The penetration of longitudinal monolayer pulses was convincingly demonstrated for the liquid-expanded phase and the transition region, but only concluded from logical arguments for the liquid-condensed state, due to the non-observable double peak. This experimental flaw is tackled within this section by a reduction of the pulse velocity, allowing an increased time resolution, and additionally by laterally shifting the excitation spot out of the central position (compare figure 8.2). As a result of the latter, the path difference between the two approaching pulses should alter the interference pattern consequently and thus would allow a better demonstration of the classical wave behavior.
For the reduction of the wave velocity, a slightly lower equilibrium pressure of the membrane, in comparison to the experiments displayed in figure 8.4, is adjusted. In accordance with section 3.4, an equilibrium pressure of 16 mN/m yields a pulse velocity of $\approx$ 0.6 m/s, resulting in a larger, time-resolved peak-to-peak distance. When additionally excited from position number two (see figure 8.2), a double peak appears as shown in the left part of figure 8.5, demonstrating the penetration of the pulses also for the liquid-condensed phase. Moreover, the single pressure pulses can be extracted by a multiple peak fit, executed with the data evaluation software *Origin*. Here, two Gaussian peaks are used to approximate the shape of the pulses.

As can be seen, the amplitude of the pulses is decreasing with increasing distance propagated. Assuming perfect penetration of pulses and with the knowledge of the exact length of the path travelled, which is gained from geometric evaluations of the experimental arrangements depicted in the right part of figure 8.5, the damping

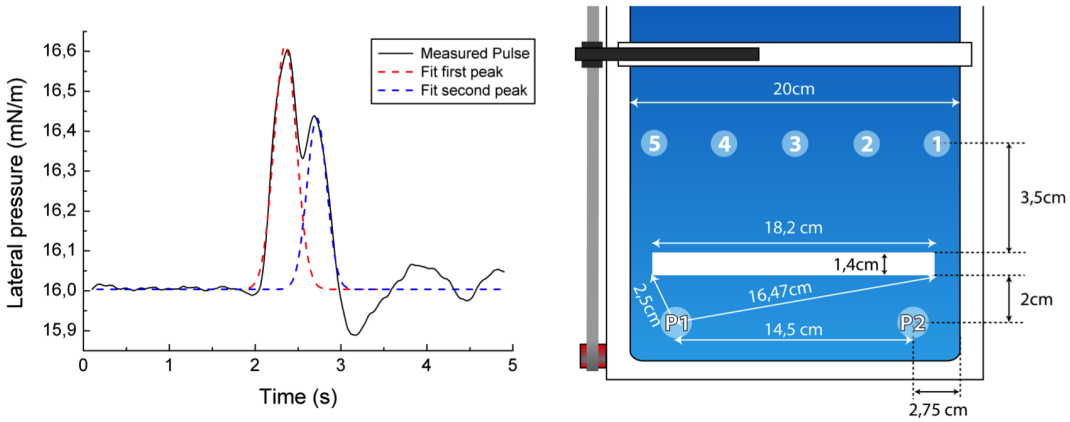

Figure 8.5.: Left: Penetration of pulses demonstrated on a DPPC membrane at 24°C at $\pi \approx 16\,\mathrm{mN/m}$. A multiple peak fit moreover extracts the single pulses from the envelope of the interference pattern, indicating the perfect penetration of pulses. **Right:** Enlarged zoom on the top view of the Langmuir trough arrangement employed for the pulse collision experiment. Lateral distances are indicated, while the overall path lengths for each respective excitation spot are summarized in table 8.1.

constant β of the lipid monolayer wave can be calculated. For this purpose, an exponentially damped pulse amplitude is assumed

$$A = A_0 \cdot \exp\left(-\frac{\Delta x}{\beta}\right) \tag{8.1}$$

, where A and A_0 are the respective amplitudes of the single pulses fitted in figure 8.5 and Δx the difference in propagation distance of the corresponding pulses. Rearrangement of equation 8.1 yields an expression for the damping constant β:

$$\beta = \frac{\Delta x}{\ln\left(\frac{A_0}{A}\right)} \tag{8.2}$$

Using the distances calculated, which are displayed for each respective excitation positions in table 8.1, one obtains:

$$\beta = 73,47\,\mathrm{cm} \pm 16,34\,\mathrm{cm} \tag{8.3}$$

This damping constant is in good agreement with literature [22, 59] and the preceding thesis concerning this subject [6], in which it was stated that the lateral dimensions of the trough ($20 - 30\,\mathrm{cm}$) are to small to experience a drastic damping of the wave.
Furthermore, the shift of the interference pattern was comprehensively studied. For this purpose, the left panel of figure 8.6 depicts the result for a consecutive shift of the excitation point from the right side of the Langmuir trough to its center. It clearly can be observed that with decreasing geometrical path difference between

the two pulses, the two pressure peaks approach each other and finally merge upon excitation from the central position. The situation reverses, when the excitation is executed from the other half of the trough (position 4 & 5 in figure 8.2; measurements not shown).

Wave path	Left sensor First pulse	Right sensor First pulse	Left sensor Second pulse	Right sensor Second pulse
Position 1	7.4 cm $\widehat{=}$ 0.12 s	21.4 cm $\widehat{=}$ 0.36 s	22.4 cm $\widehat{=}$ 0.37 s	36.4 cm $\widehat{=}$ 0.61 s
Position 2	9.6 cm $\widehat{=}$ 0.16 s	23.6 cm $\widehat{=}$ 0.39 s	18.0 cm $\widehat{=}$ 0.30 s	32.0 cm $\widehat{=}$ 0.53 s
Position 3	13.7 cm $\widehat{=}$ 0.23 s	27.6 cm $\widehat{=}$ 0.46 s	13.7 cm $\widehat{=}$ 0.23 s	27.6 cm $\widehat{=}$ 0.46 s

Table 8.1.: Summary of the path lengths according to the respective excitation position. Distances are converted into time by the assumption of a constant wave velocity of $c = 0.6\,\mathrm{m/s}$.

As conducted for the excitation from the central position (compare figure 8.4), it is attempted to calculate the pressure traces from a reference pulse by assuming classical wave behavior. Therefore, a reference pulse $\pi_t(t)$, which is measured in accordance to the trough setting displayed in figure 8.3, is shifted on the time axis by a value reflecting the time $t_{1/2}$ required for the pulse to propagate its respective path to one of the pressure sensors (see table 8.1). Additionally, the damping constant β is converted into its time pendant β_t and multiplied as an exponentially decaying factor to the shifted reference pulse. Summarizing the two pulses passing each pressure sensor upon singular excitation yields the equation:

$$\pi(t) = \pi_\mathrm{P}(t + t_1) \cdot \exp\left[-(t + t_1) \cdot \beta_t\right] + \pi_\mathrm{P}(t + t_2) \cdot \exp\left[-(t + t_2) \cdot \beta_t\right] \tag{8.4}$$

The resulting pressure traces are summarized in the right panel of figure 8.6, where each case matches the excitation situation depicted on the left panel of this figure. The similarities between the measured and calculated traces are apparent, since in both cases the distance between the double peak is decreasing and eventually the peaks are merging for the central position, demonstrating once more the classical behavior of the lipid monolayer waves. Despite the good agreement, also differences can be observed, as e.g. the asymmetric behavior of the simulated interference pattern. This might be explainable by the also asymmetric shape of the reference pulse used for calculation (compare figure 8.3).

8.3. Discussion of the Classical Wave Behavior

The results presented allow the critical discussion of lipid density waves as a possible foundation of the nerve pulse propagation. As demonstrated, the penetration

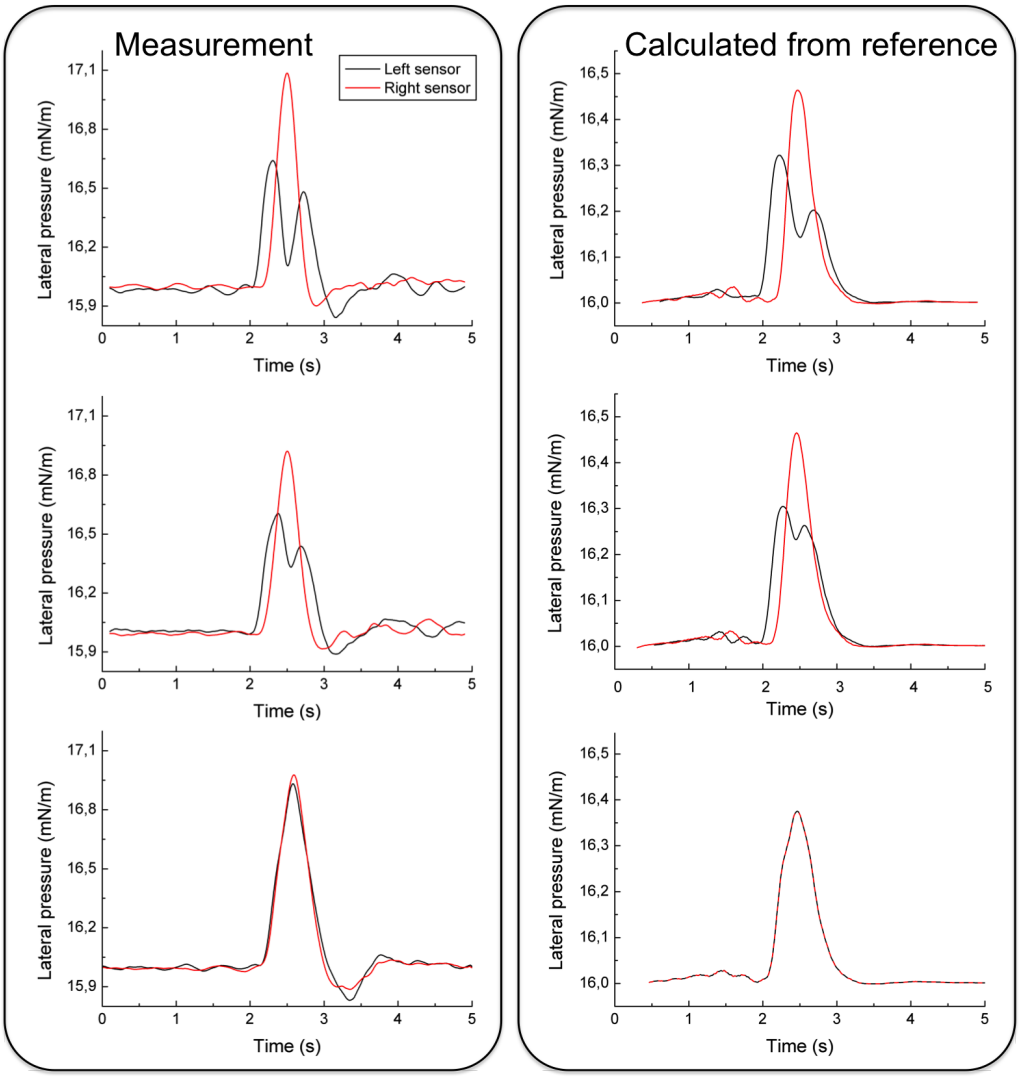

Figure 8.6.: Left panel: Collision of monolayer waves excited from the central position (3). The corresponding membrane pressures are 5, 8.5 and 22 mN/m, representing the liquid-expanded (*le*), the plateau region (*p*) and the liquid-condensed (*lc*) phase of the lipid monolayer respectively. **Right panel:** Calculation of the interference pattern by linear superposition of two reference waves. Aligned with panel on the left from top to bottom, the *le*, *p* and *lc* phases are displayed.

of density pulses is supported by the reproduction of the measured interference patterns through a linear superposition of reference measurements (see figures 8.4 & 8.6). The linear amplitude - excitation stress relation, elucidated in chapter 4, furthermore endorses the classical wave behavior of the pulses. At first sight, these results contradicts measurements executed on axons, where an annihilation of action potentials was found [120]. Also experiences made with cardiac cells support the cancellation of colliding action potential [121].
At second view it must be stated that compelling evidence of action potential an-

nihilation upon collision is hardly found in literature [18]. Moreover, in theoretical evaluations of the FitzHugh-Nagumo model [122, 123], which is a mathematically simplified version of Hodgkin and Huxley equation, it was discovered that there are indeed regimes of classical wave behavior, where the penetration of action potentials is possible [124–126]. These deviations from the complete annihilation have also been observed in vivo [121], despite the fact that these are considered to be pathologic.
The acoustic monolayer wave, which is the central subject of this thesis, has recently been proposed as a model system for cell-cell communication [23]. Velocities of the pulses measured are similar to those obtained from action potentials and furthermore it was shown that the described lateral pressure pulse is accompanied by a pulse in the membrane's surface potential [24]. Here it was shown that this type of wave, which is propagating within a lipid monolayer interface, penetrates another pulse upon collision. This is not the expected result for a model describing nervous excitation, but does also not eliminate the longitudinal wave mode as a possible model for the nerve pulse propagation, since regimes of classical wave behavior have also been elucidated from theoretical considerations [124–126]. As a consequence it needs to be stated that additional measurements are required to elucidate the full behavior of this wave upon collision of single pulses.

8.4. Summary Collision

In this chapter, the experimental finding of density pulse penetration in nanometer thin lipid monolayers is presented. Interference patterns of colliding pulses are reproduced by the linear superposition of reference measurements, thus confirming the classical wave behavior. This is executed for different thermodynamic states of the monolayer as well as various path differences for the two pressure waves, yielding a shifting interference pattern. Additionally, the damping factor for the longitudinal monolayer wave was calculated from the relative decrease in pulse amplitude of the two superimposed pressure pulses. The presented results can therefore be considered as a starting point for further experiments on lipid monolayer wave collision, including different excitation and observation methods, which could finally lead to important new insights of inter- and intracellular communication including nerve pulse propagation [120, 121].

Chapter 9: Summary and Outlook

The ability of lipid membranes to compartmentalize the structures of a cell constitutes their essential significance for life. The cell membrane separates the intra- from the extracellular environment, regulates the equilibrium of ions across the membrane and plays a key role in essential chemical processes. Furthermore, the dynamics of membranous interfaces determine among other things the exchange of metabolites, as well as the communication of the cell with its environment. Since the lipid monolayer is considered as the simplest model of a cell membrane and since its physical properties are easily accessible, it has been used throughout this thesis for the investigation of dynamic membrane properties. Two dimensional sound waves were induced by the fusion of a solvent drop with the aqueous interface of the monolayer. The time resolved observation of the membrane pressure at two laterally separated sensors enabled calculation of the pulse velocity and monitoring of the time course of the pressure variation. These experimental arrangements laid the foundation for the central aim of this thesis, which has been to empirically challenge the picture of a propagating sound wave as the basis for cell-cell communication.
This chapter summarizes the experiments conducted, combined with a short outlook on open questions and ideas to continue in this field of research.

9.1. Excitation of Lipid Monolayer Waves

In order to establish a sound foundation for all subsequent experiments, the direct and indirect excitation of lipid monolayer waves, by means of solvent molecules, has been studied. While for the direct method a solvent drop was fused with the interface of the lipid monolayer, the indirect way of excitation involved approaching the monolayer with the vapor phase of a solvent drop.

9.1.1. Direct excitation

The potency of a solvent to induce longitudinal monolayer waves was found to depend on its property to accumulate at aqueous interfaces. This could be expressed by the partition coefficient P_{OW} of the respective solvent. Upon fusion of the droplet with the monolayer, the applied solvent molecules incorporate into the lipid membrane demanding additional lateral space. This causes a displacement of the lipids

that is subsequently conducted over the entire area of the interface as a lateral pressure pulse. Despite the highly non-linear compressibility profile of the monolayer, the stress-strain relation for the pulse amplitudes was found to behave according to Hooke's law. These findings were included into a simple theory based on the idea of a sudden membrane compression, which allows to calculate the anticipated pulse amplitudes. A threshold in excitability, which occurs for low solvent concentrations, indicates the limit of the proposed theory and is explained by the concentration dependent behavior of the partition coefficient.

This rather simple method for the induction of longitudinal monolayer waves could be improved in many ways to elucidate the entire dispersion relation of the occurring wave phenomenon. Since lipids in naturally occurring membranes bare a net negative charge, an electrical method for pulse excitation seems to be feasible and has already been investigated [62]. The principle of wave excitation by a local reduction of the average area per lipid could be extended by incorporating molecules into the membrane that are able to undergo a conformational transition [60]. For this purpose, optomechanical dyes are of particular interest, but also naturally occurring proteins like rhodopsin could be used. Furthermore, by the incorporation of enzymes like acetylcholinesterase it could be probed, if the sudden production of acetic acid by the enzyme is capable of inducing a lateral pressure pulse.

9.1.2. Indirect excitation

Aside from the direct method of wave excitation, a contactless, indirect method was established. For this purpose, the vapor phase of a solvent drop is approached to the monolayer interface. This leads to a sudden increase in membrane tension, which indicates the excitation of a longitudinal wave. The velocities extracted from such pulses are found to match those of direct excitation, showing that the propagation process is independent from the respective technique used for excitation. When the drop was furthermore held at a certain, constant distance to the interface, auto-oscillations of the monolayer tension occurred. The obtained frequencies and velocities are in agreement with those obtained for direct excitation. The suggestion that the monolayer compressibility determines the restoring forces of the monolayer and thereby influences the properties of the oscillations was not verified. The frequency of the oscillations showed a remarkable stability even upon shifting the compressibility maximum towards higher membrane pressures through an increase in the system temperature.

This contact-free technique for induction of longitudinal monolayer waves was mainly studied phenomenologically and is not completely understood. The observed steep

rise and subsequent plateau region of the membrane pressure upon approach of the solvent drop indicates the occurrence of a lipid phase transition. However, it has not been possible to entirely clarify this suggestion. Also the striking stability of the oscillation frequency needs to be studied in further detail.

Based on the similarities of the pulses generated by the two excitation methods, a complete theoretical understanding of lipid monolayer waves would benefit from further investigations the indirect excitation method.

9.2. Relaxation of Lipid Monolayer Waves

Chapter 5 investigated the local relaxation of pressure pulses propagating in lipid monolayer films. A correlation is found between relaxation times and lateral compressibility of the monolayer. This is demonstrated by coinciding maxima for both parameters at the phase transition of the lipid membrane. The invariance of this relationship with respect to physical (π, T), chemical (ethanol, chloroform) and molecular (lipid type) variations is correctly predicted by theory. Based on Einstein's approach to thermodynamics, the centerpiece of which is the reversion of the Boltzmann principle and on an Onsager type ansatz, a direct correlation between relaxation time τ and lateral compressibility κ_T with the phenomenological constant L was derived. This constant is determined through the relaxation experiment by solving the correlation found between τ and κ_T for L. While a constant value for L can be found for each membrane phase, a non-linearity at the lipid phase transition clearly indicates the limitations of this theoretical approach.

The strength and beauty of the presented theory is its universality. As a consequence, all material susceptibilities can be connected to either fluctuations in their respective thermodynamic variable or to the general relaxation time of the system. This allows to predict e.g. the conductivity profile of a bilayer arrangement by investigating the phase space of the corresponding monolayer on a Langmuir trough. Future experiments should address the non-linear behavior of the phenomenological constant L at the phase transition. By using high resolution pressure jump experiments on a different lipid system as the monolayer (e.g. vesicles), it could be elucidated if the break down of linearity between thermodynamic fluxes and forces at the phase transition is a general property of lipid systems.

9.3. Influence of the Hydration Layer

To elucidate the impact of lipid-bound polymers on the properties of longitudinal monolayer waves was the main emphasis of chapter 6. Lipids with a PEG-chain conjugated to the headgroup were used to form monolayers which mimic the glycocalyx of a cell. Ethanol-induced pulses in such a monolayer were characterized by a decrease of amplitude and velocity as compared to a regular lipid monolayer. This effect was attributed to the hydrophilic nature of the polymer and the resulting increase of the monolayer's viscosity. The thickness of the hydration layer which is dragged along with a pulse was found to correlate with the polymer's length and its surface pressure dependent molecular conformation. Overall, PEG linearizes the velocity profile and strongly diminishes the pulse amplitudes due to an increased viscous drag.

In addition to the presented experiments an expansion towards higher membrane pressures of the monolayer would be of interest. This is expected to induce the so-called brush state of the PEG moieties, resulting in a rheological transition and an elastic membrane (storage modulus G' > loss modulus G") [92, 99]. As a consequence of this transition, the properties of the monolayer wave such as damping, relaxation and velocity should change drastically. Moreover, experiments with different hydrophilic moieties conjugated to the lipid headgroup (e.g. lactose instead of PEG) would allow to test for generality of the phenomenon and would thereby contribute to the understanding of pressure pulses that might propagate in cell membranes.

9.4. Effects of Lanthanides

In chapter 7, the influence of trivalent ions on lipid monolayer and in particular on pressure pulses therein was discussed. The focus was mainly set on the lanthanide Gadolinium, which has been described in the literature as a potent blocker of mechanosensitive ion channels. A strong influence of even micromolar concentrations of Gadolinium on the static properties of the monolayer was observed in π-A-isotherms and fluorescence microscopic images. In the latter, macroscopic liquid-condensed domains appeared upon injection of Gadolinium to the aqueous sub phase. This supported the result of a membrane compaction due to Gadolinium as has been found in π-A-isotherms. Moreover, the dynamic properties of the membrane were altered. In particular, a reduction of excitability was found with a complete block of pressure pulses for concentrations above $c \approx 10\,\mu$Mol of Gd^{3+}. This characteristic behavior was also observed for other lanthanides such as Lanthanum and Neodymium.

It would be an important next step to investigate the influence of these rare earth ions on the conductivity across pure lipid bilayers. This could be achieved by introducing e.g. Gd^{3+} to a black lipid membrane setup. In combination with previous reports in the literature [114] the results presented in this thesis predict an inhibition of membrane currents in pure lipid bilayers in the presence of trivalent ions. This would support the suggestion found in literature of a lipid-based effect for the blockage of mechanosensitive protein ion channels.

9.5. Collision of Lipid Monolayer Waves

The demonstration of the classical wave behavior for solvent induced density pulses comprised the last chapter of this thesis. Two pulses display interference patterns upon collision which can be reproduced by the linear superposition of reference measurements. These experiments were performed for different thermodynamic states of the monolayer as well as various path differences for the two pressure waves. Ultimately, a shifting interference pattern was obtained. As an additional result, the damping factor for the longitudinal monolayer wave was calculated from the relative decrease in pulse amplitude of the two superimposed pressure pulses.

The establishment of an experimental setup that is capable of inducing two mutually approaching interfacial waves is a key step in order to study the collision of two dimensional density pulses, propagating in lipid monolayers. Thus, the results presented in chapter 8 can be expanded by the application of different pulse excitation methods (electrical, mechanical, optical), which would allow to probe a wider range of the frequency spectrum. An additional elongation of the distance between the two pressure sensors would increase the time required for pulse propagation and thereby improve the resolution of the single pulses. This would serve to study possible variations of the wave properties as e.g. an increase in the pulse velocity, predicted by theoretical consideration on colliding solitons.

9.6. Conclusion

The dynamics of lipid interfaces affect many functions of cells and are therefore crucial for life. In particular pressure pulses propagating in lipid membranes are of interest, since they might as well conduct information. This was the motivation to study lipid monolayer waves and to advance towards a model that could more realistically mimic the cell membrane. The experimental results presented within this thesis demonstrate that the properties of a wave such as amplitude, velocity and relaxation time are tightly coupled to the state of the lipid monolayer. Mim-

icking of the hydrophilic coating of cells by introducing PEG-lipids led to damping, but did not abolish pulse propagation over macroscopic distances. Trivalent ions displayed a strong influence on structure and polymorphism of the lipid monolayer and were able to block pulse excitation. Moreover it was shown that the pressure pulses behave as classical, longitudinal waves, as was elucidated from pulse collision experiments. In conclusion, the variety of the presented results provide a solid basis for a scientific debate on the possible contribution of pulses in lipid layers to cell-cell communication.

Appendix A: Thermodynamic relations and derivations

A.1. Derivation of the Poisson-Boltzmann equation

The movement of ions in vicinity of a charged plate is governed by the electrochemical potential μ_i for the i^{th} ion, which is comprised by the competing contributions of the ordering electric potential of the surface charge density σ and the order destroying maximization of entropy due to thermal motion:

$$\mu_i = ez_i\psi + kT\ln(n_i) \tag{A.1}$$

Integration leads to a regular Boltzmann equation, where the integration constant $n_0^{(i)}$ is supposed to be the bulk concentration of the i^{th} ion in a distance far apart from the charged surface:

$$n_i = n_0^{(i)} \exp\left(\frac{-ez_i\psi}{kT}\right) \tag{A.2}$$

The *Poisson equation* provides a relationship between the potential ψ and the charge density σ. In this case, we have to consider the positive and negative charges in the surrounding media:

$$\nabla^2\psi(\vec{r}) = -\frac{4\pi}{\epsilon_W}\rho(\vec{r}) = -\frac{4\pi e}{\epsilon_W}\left[ez_+n_+(\vec{r}) + ez_-n_-(\vec{r})\right] \tag{A.3}$$

Combining equation A.2 and A.3 gives the *Poisson-Boltzmann equation*

$$\nabla^2\psi(\vec{r}) = -\frac{4\pi e}{\epsilon_W}\left[z_+n_+\exp\left(\frac{-ez_+\psi(\vec{r})}{kT}\right) + z_-n_-\exp\left(\frac{-ez_-\psi(\vec{r})}{kT}\right)\right] \tag{A.4}$$

A.2. Derivation of the Debye-Hückel length

Discussing two simple cases in which the Poisson-Boltzmann equation can be solved analytically:

1. No ions in solution $n_0^{(-)} = 0$; $n_0^{(+)} = n_0$

$$\nabla^2\psi(\vec{r}) = -\frac{4\pi e n_0}{\epsilon_W}\exp\left(\frac{-e\psi(\vec{r})}{kT}\right) \tag{A.5}$$

2. 1:1 ion solution (NaCl case) $n_0^{(-)} = n_0^{(+)} = n_0$

$$\nabla^2\psi(\vec{r}) = -\frac{4\pi e}{\epsilon_W}\left[n_0\exp\left(\frac{-e\psi(\vec{r})}{kT}\right) - n_0\exp\left(\frac{-e\psi(\vec{r})}{kT}\right)\right] = \frac{8\pi e^2 n_0}{\epsilon_W}\sinh\left(\frac{e\psi}{kT}\right) \tag{A.6}$$

This non-linear, differential equation can be solved by expanding the hyperbolic sine and using only the linear term to transform equation A.6 into a linear differential equation.

$$\nabla^2\psi(\vec{r}) = -\frac{8\pi e^2 n_0}{\epsilon_W kT}\psi(\vec{r}) \quad \Rightarrow \quad \nabla^2\psi(\vec{r}) = \lambda_D^{-2}\psi(\vec{r}) \tag{A.7}$$

Here, $\lambda_D = \left(8\pi e^2 n_0/\epsilon_W kT\right)^{-1/2} \propto n_0^{-1/2}$ is called the Debye-Hückel screening length.

Appendix B: Details of materials and methods

B.1. Description of used lipids

- **DPPC:** 1,2-dipalmitoyl-sn-glycero-3-phosphocholine is a phospholipid comprised of two palmitic acids and one phosphocholine group attached to the glycerol backbone. In the human body it is most prominent in the lung surfactant, where it among others prevents the collapse of the alveole. The phosphocholine headgroup is neutrally charged at neutral pH, since the negative phosphoric acid group and the positively charged choline group are neutralizing each other. This results in a strong dipole moment. Its molar weight is $M = 734.039 \frac{g}{mol}$
- **DPPG:** 1,2-dipalmitoyl-sn-glycero-3-phospho-(1'-rac-glycerol) is the second most common lipid in the lung surfactant and consitsts of the same fatty acids as DPPC. The distinguishing property results from the phosphoglycerol headgroup, which is negatively charged at neutral pH. Thus, membranes formed from DPPG bear a negative surface charge, attracting and interacting with positively charged ions more efficiently. Its molar weight is $M = 744.952 \frac{g}{mol}$
- **DSPE-PEG(350):** 1,2-distearoyl-sn-glycero-3-phosphoethanolamine-N-(polyethylene glycol)-350] is lipid with a poly(ethylene glycol) moiety of 7 monomers attached to the lipid headgroup. Its molar weight is $M = 1131.500 \frac{g}{mol}$
- **DSPE-PEG(2000):** 1,2-distearoyl-sn-glycero-3-phosphoethanolamine-N-(polyethylene glycol)-2000] is a standard PEG-lipid. A poly(ethylene glycol) moiety with 45 monomers attached to the lipid headgroup. Its molar weight is $M = 2790.486 \frac{g}{mol}$

B.2. Fabrication of lipid solutions

All lipids used in this thesis were purchased from *Avanti Polar Lipids* as powder or already solved. The lipid solutions used to spread monolayers were adjusted to a concentration of $10 \frac{mg}{ml}$.

- **DPPC:** This lipid was mostly purchased in chloroform solution with a concentration of $10\frac{mg}{ml}$ and therefore used directly. When obtained as powder, $10mg$ were weighted into a well cleaned sample vial. The exact weight m is then further used to precisely measure the volume $V = m \cdot 0,1\frac{mg}{ml}$ of chloroform with a micro syringe, in order to obtain the desired $10\frac{mg}{ml}$ DPPC solution.

- **DPPG:** This lipid was mostly purchased in so-called *magic* solution with a concentration of $10\frac{mg}{ml}$ and therefore directly used. The *magic* solution consists of chlorform-methanol-water in a ratio of 65:35:8. When obtained as powder, $10mg$ were weighted into a well cleaned sample vial and since this lipid is insoluble within chloroform, the *magic* solution was used. Thus, the exact weight m is then further used to precisely measure the volume $V_c = m \cdot \frac{65}{108} \cdot 0,1\frac{mg}{ml}$ of chloroform, $V_m = m \cdot \frac{35}{108} \cdot 0,1\frac{mg}{ml}$ of methanol and $V_w = m \cdot \frac{8}{108} \cdot 0,1\frac{mg}{ml}$ of water with a micro syringe to yield a solution of $10\frac{mg}{ml}$ DPPG solution.

- **DPPC DPPG (10%):** The lipid mixture can not be purchased and is therefore produced from its single components. For this purpose, DPPC with a concentration of $20\frac{mg}{ml}$ is transferred by means of a micro syringe in to a well cleaned sample vial. The volume transferred can be calculated into the mass of DPPC lipids m_{DPPC} within the solution. In order to obtain the correct ratio of 9:1, the molar weights of both lipids need to be considered. Thus volume of DPPG lipids necessary can be calculated as:

$$V_{\mathrm{DPPG}} = \frac{1}{9} \cdot \left(\frac{c_{\mathrm{DPPC}}}{c_{\mathrm{DPPG}}}\right) \cdot \left(\frac{M_{\mathrm{DPPG}}}{M_{\mathrm{DPPC}}}\right) \cdot V_{\mathrm{DPPC}}$$

  When DPPG enters the chloroform solution, it spontaneously forms a white precipitate according to its low solubility within chloroform. This was the reason for the higher starting concentration of DPPC so that now the resulting solution ca be rediluted with methanol and water to regain the *magic* solution.

$$V = \left[(m_{\mathrm{DPPG}} + m_{\mathrm{DPPG}}) \cdot 0,1\frac{ml}{mg}\right] - V_{\mathrm{DPPC}} + V_{\mathrm{DPPG}}$$

  For DPPC DPPG (10%) mostly chloroform is in the solution yet. Therefore the rest volume must be mostly filled with methanol. But in practice, the calculated volume must be slowly added with methanol, water and chloroform until DPPG is dissolving again.

- **DSPE-PEG(350):** This lipid was purchased in chloroform solution with a concentration of $10\frac{mg}{ml}$ and therefore used directly.

- **DSPE-PEG(2000):** This lipid was purchased in chloroform solution with a concentration of $10\frac{mg}{ml}$ and therefore used directly.

B.3. Fabrication of lipid and buffer solutions

Ringer solution

For the fabrication of the ringer solution a premixed powder with all ingredients necessary was purchased from *Sigma Aldrich*. The content of the premix, sufficient to produce 1ℓ of the ringer solution, is displayed in table B.1 and at first dissolved in $0,9\ell$ of ultra pure water. Subsequently, $1,26g$ of sodium bicarbonate ($NaHCO_3$) are added to the solution, which works together with the phosphate as a buffer system. In the following, the volume is supplemented with water to yield 1ℓ of solution. This mixture normally should result in a pH$\approx 7,4$, which is checked by a regular pH electrode and if necessary adjusted with $NaOH$.

Component	**Mass in g (converts to $\frac{g}{\ell}$ in solution)**
D-Glucose	1,8
Magnesium chloride ($MgCl$)	0,0468
Potassium chloride (KCl)	0,34
Sodium chloride ($NaCl$)	7
Monosodium phosphate (NaH_2PO_4)	0,1
Disodium phosphate (Na_2HPO_4)	0,18

Table B.1.: Substances in the premix and necessary to produce 1ℓ of ringer solution

HEPES buffer

The HEPES buffer is widely used throughout this thesis to study the influence of Gadolinium onto static and dynamic properties of lipid membranes. Since the entire experiment was motivated by the work of Yang and Sachs [112], who blocked mechanosensitive ion-channels by means of Gd^{3+}, the buffer system applied in this thesis was produced by the same recipe. Therefore, $150\frac{mmol}{\ell}$ of sodium chloride (NaCl), $10\frac{mmol}{\ell}$ of 4-(2-hydroxyethyl)-1-piperazineethanesulfonic acid (HEPES) are solved within 1ℓ of ultra pure water. The corresponding masses m necessary can be calculated via:

$$m = c \cdot M \cdot V$$

and are displayed in table B.2 Here, c is the final concentration of the salt with a molar mass M, dissolved in a solution of volume V. The zwitterionic HEPES

Component	**Molar mass in** $\frac{g}{mol}$	**Mass in** g
Sodium chloride ($NaOH$)	58,44	8,766
HEPES	238,3	2,383

Table B.2.: Substances necessary to produce 1ℓ of HEPES buffer

molecule serves here as the buffer system. The dissolved salts normally yielded a pH$\approx 5,6$, what was adjusted to pH$\approx 7,4$ by means of $NaOH$.

B.4. Fabrication of ethanol & acetic acid solutions

Solutions of different concentrations of ethanol & acetic acid were produced by dilution of the pure solvent, purchased from Sigma Aldrich (USA) and used without further purification. Density and molar mass values were obtained from the associated data sheet, allowing the calculation of the molar concentration of the pure solvent solution and consecutively the dilution factors to reach the required concentrations. Solvents were diluted with bidistilled, ultrapure water to prevent any type of contamination and possible error sources. In the case of ethanol, the following calculations have been used to fabricate the solutions applied in this thesis: The dif-

solvent	**molar mass**	**density**	**molar concentration**	V_{water}	V_{solvent}
	g/mol	g/cm^3	mol/ℓ	$m\ell$	$m\ell$
Methanol	32,04	0,79	24,66	0,406	0,594
Ethanol	46,07	0,79	17,15	0,583	0,417
Propanol	60,10	0,80	13,31	0,751	0,249
Butanol	74,12	0,81	10,93	0,915	0,085
Formic Acid	46,03	1,22	26,50	0,377	0,623
Acetic Acid	60,05	1,05	17,49	0,572	0,428
Propionic Acid	74,08	0,99	13,36	0,748	0,252
Butyric Acid	88,11	0,96	10,90	0,918	0,082

Table B.3.: Properties of the investigated solvents and volume used to fabricate solutions of a standardized 10 $\frac{mol}{\ell}$ concentration. Molar mass, density, solubility adapted from the respective Sigma Aldrich data sheets and controlled with [65]

ficulty of butanol being only solvable in water by 7,9% was overcome by introducing

only a small amount of water to a 100% butanol solution to yield an absolut molar concentration of $10\frac{mol}{\ell}$.

B.5. Relaxation times for different excitation solvents

Relaxation times as evaluated from pressure pulses in a DPPC monolayer at 24°C, excited with chloroform and pentane. Both figures display the correlation between isothermal compressibility and relaxation times, indicated by the coinciding maxima. Differences in absolute numbers and course of the relaxation times might be due to the influence of the solvent on the excitation process.

Chloroform excitation

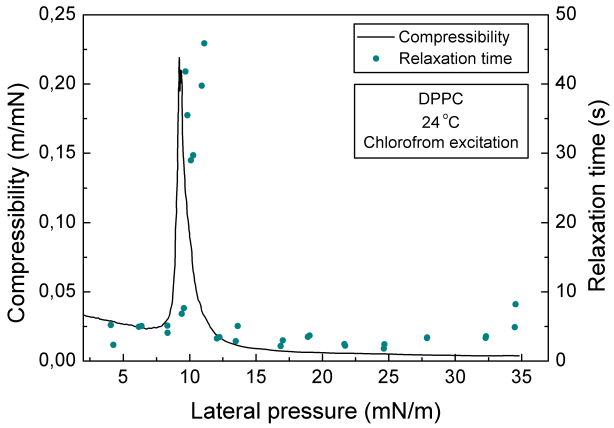

Figure B.1.: Invariance of the compressibility-relaxation time correlation (derived in chapter 5 with respect to the change of excitation solvent. Here: Chloroform

Pentane excitation

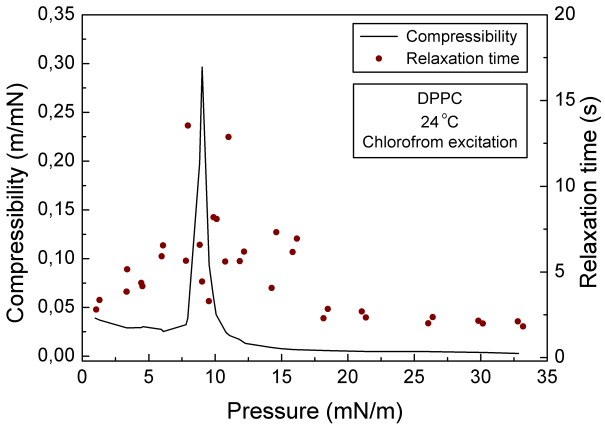

Figure B.2.: Invariance of the compressibility-relaxation time correlation (derived in chapter 5 with respect to the change of excitation solvent. Here: Pentane

B.6. Solubilities of threefoldly charged ions

Table B.4 displays the solubility of hydroxides of threefoldly charged ions and thus determines the pH dependent solubility of these ions within ultrapure water. Thus, Aluminum precipitates even at micromolar concentrations at $\mathrm{pH} = 7,4$, while most rare earth ions stay in the solution.

Element	pL
$In(OH)_3$	33,2
$La(OH)_3$	18,7
$Nd(OH)_3$	21,5
$Pr(OH)_3$	22,4
$Sc(OH)_3$	30,7
$Sm(OH)_3$	23,4
$Tb(OH)_3$	23,2
$Y(OH)_3$	24,5

Element	pL
$Al(OH)_3$	32,9
$Cr(OH)_3$	30,2
$Co(OH)_3$	43,8
$Eu(OH)_3$	26,9
$Fe(OH)_3$	38,6
$Ga(OH)_3$	35,1
$Gd(OH)_3$	22,7

Table B.4.: Solubility of the hydroxides of threefoldly charged ions. Values are adapted from [129]

B.7. Influence of tetrodotoxin on DPPC DPPG (10%) isotherms

The extremly dangerous neurotoxin tetrodotoxin (TTX) was investigated towards its influence on lipid monolayers. Its capability of blocking specifically voltage and ligand gated sodium channels [130] indicates a strong interaction with the axon membrane. In order to elucidate any effects on the pure lipids, π-A-isotherms of charged and uncharged lipid systems under the influence of TTX are studied and presented in B.3. In almost all cases, a slight upwards shift in the phase transition pressure can be observed. These unexpectedly little effects might be explainable by the low solubility of TTX. While the toxin needs to be solved within a buffer system at $\mathbf{pH} = 4,7$, it is hardly solvable at a regular $\mathbf{pH}$ of $7,4$. Thus, the diminshed effects might be a simple percipitation of TTX, which prevents the interaction with the membrane.

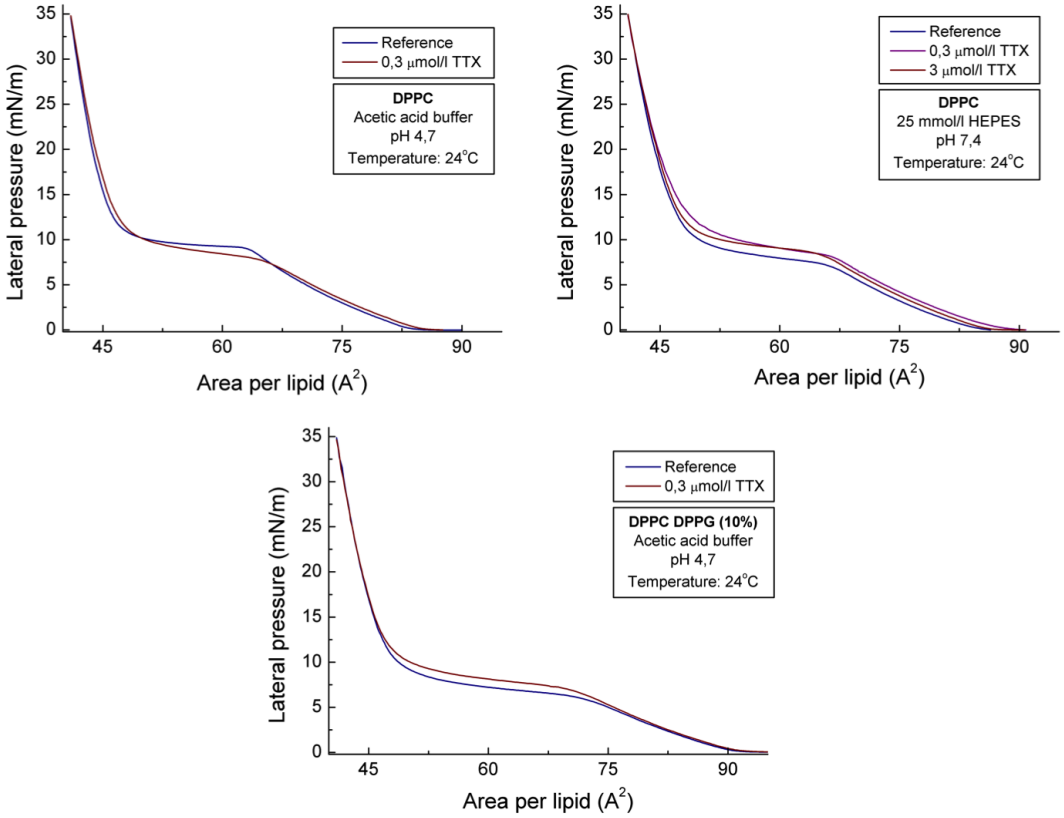

Figure B.3.: Isotherms of DPPC and DPPC DPPG (10%) monolayers under the influence TTX. Only slight changes indicate minor interaction.

Bibliography

1. Barbara, J.-G. & Clarac, F. Historical concepts on the relations between nerves and muscles. *Brain research* **1409,** 3–22. ISSN: 1872-6240 (Aug. 2011).
2. Wells, D. A. *The science of common things: a familiar explanation of the first principles of physical science. For schools, families, and young students.* (Ivison, 1859).
3. Circuitstoday.com. <http://www.circuitstoday.com/working-of-a-capacitor>.
4. Gillard. *Leçons de Physique* (Vuibert et Nony, 1904).
5. Hodgkin, A. L. & Huxley, A. F. A Quantitative Description of Membrane Current and its Application to Conduction and Excitation in Nerve. *Society for Mathematical Biology* **52,** 25–71 (1990).
6. Griesbauer, J. *Akkustik und Dynamik von Lipid-Monolayern im Licht der Nervenreizleitung* PhD thesis (2011), 180.
7. Tasaki, I. *Physiology and Electrochemistry of Nerve Fibers* 348 (1981).
8. Tasaki, I. Rapid Structural Changes in Nerve Fibers and Cells Associated with Their Excitation Processes. *The Japanese journal of physiology* **49,** 125–138 (1999).
9. Tasaki, I., Kusano, K. & Byrne, P. Rapid mechanical and thermal changes in the garfish olfactory nerve associated with a propagated impulse. *Biophysical journal* **55,** 1033–1040 (1989).
10. Tasaki, I., Watanabe, A, Sandlin, R & Carnay, L. Changes in fluorescence, turbidity, and birefringence associated with nerve excitation. *Proceedings of the National Academy of Sciences of the United States of America* **61,** 883 (1968).
11. Abbott, B. C. Heat production in nerve and electric organ. *The Journal of general physiology* **43,** 119–27. ISSN: 0022-1295 (May 1960).
12. Abbott, B., Howarth, J. & Ritchie, J. The initial heat production associated with the nerve impulse in crustacean and mammalian non-myelinated nerve fibres. *The Journal of Physiology* **178,** 368 (1965).

13. Howarth, J., Keynes, R. & Ritchie, J. The origin of the initial heat associated with a single impulse in mammalian non-myelinated nerve fibres. *The Journal of physiology* **194,** 745 (1968).

14. Coster, H. G. Heat production and absorption during excitation in nerve. *Journal of theoretical biology* **54,** 225–7. ISSN: 0022-5193 (Oct. 1975).

15. Kaufmann, K. *Action Potentials and Electrochemical Coupling in the Macroscopic Chiral Phospholipid Membrane* 75 (1989).

16. Heimburg, T. & Jackson, A. D. On soliton propagation in biomembranes and nerves. *Proceedings of the National Academy of Sciences of the United States of America* **102,** 9790–5. ISSN: 0027-8424 (July 2005).

17. Andersen, S. r. S. L., Jackson, A. D. & Heimburg, T. Towards a thermodynamic theory of nerve pulse propagation. *Progress in neurobiology* **88,** 104–13. ISSN: 1873-5118 (June 2009).

18. Lautrup, B, Appali, R, Jackson, a. D. & Heimburg, T. The stability of solitons in biomembranes and nerves. *The European physical journal. E, Soft matter* **34,** 1–9. ISSN: 1292-895X (June 2011).

19. Lucassen, J & Van Den Tempel, M. Longitudinal waves on visco-elastic surfaces. *Journal of Colloid and Interface Science* **41,** 491–498. ISSN: 00219797 (Dec. 1972).

20. Lucassen, J. & Van Den Tempel, M. Dynamic measurements of dilational properties of a liquid interface. *Chemical Engineering Science* **27,** 1283–1291. ISSN: 00092509 (June 1972).

21. Lucassen, J. Longitudinal capillary waves. Part 2. -Experiments. *Transactions of the Faraday Society* **64,** 2221–2229. ISSN: 0014-7672 (1968).

22. Lucassen, J. Longitudinal Capillary Waves Part 1 - Theory. *Trans. Faraday Soc.* **64,** 2221–2229 (1968).

23. Griesbauer, J., Bössinger, S., Wixforth, A. & Schneider, M. Propagation of 2D Pressure Pulses in Lipid Monolayers and Its Possible Implications for Biology. *Physical Review Letters* **108,** 1–5. ISSN: 0031-9007 (May 2012).

24. Griesbauer, J., Bössinger, S., Wixforth, A. & Schneider, M. F. Simultaneous Propagating Voltage and Pressure Pulses in Lipid Monolayers and their Chemical Excitation. *Physical Review E - submitted* (2012).

25. Gaines, G. & Others. *Insoluble monolayers at liquid-gas interfaces* <http://en.scientificcommons.org/9254662> (Interscience New York, 1966).

26. Cevc. *Phospholipids Handbook* (Marcel Dekker, New York, NY, 1993).

27. Heimburg, T. *Thermal Biophysics of Membranes* 378. ISBN: 3527404716 (Wiley-VHC, 2007).

28. Barnes, G. T. & Gentle, I. *Interfacial Science - An introduction* 247 (Oxford University Press, New York, NY, 2005).

29. Sacré, M. M. & Tocanne, J. F. Importance of glycerol and fatty acid residues on the ionic properties of phosphatidylglycerols at the air-water interface. *Chemistry and physics of lipids* **18,** 334–54. ISSN: 0009-3084 (Apr. 1977).

30. Tanford, C. *The hydrophobic effect: formation of micelles and biological membranes* ISBN: 9780471048930. <http://books.google.de/books?id=079pAAAAMAAJ> (Wiley, 1980).

31. Singer, S. J. & Nicolson, G. L. The fluid mosaic model of the structure of cell membranes. *Science (New York, N.Y.)* **175,** 720–31. ISSN: 0036-8075 (Feb. 1972).

32. Mouritsen, O. G. & Bloom, M. Mattress model of lipid-protein interactions in membranes. *Biophysical journal* **46,** 141–53. ISSN: 0006-3495 (Aug. 1984).

33. Schilpp, P. A. *Albert Einstein: Autobiographical Notes* 95. ISBN: 0875483526 (Open Court Pub Co., 1979).

34. Steppich, D. *et al.* Thermomechanic-electrical coupling in phospholipid monolayers near the critical point. *Physical Review E* **81,** 1–5. ISSN: 1539-3755 (June 2010).

35. Einstein, A. On the Present Status of The Radiation of Problem. *Physikalische Zeitschrift* **10,** 185–193 (1909).

36. Einstein, A. Theory of the Opalescence of homogenous fluids and liquid mixtrues near the critical state. *Annalen der Physik* **33,** 1275–1298 (1910).

37. Einstein, A. On the present state of the problem of the specific heat. *Abhandlungen der Deutschen Bunsen Gesellschaft* **3,** 330–352 (1911).

38. Schrödinger, E. *Mein leben, meine Weltansicht* <http://scholar.google.com/scholar?hl=en&btnG=Search&q=intitle:Mein+Leben,+meine+Weltansicht#0> (P. Zsolnay, Wien, Hamburg: Zsolnay., 1985).

39. Wunderlich, B *et al.* Phase-state dependent current fluctuations in pure lipid membranes. *Biophysical journal* **96,** 4592–7. ISSN: 1542-0086 (June 2009).

40. Blicher, A., Wodzinska, K., Fidorra, M., Winterhalter, M. & Heimburg, T. The temperature dependence of lipid membrane permeability, its quantized nature, and the influence of anesthetics. *Biophysical journal* **96,** 4581–91. ISSN: 1542-0086 (June 2009).

41. Grabitz, P, Ivanova, V. & Heimburg, T. Relaxation kinetics of lipid membranes and its relation to the heat capacity. *Biophysical journal* **82,** 299–309 (2002).

42. Andelman, D. Electrostatic properties of membranes: the Poisson-Boltzmann theory. *Handbook of biological physics* **1,** 603–642 (1995).

43. Israelachvili, J. *Intermolecular and Surface Forces* 450 (Academic Press, 1992).

44. Träuble, H, Teubner, M, Woolley, P & Eibl, H. Electrostatic interactions at charged lipid membranes. I. Effects of pH and univalent cations on membrane structure. *Biophysical Chemistry* **4,** 319–342 (1976).

45. Jähnig, F. Electrostatic free energy and shift of the phase transition for charged lipid membranes. *Biophysical chemistry* **4,** 309–18. ISSN: 0301-4622 (July 1976).

46. Yang, H. *et al.* Effects of Na+, K+, and Ca2+ on the structures of anionic lipid bilayers and biological implication. *The journal of physical chemistry. B* **114,** 16978–88. ISSN: 1520-5207 (Dec. 2010).

47. Langmuir, I. The mechanism of the surface phenomena of flotation. *Trans. Faraday Soc.* **15,** 62–74 (1920).

48. Blodgett, K. Films built by depositing successive monomolecular layers on a solid surface. *Journal of the American Chemical Society* **57,** 1007–1022 (1935).

49. Albrecht, O., Gruler, H, Sackmann, E & Others. Polymorphism of Phospholipid Monolayer. *Journal De Physique* **39,** 301–313 (1978).

50. Keller, S. & McConnell, H. Stripe Phases in Lipid Monolayers near a Miscibility Critical Point. *Physical Review Letters* **82,** 1602–1605. ISSN: 0031-9007 (Feb. 1999).

51. Benvegnu, D. & McConnell, H. Line Tension between Liquid Domains in Lipid Monolayers. *The Journal of Physical Chemistry,* 6820–6824 (1992).

52. Meschede, D. *Gerthsen Physik* 23rd ed. (Springer, Berlin, 2005).

53. Lucassen, J & Hansen, R. Damping of Waves on Monolayer-Covered Surfaces - II. Influence of Bulk-to-Surface Diffusional Interchange on Ripple Characterisitcs. *Journal of Colloid and Interface Science* **23,** 319–328. ISSN: 00219797 (Mar. 1967).

54. Espinosa, G., López-Montero, I., Monroy, F. & Langevin, D. Shear rheology of lipid monolayers and insights on membrane fluidity. *Proceedings of the National Academy of Sciences* **108,** 6008 (2011).

55. Evans, R., Williams, M. & Tinoco, J. Surface viscosities of phospholipids alone and with cholesterol in monolayers at the air-water interface. *Lipids* **15,** 524–533. ISSN: 0024-4201 (July 1980).

56. Möhwald, H. in *Phospholipid Handbook* (1987). <http://iopscience.iop.org/0295-5075/4/6/010>.

57. Noskov, B., Alexandrov, D., Loglio, G & Miller, R. Characterisation of adsorbed polymer film structure by dynamic surface tension and dilational elasticity. *Colloids and Surfaces A: Physicochemical and Engineering Aspects* **156,** 307–313. ISSN: 09277757 (Oct. 1999).

58. Noskov, B., Alexandrov, D. & Miller, R. Dynamic Surface Elasticity of Micellar and Nonmicellar Solutions of Dodecyldimethyl Phosphine Oxide. Longitudinal Wave Study. *Journal of colloid and interface science* **219,** 250–259. ISSN: 1095-7103 (Nov. 1999).

59. Lucassen, J. Longitudinal Capillary Waves Part 2. - Experiments. *Trans. Faraday Soc.* 2230–2235 (1968).

60. Suzuki, M., Möbius, D. & Ahuja, R. Generation and transmission of a surface pressure impulse in monolayers. *Thin Solid Films* **138,** 151–156. ISSN: 0040-6090 (Apr. 1986).

61. Landau, L. D. & Lifshitz, E. M. *Fluid Mechanics, Second Edition: Volume 6 (Course of Theoretical Physics)* 2nd ed. ISBN: 0750627670. <http://www.amazon.com/exec/obidos/redirect?tag=citeulike07-20\&path=ASIN/0750627670> (Butterworth-Heinemann, Jan. 1987).

62. Griesbauer, J., Wixforth, A. & Schneider, M. F. Wave propagation in lipid monolayers. *Biophysical journal* **97,** 2710–6. ISSN: 1542-0086 (Nov. 2009).

63. Lucassen-Reynders, E. Properties of capillary waves. *Advances in Colloid and Interface Science* **2,** 347–395 (Mar. 1970).

64. Dr. Sangster, J. <http://logkow.cisti.nrc.ca/logkow/>.

65. Seilnacht, T. <http://www.seilnacht.com/>.

66. Paschke, A. & Schüürmann, G. Concentration Dependence of the Octanol/Water Partition Coefficients of the Hexachlorocyclohexane Isomers. *Chemical engineering* **23,** 666–670 (2000).

67. Lee, S. H. & Lee, S. B. Octanol/water partition coefficients of ionic liquids. *Journal of Chemical Technology and Biotechnology* **84,** 202–207. ISSN: 02682575 (Feb. 2009).

68. Nomura, T & Kurihara, K. Effects of changed lipid composition on responses of liposomes to various odorants: possible mechanism of odor discrimination. *Biochemistry* **26,** 6141–5. ISSN: 0006-2960 (Sept. 1987).

69. Nomura, T & Kurihara, K. Liposomes as a model for olfactory cells: changes in membrane potential in response to various odorants. *Biochemistry* **26,** 6135–40. ISSN: 0006-2960 (Sept. 1987).

70. Koyama, N & Kurihara, K. Effect of Odorants on Lipid Monolayers from Bovine Olfactory Epithelium. *Nature* **236,** 402–404 (1972).

71. Okahata, Y, En-na, G & Ebato, H. Synthetic chemoreceptive membranes. Sensing bitter or odorous substances on a synthetic lipid multibilayer film by using quartz-crystal microbalances and electric responses. *Analytical chemistry* **62,** 1431–8. ISSN: 0003-2700 (July 1990).

72. Okahata, Y. & Shimizu, O. Olfactory Reception on a Multibilayer-Coated Piezoelectric Crystal in a Gas Phase. *Langmuir* **3,** 1171–1172. ISSN: 0036-8075 (Oct. 1987).

73. Papahadjopoulos, D., Jacobson, K., Nir, S. & Isac, I. Phase Transitions in Phospholipid Vesicles Fluorescence Polarization and Permeability Mearuements Concerning the Effect of Temperature and Cholesterol. *Biochimica et Biophysica Acta (BBA)-Biomembranes* **311,** 330–348 (1973).

74. Seeger, H. M., Aldrovandi, L., Alessandrini, A. & Facci, P. Changes in single K(+) channel behavior induced by a lipid phase transition. *Biophysical journal* **99,** 3675–83. ISSN: 1542-0086 (Dec. 2010).

75. Teissie, J. Fluorescence temperature jump relaxations of dansylphosphatidylethanolamine in aqueous dispersions of dipalmitoylphosphatidylcholine during the gel to liquid-crystal transition. *Biochimica et Biophysica Acta (BBA)-Biomembranes* **555,** 553–557 (1979).

76. Boehm, K., Guddorf, J. & Hinz, H.-J. Application of pressure-modulated differential scanning calorimetry to the determination of relaxation kinetics of multilamellar lipid vesicles. *Biophysical chemistry* **126,** 218–27. ISSN: 0301-4622 (Mar. 2007).

77. Schiewek, M. & Blume, A. Pressure jump relaxation investigations of lipid membranes using FTIR spectroscopy. *European biophysics journal : EBJ* **38,** 219–28. ISSN: 1432-1017 (Feb. 2009).

78. Gruenewald, B., Blume, A. & Watanabe, F. Kinetic investigations on the phase transition of phospholipid bilayers. *Biochimica et Biophysica Acta (BBA)-Biomembranes* **597,** 41–52 (1980).

79. Elamrani, K. & Blume, A. Phase Transition Kinetics of Phosphatidic Acid Bilayers. *Biochemistry* **22,** 84–90 (1983).

80. Seeger, H., Gudmundsson, M. & Heimburg, T. The influence of anesthetics, neurotransmitters and antibiotics on the relaxation processes in lipid membranes. *Arxiv preprint physics/0703022* **111,** 13858–13866 (2007).

81. Kaatze, U, Henze, R & Pottel, R. Dielectric Relaxation and Molecular Motions in C-14 Lecithin-Water Systems. *Chemistry and Physics of Lipids* **25,** 149–177 (1979).

82. Strom-Jensen, P., Magin, R. & Dunn, F. Ultrasonic evidence for structural relaxation in large unilamellar liposomes. *Biochimica et Biophysica Acta* **769,** 179–186 (1984).

83. Kanehisa, M. I. & Tsong, T. Y. Cluster model of lipid phase transitions with application to passive permeation of molecules and structure relaxations in lipid bilayers. *Journal of the American Chemical Society* **100,** 424–432. ISSN: 0002-7863 (Jan. 1978).

84. Bössinger, S., Griesbauer, J., Ziade, E., Nuschele, S. & Schneider, M. F. Thermodynamic-state dependent relaxation in lipid monolayers. *PRE - in review* (2012).

85. Onsager, L. Reciprocal relations in irreversible processes. *Physical Review.* <http://prola.aps.org/abstract/PR/v37/i4/p405_1> (1931).

86. Onsager, L. Reciprocal relations in irreversible processes II. *Physical Review.* <http://prola.aps.org/abstract/PR/v37/i4/p405_1> (1931).

87. Heimburg, T. Mechanical aspects of membrane thermodynamics. Estimation of the mechanical properties of lipid membranes close to the chain melting transition from calorimetry. *Biochimica et biophysica acta* **1415,** 147–62. ISSN: 0006-3002 (Dec. 1998).

88. Einstein, A. Theoretical Remarks on Brownian Motion. *Annalen der Physik* **13,** 41–42 (1907).

89. Antonov, V. F., Petrov, V. V., Molnar, a. a., Predvoditelev, D. a. & Ivanov, a. S. The appearance of single-ion channels in unmodified lipid bilayer membranes at the phase transition temperature. *Nature* **283,** 585–586. ISSN: 0028-0836 (Feb. 1980).

90. Silbernagel, S. & Despopoulos, A. *Taschenbuch der Physiologie* 6th ed. ISBN: 3135677060 (Thieme, Stuttgart, 2003).

91. Schneider, M. F., Lim, K., Fuller, G. G. & Tanaka, M. Rheology of glycocalix model at air/water interface. *Physical Chemistry Chemical Physics* **4,** 1949–1952. ISSN: 14639076 (May 2002).

92. Naumann, C. a. *et al.* Rheological Properties of Lipopolymer - Phospholipid Mixtures at the Air-Water Interface: A Novel Form of Two-Dimensional Physical Gelation. *Macromolecules* **34,** 3024–3032. ISSN: 0024-9297 (Apr. 2001).

93. Ruiz, M. <http://php.med.unsw.edu.au/cellbiology/index.php?title=Cell_Membranes_and_Compartments>.

94. Kim, B. H. C. & W, M. Adsorption Layer Effects on Surface Waves at the Polyethyleneoxide (PEO) Solution/Air Interface. *EPL (Europhysics Letters)* **29,** 555. ISSN: 0295-5075 (1995).

95. Steinmetz, N. F. & Manchester, M. PEGylated viral nanoparticles for biomedicine: the impact of PEG chain length on VNP cell interactions in vitro and ex vivo. *Biomacromolecules* **10,** 784–92. ISSN: 1526-4602 (Apr. 2009).

96. Gennes, P. D. Conformations of polymers attached to an interface. *Macromolecules* **1075,** 1069–1075 (1980).

97. Alexander, S. Adsorption of chain molecules with a polar head a scaling description. *Journal de physique.* <http://hal.archives-ouvertes.fr/jpa-00208666/> (1977).

98. Baekmark, T., Elender, G. & Lasic, D. Conformational Transitions of Mixed Monolayers of Phospholipids and Poly (ethylene oxide) Lipopolymers and Interaction Forces with Solid Surfaces. *Langmuir,* 3975–3987 (1995).

99. Naumann, C., Brooks, C., Fuller, G., Knoll, W & Frank, C. Viscoelastic Properties of Lipopolymers at the Air-Water Interface: A Combined Interfacial Stress Rheometer and Film Balance Study. *Langmuir* **15,** 7752–7761 (1999).

100. Hammoudah, M. M. *et al.* Interactions of La3+ with phosphatidylserine vesicles Binding, phase transition, leakage, 31P-NMR and fusion. *Biochimica et Biophysica Acta (BBA) - Biomembranes* **645,** 102–114. ISSN: 0005-2736 (June 1981).

101. Cevc, G. Isothermal lipid phase transitions. *Chemistry and physics of lipids* **57,** 293–307. ISSN: 0009-3084 (Mar. 1991).

102. Hauser, H, Phillips, M. C., Levine, B. a. & Williams, R. J. Ion-binding to phospholipids. Interaction of calcium and lanthanide ions with phosphatidylcholine (lecithin). *European journal of biochemistry / FEBS* **58,** 133–44. ISSN: 0014-2956 (Oct. 1975).

103. Li, X. M., Zhang, Y. F., Ni, J. Z., Chen, J. W. & Hwang, F. Effect of lanthanide ions on the phase behavior of dipalmitoylphosphatidylcholine multilamellar liposomes. *Journal of inorganic biochemistry* **53,** 139–49. ISSN: 0162-0134 (Feb. 1994).

104. Hwang, F., Zhao, D.-q., Chen, J.-w., Chen, X.-h. & Ni, J.-z. Effect of lanthanum ions on the lipid polymorphism of phosphatidylethanolamines. *Chemistry and Physics of Lipids* **82,** 73–77. ISSN: 00093084 (July 1996).

105. Seelig, J, Lehrmann, R & Terzi, E. Domain formation induced by lipid-ion and lipid-peptide interactions. *Molecular membrane biology* **12,** 51–7. ISSN: 0968-7688 (1995).

106. Chowdhry, B. Z., Lipka, G, Dalziel, a. W. & Sturtevant, J. M. Effect of lanthanum ions on the phase transitions of lecithin bilayers. *Biophysical journal* **45,** 633–5. ISSN: 0006-3495 (Mar. 1984).

107. Sabin, J *et al.* Interaction of Gadolinium with Phospholipid Bilayer Membranes. *Journal of Thermal Analysis and Calorimetry* **87,** 199–203 (2007).

108. Cheng, Y *et al.* Gadolinium induces domain and pore formation of human erythrocyte membrane: an atomic force microscopic study. *Biochimica et biophysica acta* **1421,** 249–60. ISSN: 0006-3002 (Oct. 1999).

109. Cheng, Y, Chen, B, Lu, J & Wang, K. The reaction of lanthanide ions with n-doxyl stearic acids and its utilization for the ESR study on the permeability of lipid-bilayer of erythrocyte membrane to gadolinium ions. *Journal of inorganic biochemistry* **69,** 1–7. ISSN: 0162-0134 (Feb. 1998).

110. Ermakov, Y. A., Averbakh, A. Z., Yusipovich, A. I. & Sukharev, S. Dipole potentials indicate restructuring of the membrane interface induced by gadolinium and beryllium ions. *Biophysical journal* **80,** 1851–62. ISSN: 0006-3495 (Apr. 2001).

111. Tanaka, T., Tamba, Y., Masum, S. M., Yamashita, Y. & Yamazaki, M. La(3+) and Gd(3+) induce shape change of giant unilamellar vesicles of phosphatidylcholine. *Biochimica et biophysica acta* **1564,** 173–82. ISSN: 0006-3002 (Aug. 2002).

112. Yang, X. C. & Sachs, F. Block of stretch-activated ion channels in Xenopus oocytes by gadolinium and calcium ions. *Science (New York, N.Y.)* **243,** 1068–71. ISSN: 0036-8075 (Feb. 1989).

113. Adding, L. C., Bannenberg, G. L. & Gustafsson, L. E. Basic experimental studies and clinical aspects of gadolinium salts and chelates. *Cardiovascular drug reviews* **19,** 41–56. ISSN: 0897-5957 (Jan. 2001).

114. Ermakov, Y. A., Kamaraju, K., Sengupta, K. & Sukharev, S. Gadolinium ions block mechanosensitive channels by altering the packing and lateral pressure of anionic lipids. *Biophysical journal* **98,** 1018–27. ISSN: 1542-0086 (Mar. 2010).

115. Cantor, R. S. The lateral pressure profile in membranes: a physical mechanism of general anesthesia. *Toxicology letters* **100-101,** 451–8. ISSN: 0378-4274 (Nov. 1998).

116. Cantor, R. S. The influence of membrane lateral pressures on simple geometric models of protein conformational equilibria. *Chemistry and physics of lipids* **101,** 45–56. ISSN: 0009-3084 (Aug. 1999).

117. Alexy, T. *et al.* Effect of lanthanum on red blood cell deformability. *Biorheology* **44,** 361–73. ISSN: 0006-355X (Jan. 2007).

118. Gullingsrud, J. & Schulten, K. Lipid bilayer pressure profiles and mechanosensitive channel gating. *Biophysical journal* **86,** 3496–509. ISSN: 0006-3495 (June 2004).

119. Boland, L. M., Brown, T. a. & Dingledine, R. Gadolinium block of calcium channels: influence of bicarbonate. *Brain research* **563,** 142–50. ISSN: 0006-8993 (Nov. 1991).

120. Tasaki, I. Collision of two nerve impulses in the nerve fibre. *Biochimica et Biophysica Acta* **3,** 494–497 (1949).

121. Steinhaus, B., Spitzer, K. & Isomura, S. Action Potential Collision in Heart Tissue - Computer Simulations and Tissue Experiments. *IEEE transactions on bio-medical engineering* **BME-32,** 731–742 (1985).

122. Fitzhugh, R. Impulses and Physiological States in Theoretical Models of Nerve Membrane. *Biophysical Journal* **1,** 445–466. ISSN: 00063495 (July 1961).

123. Nagumo, J, Arimoto, S & Yoshizawa, S. An Active Pulse Transmission Line Simulating Nerve Axon. *Proceedings of the IRE* **117,** 2061–2070 (1962).

124. Aslanidi, O. V. & Mornev, O. a. Can colliding nerve pulses be reflected? *Journal of Experimental and Theoretical Physics Letters* **65,** 579–585. ISSN: 0021-3640 (Apr. 1997).

125. Aslanidi, O. Soliton-Like Regimes and Excitation Pulse Reflection (Echo) in Homogeneous Cardiac Purkinje Fibers: Results of Numerical Simulations. *Journal of Biological Physics* **211590,** 149–164 (1999).

126. Argentina, M, Coullet, P & Krinsky, V. Head-on collisions of waves in an excitable FitzHugh-Nagumo system: a transition from wave annihilation to classical wave behavior. *Journal of theoretical biology* **205,** 47–52. ISSN: 0022-5193 (July 2000).

127. Heimburg, T. & Jackson, A. D. The thermodynamics of general anesthesia. *Biophysical journal* **92,** 3159–65. ISSN: 0006-3495 (May 2007).

128. Appali, R., Lautrup, B. & Heimburg, T. Soliton Collision in Biomembranes and Nerves-A Stability Study. *Scientific Computing in Electrical Engineering. Mathematics in Industry* **16** (eds Michielsen, B. & Poirier, J.-R.) 205–212 (2012).

129. Rausch, R. <http://www.periodensystem-online.de>.

130. Watanabe, A., Tasaki, I., Singer, I. & Lerman, L. Effects of Tetrodotoxin on Excitability of Squid Giant Axons in Sodium-Free Media. *Science,* 95–97 (1966).

Acknowledgment

A PhD thesis is not only a compendium of a three years hard work, but also a wonderful time, where one is allowed to pursue his own ideas and dreams. Luckily, this road was loaded with friends, who made these three years absolutely unforgettable and without whom I would have never reached my goals. In particular I want to mention and thank:

My professor and advisor ***Prof. Matthias Schneider***. Not only for the possibility of spending almost two and a half years in Boston to work on such a fascinating topic, but also for the trust into my self-reliance; the late night talks, filled with beer, about my work or physics in general; the soccer games we played and watched together and the ability of always reviving my fascination for this research, when I seemed drowning in not working experiments. Thank you, for these wonderful years that wouldn't have been possible without you.

My professor ***Prof. Achim Wixforth***, who supported me ever since I met him in the first semester of my studies. Thanks for giving me the confidence and freedom to pursue all these goals and ideas of mine.

Prof. Armin Reller for writing the second review for this thesis.

Special thanks also to my students, ***Elbara Ziade, Dan King and Frank Fu***, who did part of the work presented in this thesis and made working in the lab such a great time.

My Indian labmate "canelito" ***Shamit Shrivastava*** for his help and expertise during the fluorescence experiments, but also for his highly suggestive comments and jokes.

Christoph Westerhausen for the late night lab sessions and the crazy roadtrips.

Andreas Hartmann for being a friend and lab partner during my studies and PhD.

Thanks also to the entire ***Team of the EP1*** at the University of Augsburg for integrating me so well after my return. Somehow I never really felt as if I was gone for more than two years.

Konrad Kaufmann for his incomparable and unique character. Regardless whether I met you as a researcher, philosopher or musician; thank you for broadening my horizon in all these discussions and jam sessions.

One of the most precious experiences during my PhD was certainly to share my apartment with my Colombian friends ***Valeria Rueda and Benjamin Iriarte***. Appreciation for good food, coffee, music and life I learned from Valeria, while Ben filled our late night talks with the best stories about women and math. Thanks for this great year we shared.

Unforgettable and almost legendary was the band I played with in Boston. Thank you, ***David and Srikant*** for great jam sessions, the "Turducken" and your friendship.

Not to forget my most favorite Austrian ***Christian Fillafer***. Thank you for being such a great labmate and for taking so much effort in correcting the logical mistakes and typos of my thesis. In particular I'm grateful to you and your wife ***Gina Fillafer*** for granting me asylum in my last weeks in the USA, which simplified my life and made my transition back to Germany such a smooth process.

Especially I want to thank my colleague, roommate and friend ***Josef Griesbauer***. Three years ago, I would never have thought that two such opposed characters could spend such an "sau"-awesome time together. But living, working, exercising, travelling and partying together forged this unique friendship that changed my way of thinking far beyond the borders of physics and hopefully will last forever. Thanks for this unforgettable time and till our next beer at Red Bones!!!

My brother ***Michael Bössinger*** for the intense discussions about the economic order, the financial system and many other business related topics that almost make me an expert in these type of questions. But also for the appreciative and motivating competition and the friendship that connects us.

Last but not least I'd like to thank my parents ***Hannelore and Otto Bössinger*** for all their support during my studies and my PhD. Because of your confidence in me, I am able to reach my goals and dreams. Thank you!

L E B E N S L A U F

von Diplom Physiker

Stefan Bössinger

geboren am 6. Oktober 1982

STUDIUM

2003 - 2008	**University Augsburg** Physik Studium mit Nebenfach Chemie - *Note: 1,1*
2006 - 2008	**Bayerische EliteAkademie, München** Förderinstitution
2009 - 2012	**University Augsburg & Boston University** Promotion Biophysik

AUSLANDSAUFENTHALTE

2006 - 2007	**University of Santa Barbara (USA)** Forschungspraktikum Halbleiter
2009 - 2011	**Boston University (USA)** Forschungsaufenthalt mit Laborumzug

BERUFSPRAXIS

2000 - 2004	**Fujitsu Siemens & MAN, Augsburg** Ferienjobs in der Fertigung
2005 - 2007	**Exp. Physik 1, Augsburg** Wissenschaftsassistent & Übungsgruppenleiter

STIPENDIEN

2009 - 2012	**Elitenetzwerk Bayern** Doktorandenkolleg
2010	**DAAD** Promotionsstipendium

FACHLICHE KENNTNISSE

Sprachen	**Englisch** - fließend, **Französisch** - Grundkenntnisse
IT	Mac OS, C#, MS Office, Adobe Illustrator & Photoshop, Origin

SONSTIGES ENGAGEMENT

Nachhilfelehrer, Fußballtrainer, Musik (Saxophon, Gitarre, Klavier)
Begeisterter Sportler: u.a. NYC Marathon 2011

Augsburg, September 20, 2012

Stefan Bössinger